Fluid Flow and Heat Transfer Studies of Two−Phase Flow Inside Microchannels

A Dissertation
Submitted in partial fulfillment of the requirements for
the award of the Degree of

DOCTOR OF PHILOSOPHY

in

MECHANICAL ENGINEERING

by

S.V.B.VIVEKANAND
(Roll No.: 714012)

Under the Supervision of

Dr. V.R.K. Raju
Associate Professor
Mechanical Engineering Department

DEPARTEMENT OF MECHANICAL ENGINEERING
NATIONAL INSTITUTE OF TECHNOLOGY,
WARANGAL (TS), INDIA−506004,
November, 2019

Fluid Flow and Heat Transfer Studies of Two−Phase Flow Inside Microchannels

A Dissertation
Submitted in partial fulfillment of the requirements for
the award of the Degree of

DOCTOR OF PHILOSOPHY

in

MECHANICAL ENGINEERING

by

S.V.B.VIVEKANAND
(Roll No.: 714012)

Under the Supervision of

Dr. V.R.K. Raju
Associate Professor
Mechanical Engineering Department

DEPARTEMENT OF MECHANICAL ENGINEERING
NATIONAL INSTITUTE OF TECHNOLOGY,
WARANGAL (TS), INDIA−506004,
November, 2019

राष्ट्रीय प्रौद्योगिकी संस्थान वारंगल National Institute of Technology Warangal

Department of Mechanical Engineering

CERTIFICATE

This is to certify that the dissertation work entitled **— FLUID FLOW AND HEAT TRANSFER STUDIES OF TWO−PHASE FLOW INSIDE MICROCHANNELS**, which is being submitted by **Mr. S.V.B. VIVEKANAND (**Roll No. 714012), is a bonafide work submitted to the Department of Mechanical Engineering, National Institute of Technology, Warangal in partial fulfillment of the requirement for the award of the degree of **Doctor of Philosophy in Mechanical Engineering.**

To the best of our knowledge, the work incorporated in this thesis has not been submitted elsewhere for the award of any degree.

Dr. V.R.K. Raju
Supervisor
Department of Mechanical Engineering
National Institute of Technology
Warangal- 506004

Prof. N. Selvaraj
Head of the Department
Department of Mechanical Engineering
National Institute of Technology
Warangal-506004

NATIONAL INSTITUTE OF TECHNOLOGY, WARANGAL – 506004

Mechanical Engineering Department

APPROVAL SHEET

This Thesis entitled **"Fluid Flow and Heat Transfer Studies of Two−Phase Flow Inside Microchannels"** by **Mr. S.V.B. Vivekanand (Reg. No. 714012)** is approved for the degree of Doctor of Philosophy.

Examiner

Prof. Swarup Kumar Mahapatra (SMS, IIT Bhubaneswar)

Supervisor

Dr. V.R.K. Raju (Assoc. Prof., MED)

Chairman

Prof. N. Selvaraj

MED, NIT Warangal

DECLARATION

This is to certify that the work presented in the thesis entitled. **"FLUID FLOW AND HEAT TRANSFER STUDIES OF TWO−PHASE FLOW INSIDE MICROCHANNELS"** is a bonafide work done by me under the supervision of Dr. V.R.K. Raju, Associate Professor, Department of Mechanical Engineering, NIT Warangal, India and was not submitted elsewhere for the award of any degree.

I declare that this written submission represents my ideas in my own words and where others' ideas or words have been included, I have adequately cited and referenced the original sources. I also declare that I have adhered to all principles of academic honesty and integrity and have not misrepresented or fabricated or falsified any idea / data / fact / source in my submission. I understand that any violation of the above will be a cause for disciplinary action by the Institute and can also evoke penal action from the sources which have thus not been properly cited or from whom proper permission has not been taken when needed.

S.V.B.Vivekanand

(Roll No.: 714012)

Date:

Dedicated to

My Parents (Shri. S. Sankara Rao & Smt. Jaya Lakshmi) & My Wife (Mrs. Ashwini Panchal)

ACKNOWLEDGMENT

Foremost, Praise to God. Afterwards, I would like to express my deep sense of gratitude and sincere thanks to my supervisor **Dr. V.R.K. Raju** for his invaluable insights, guidance, continuous support, and encouragement during the course of this research. This work could not have been possible without his innovative problem definition, technical advice and continuous inspiration. His meticulous approach in dealing with complex problems and critical comments at each stage during the progress of this work brings this thesis up to this form.

I express my sincere thanks to Director NIT Warangal **Prof. N. V. Ramana Rao** for providing all academic and administrative help during the course of my work.

I like to extend my sincere thanks to **Prof. P. Bangaru Babu**, Chairman (Doctoral Scrutiny Committee), Head of the Mechanical Engineering Department and to the members of DSC, **Prof. S. Srinivasa Rao**, Department of Mechanical Engineering, **Dr. D. Jaya Krishna**, Associate Professor, Department of Mechanical Engineering, and **Dr. Ajey Kumar Patel**, Assistant Professor, Department of Civil Engineering, for all the support bestowed on me by suggesting and verifying the research work.

Moral support, encouragement and help provided to me throughout this research journey by several of my faculties and friends are gratefully acknowledged; in particular I mention, **Shri. G.R.K. Gupta**, Associate Professor, Department of Mechanical Engineering, **Dr M. Raja Vishwanathan**, Asstistant Professor, Department of H&SS, my co-scholars: Dr. G. Prabhakar Rao, **T. Manoj Dundi**, **S. Chandrasekhar**, **R. Shasidhar**, and **K. Siva Prasad**. I am also grateful to **Dr. Raghvendra Gupta**, Associate Professor, Department of Chemical Engineering, IIT Guwahati, for his invaluable insights during this journey. I extend my deep sense of gratitude to **Dr. Jaya Mishra**, Associate Professor, Communication skills, RCET Bhilai, for assisting me in completing my work.

I could not have completed my doctoral study without the inspiration of my parents, my wife, brother-in-law, and my beloved sister. Whenever I felt depressed or faced any problem they were always beside me. Words can hardly acknowledge the support I received from them. The list is unending. There are many people who are responsible to make this journey so enjoyable. I am carrying the memory of all of them in my heart.

(**S.V.B. VIVEKANAND**)

ABSTRACT

Two-phase heat transfer in microchannel has been an interesting topic of research to many researchers since the increasing loads of heat fluxes in the electronic components are reaching the limits of single-phase cooling techniques. The two-phase flow and heat transfer inside microchannels are affected by several factors, such as wettability, wall boundary conditions, wall motion, and channel orientation. Most of the studies available in the literature deal with: (i) stationary walls of the channel, and (ii) constant heat flux or isothermal wall boundary conditions. Apart from that the effect of (a) contact angle on the flow physics, and (b) channel orientation on the evaporation heat transfer characteristics have also not been explored in detail earlier.Thus, the present study aims at exploring the two-phase flow and heat transfer behavior at microscale,through which higher heat fluxes can be removed.

This thesis addresses the flow physics and heat transfer characteristics of the two-phase flow with and without undergoing any phase changing process. Gas-liquid and liquid-liquid Taylor flows represent the cases where the phase change does not take place. Whereas, flow boiling of water inside a microchannel has also been studied in which the phase change takes place. A wide range of parameters affecting the two-phase fluid flow and heat transfer behavior has been identified and new methods have been conceived for achieving better enhancement in the two-phase heat transfer rates.

The hydrodynamics of gas-liquid Taylor flow in a two-dimensional T-junction microchannel has been numerically examined, where the volume of fluid interface capturing technique is employed. The effect of inlet fluid velocity and the wall contact angle on the flow parameters such as gas and liquid slug lengths, and pressure drop has been studied. The wall wettability is found to have a significant effect on the pressure drop inside the channel. The pressure drop decreases with the contact angle in hydrophilic channels. Whereas, in hydrophobic cases the pressure drop increases. In addition, the bubble shape becomes asymmetric due to the increase in drag forces in the hydrophobic channels.

In this thesis, the flow physics and thermal behavior of liquid-liquid Taylor flow in a two-dimensional, axi-symmetric circular microchannel is presented. The gradient-adaptation technique has been employed for the capturing of thin liquid films. The wall of the circular microchannel is subjected to isothermal and constant heat flux boundary conditions in individual cases in order to determine the influence of thermal wall boundary conditions on the heat transfer rates during the flow. A significant increase in the Nusselt number in slug

flow in contrast to single-phase flow has been witnessed by using both the boundary conditions individually.

Further, the heat transfer characteristics of liquid-liquid Taylor flow inside the rectangular micro-parallel plates prescribed with modulated temperature boundary conditions have been examined. The effects of amplitude and frequency of the sinusoidal wall temperature profile of the time-averaged Nusselt number have been investigated. The temperature modulation has been found to increase the average heat transfer of the two-phase flow in contrast to liquid-only flow as well as the two-phase flow without modulation.

The thermal behavior of a liquid-liquid Taylor flow in rectangular microchannel having its walls imposed by small modulated motion in the transverse direction of the fluid flow under constant heat flux boundary condition has also been studied. The effects of amplitude and frequency of the modulated wall motion on the film thickness, droplet shape, and time-averaged Nusselt number have been investigated. The modulated wall motion has a significant effect on the two-phase heat transfer rate due to the presence of small vortices of the two-phase interface at a particular value of frequency. The average Nusselt number increased with the increase in amplitude when the frequency of modulated wall motion was kept constant.

The heat transfer studies of the two-phase flow of water undergoing evaporation inside a rectangular microchannel have been carried out. The purpose of this work is to investigate computationally effect of gravity on the heat transfer behavior of the two-phase flow of water undergoing phase change. The inclination of the channel varied from -90^0 (vertically downward) to 90^0 (vertically upward) to study the effect of gravity on the two phase heat transfer during the flow. The heat transfer coefficient was found to be the highest for an inclination angle of 45^0 as compared to all other orientations. It was observed that for a given heat flux, the boiling heat transfer coefficient increases significantly at a very high quality region, in contrast to the low quality region where it remains roughly unchanged due to partial dry out.

This research provides some important results and discussion on various parameters influencing high amounts of heat fluxes, which further could be used for optimizing engineering devices, such as semiconductor devices.

Keywords: Evaporation, Heat transfer, Microchannel, Modulation, Pressure drop, Taylor flow.

CONTENTS

LIST OF FIGURES

LIST OF TABLES

NOMENCLATURE

a	constant (-)
b	constant (-)
C	Courant number (-)
Ca	Capillary number(-)
D	diameter (m)
E	Energy per unit mass (J/kg)
f	apparent friction factor(-)
F	body force vector (kg m-2 s^{-2})
G	Mass flux ($kg\ m^{-2}\ s^{-1}$)
h	channel width (m)
h	convection heat transfer coefficient (W m^{-2} K^{-1})
k	interface curvature (m^{-1})
k	thermal conductivity (W m^{-1} K^{-1})
L	length (m)
Nu	Nusselt number(-)
N_{UC}	no. of unit cells (-)
P	pressure (Pa)
Pe	Peclet number(-)
q	heat flux (W m^{-2})
R	microchannel radius (m)
Re	Reynolds number(-)
S_α	mass source term (kg/m^3 s)
S_h	Energy source term (kg/ms^3)
t	time (s)
T	temperature (K)
U_S	slug velocity (m/s)
U_b	bubble velocity (m/s)
U_{TP}	mixture velocity (m/s)
u_{cell}	unit cell velocity (m/s)
V	velocity (m/s)
w	relative velocity of bubble w.r.t slug (m/s)
We	Weber number
y	Location along the width of the channel (m)

Greek letters

a	Amplification factor (-)
α	dispersed phase volume fraction
β	homogeneous void fraction
δ	film thickness (m)
Δx_{cell}	unit cell length (m)
λ_m	roots of second order Bessel function
ω	frequency (rad/s)
μ	dynamic viscosity (Pas)
ρ	density (kg/m^3)

σ	surface tension coefficient (N/m)
Θ	contact angle (degree ^{o})
θ	dimensionless temperature

Subscripts

a	advancing
avg	average
b	bubble
bm	bulk mean
c	continuous/carrier phase
c	cold wall
C	capillary
CA	contact angle effect
d	dispersed phase
eff	effective
F	film
FD	film to droplet
FS	film to slug
G	gas phase
h	hydraulic
h	heated wall
hyd	Hydrodynamic entrance
h_{lv}	Latent heat (J/kg)
H	horizontal direction
i	i^{th} phase
L	liquid phase
L	lower wall
MF	Moving film
r	receding
SP	single phase
SF	Stagnant film
s	Saturated state
S	liquid slug
TP	two-phase
U	upper wall
UC	unit cell
v	vapor phase
V	vertical direction
w	wall
x	axial direction
o	static

CHAPTER 1 INTRODUCTION AND LITERATURE SURVEY

1 Introduction

The use of semiconductor devices such as high-speed computers, microprocessors, commercial electronic equipment has been increasing exponentially these days due to their fast response and capabilities in meeting the needs of human beings in several aspects. This has led to higher generation of heat fluxes in these devices which must be dissipated at faster rates to ensure the durability of these devices. Hence, faster and efficient cooling has become a prime importance for the application of above-mentioned devices. Several cooling techniques have been developed for fast and effective cooling such as spray cooling (Fabbri et al. 2005), microchannels (Morini 2004), and jet impingement (Jeffers et al. 2009). However, it is still being explored by many researchers to find better cooling methods. Out of the above-mentioned techniques, microchannels ($0.1 < d < 1$mm) are found to be effective in removing high heat fluxes. Small surface-to-volume ratio and superior heat and mass transfer properties are the major key reasons for the rapid demand of microchannel reactors over conventional reactors. Due to recent advancements in microfabrication technologies, the application of microchannels has increased tremendously. It is now effectively possible to miniaturize all kinds of systems like mechanical, fluidic, electrochemical, and thermal, down to micrometric sizes. Many industries like biomedical, food processing, electronic and manufacturing are now looking towards miniaturized devices because of their remarkable properties. With the small dimensions of microchannels, it has become possible to achieve high throughput by using simple microreactor units, thereby reducing the cost and time of re-design, production, and development, unlike macroreactors. These microreactors have been largely used in single-phase forced convection cooling techniques. Earlier, in single-phase

forced convection cooling, air was used as the coolant to dissipate the heat fluxes in the electronic equipment. However, the increasing levels of power-density in electronic devices are reaching the limits of single-phase cooling techniques. Hence, it is necessary to switch to two-phase flow cooling methods due to their capability in removing high amounts of heat fluxes.

Two-phase flow is the type of multiphase flow, which occurs due to a significant change in the interfacial phenomenon because of the flow of two fluids, either gas-liquid or liquid-liquid, inside a channel or a tube.Two-phase flow can be broadly classified into two types: (i) undergoing a phase changing process, and (ii) without undergoing a phase changing process. The former type includes boiling and condensation problems, whereas, the latter type includes flows such as bubbly-dispersed, slug-annular, churn, and slug flows. These flow regimes are distinguished on the basis of a flow regime map (Fig. 1.1) which shows the relationship between the superficial velocities (U_s) of the fluids. Out of these two-phase flows, slug flow (also known as Taylor flow) covers a considerable region in the flow regime map which indicates that it operates for a large range of the superficial velocity of the two fluids (Dai et al. 2015; Leung et al. 2010; Gupta et al. 2010b; Fukagata et al. 2007; Triplett, Ghiaasiaan, Abdel-Khalik & Sadowski 1999). Slug flow is characterized by the segmentation of primary phase fluid with the secondary phase fluid which is dispersed inside the flow channel. These flows are of two types, namely, liquid-liquid (LL) and gas-liquid (GL) slug flows depending on the phase of the dispersed phase fluid. Slug flow is known to be very effective in heat and mass transfer applications because of its unique ability to create recirculation (Taylor vortices) inside the droplets/bubbles and slugs (Bauer et al. 2006; Abiev & Lavretsov 2012; Abiev 2013). Several researchers have contributed their efforts in understanding the physics of two-phase Taylor flow because of its various benefits associated with flow and heat transfer applications (He et al. 2010; Horvath et al. 1973; Lakehal et al. 2008; Triplett, Ghiaasiaan, Abdel-Khalik, LeMouel, et al. 1999; Leung et al. 2012).

This chapter discusses some of the fundamentals of the fluid mechanics and heat transfer along with a brief introduction of two-phase flow which forms the foundation for the objectives of the research work discussed in the subsequent chapters.

1.1 Hydrodynamics of Single-phase flows

Fluid flow through a pipe finds its major applications in heating and cooling problems, and also in the distribution network of fluids. Very often, forced convection technique is used to

pass the fluid through the pipes. Due to fluid flow through the pipe, fluid friction comes into picture which has a significant effect on the pressure drop across the channel. In the fluid flow through pipes, the velocity of the fluid is zero at the wall due to no-slip conditions and the maximum velocity occurs at the center of the pipe. By using the principle of conservation of mass one can obtain the average velocity (u_{avg}) at a given cross-section of the pipe using Eq. 1.1.

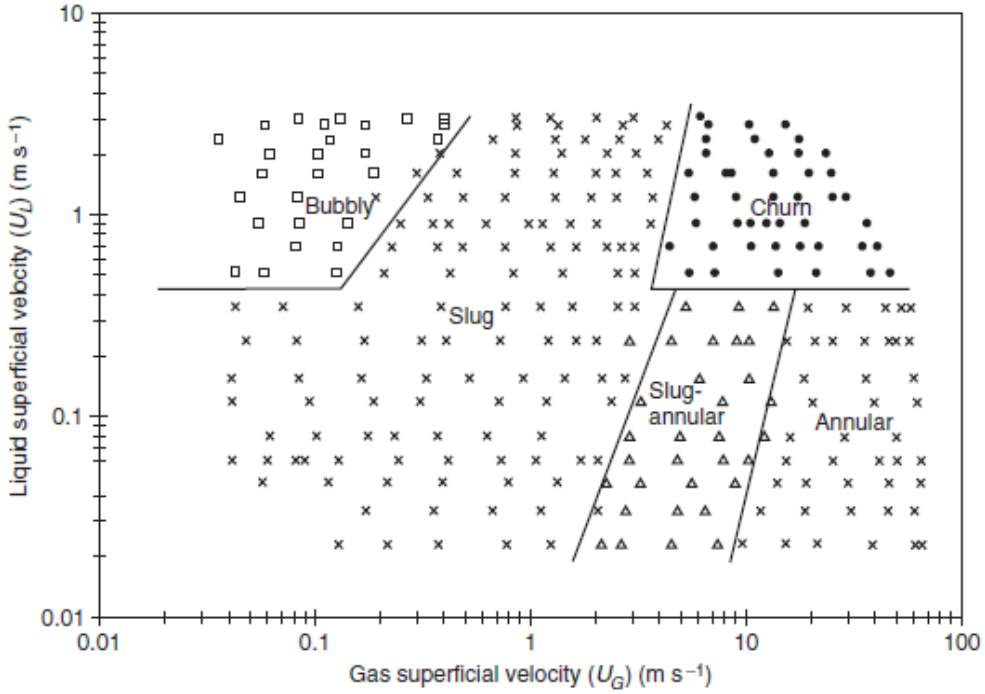

Fig. 1.1. Flow regime map (Gupta et al. 2010b).

$$u_{avg} = \frac{\int_{A_c} \rho u(r)\, dA_c}{\rho A_c} = \frac{\int_0^R \rho u(r)\, 2\Pi r dr}{\rho \Pi R^2} = \frac{2}{R^2}\int_0^R u(r)\, r dr \tag{1.1}$$

whereρ is the fluid density, R is the radius of the circular pipe, A_c cross-sectional area, and $u(r)$ velocity profile as the function of the radius of the tube or pipe.

Hydrodynamic Boundary layer development

Figure 1.2 shows the development of the velocity boundary layer in the pipe flow. The flow region, in which the effects of shear forces (arising due to the viscosity of fluid) are observed, is known as the velocity or hydrodynamic boundary layer. This layer divides the flow into two regions, namely, the core region where the flow is irrotational and the fluid is essentially having uniform velocity across the flow, and the second region is the boundary layer region

where the fluid friction is not negligible and the viscosity effects are significant. In this region, the boundary layer thickness increases along the direction of flow and finally reaches the pipe center as shown in Fig. 1.2. The point at which the boundary layer merges with centerline is called as the hydrodynamic entrance point, and the length from the inlet to the hydrodynamic entrance point is called as the hydrodynamic entrance length, L_h given by Eq. (1.2). Since the velocity boundary layer increases till this point as the velocity profile develops, the flow is called as hydrodynamically developing flow. The flow beyond this point is called as hydrodynamically fully developed flow and the velocity profile does not change afterwards.

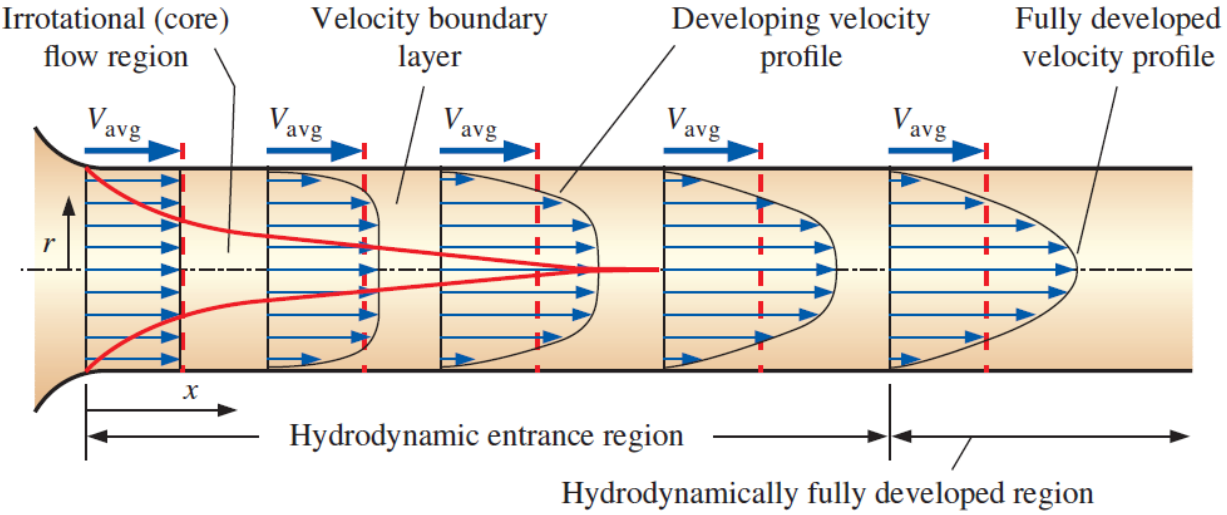

Fig. 1.2. Development of the velocity boundary layer in a pipe (Cengel & Cimbala 2017).

$$L_{h,laminar} = 0.05ReD \tag{1.2}$$

The velocity profile in the fully developed region is parabolic profile, given by Eq. (1.3).

$$u(r) = 2u_{avg}\left(1 - \frac{r^2}{R^2}\right) \tag{1.3}$$

Pressure drop

In pipe flows, pressure drop plays a key role in pumping power requirements. The total pressure drop during a fluid flow can be evaluated from Hagen-Poiseuille's equation (Eq. 1.4),

$$\Delta P = \frac{8\mu L u_{avg}}{R^2} \tag{1.4}$$

In terms of friction factor, it is expressed as

$$\Delta P = f\frac{L}{D}\frac{\rho {u_{avg}}^2}{2} \tag{1.5}$$

where $\frac{\rho {u_{avg}}^2}{2}$ is dynamic pressure, and f is a Darcy friction factor given by Eq. (1.6) for fully developed laminar flow in a circular pipe.

$$f = \frac{64\mu}{\rho D u_{avg}} = \frac{64}{Re} \tag{1.6}$$

1.2 Heat transfer in single-phase flows

Heat is the amount of energy that can be transferred from one system to another due to the temperature differences. There are three modes of heat transfer: conduction, convection and radiation while the form of heat transfer considered in this thesis is internal forced convection heat transfer.

Convection heat transfer

The transfer of heat from one position to another due to the motion of fluids is termed as a convection heat transfer. This mode of heat transfer is also called often as Newton's law of cooling. Convection is the dominant mode of heat transfer in gases and liquids except for solids where conduction is the dominant mode of heat transfer. Mathematically Newton's law of cooling is given as:

$$\dot{Q} = hA_s(T_w - T_b) \tag{1.7}$$

Where $\dot{Q}$ is the heat transfer rate (W); h is heat transfer coefficient (W/m^2/K); T_w is wall temperature (K), and T_b is bulk mean or cup mixing temperature (K).

*Bulk mean temperature:*The ratio of the rate of flow of enthalpy through a cross-section to that of the rate of flow of heat capacity through the cross-section is defined as bulk mean or cup-mixing temperature. At any cross-section x, the bulk mean temperature can be obtained by equation (1.8):

$$T_{B_x} = \frac{\int_0^R \rho u(r) c_p T 2\Pi r dr}{\int_0^R \rho u(r) c_p \, 2\Pi r dr} \tag{1.8}$$

where ρ is the fluid density (kg/m^3), R is the radius of the circular pipe (m), c_p is the specific heat capacity of the fluid (J/kgK), and $u(r)$ velocity profile as the function of the radius of the tube or pipe, T is the temperature of the fluid (K).

Heat transfer coefficient

The total heat transfer rate absorbed by the fluid per unit area at any given axial location must be equal to the heat exchanged by conduction through the wall (Fourier's conduction law at $r = R$), hence the heat transfer coefficient is obtained as:

$$h = \frac{k_f \left(\frac{dT}{dr}\right)_{r=R}}{T_w - T_B} \tag{1.9}$$

Thermal boundary layer development

Figure 1.3 shows the development of the thermal boundary layer during a pipe flow under heating conditions. Similar to the hydrodynamic entrance length, a thermal entrance region, as shown in Figure 1.3, develops in channels when a cold fluid (at a temperature below the channel wall temperature) enters a hot channel or vice versa. The thermal entry length is calculated by Eq. (1.10).

$$L_{thermal} = 0.05RePrD \tag{1.10}$$

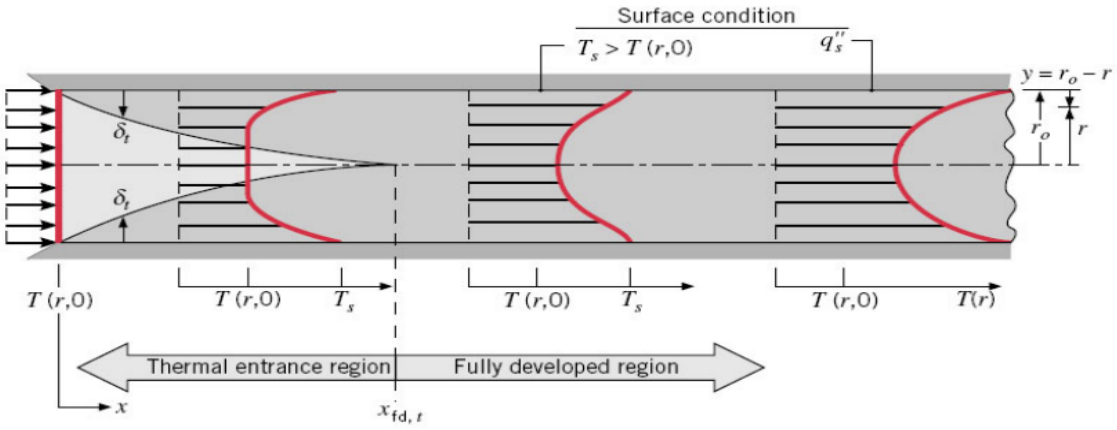

Fig. 1.3. Development of thermal boundary layer during heat transfer inside a pipe flow (Cengel & Cimbala 2017).

The heat can be supplied to the channel either in the form of constant heat flux (Neumann boundary condition) or constant temperature condition (Diritchlet boundary condition).

Constant heat flux

In circular channels, under constant wall heat flux conditions and constant thermophysical properties of the working fluid, the channel wall temperature and the bulk mean temperature of the fluid increases linearly along the axis. The temperature profiles at all cross-sections are

also similar and axially symmetric. The temperature profile in terms of the centerline fluid temperature T_c is given in Eq. (1.11) below:

$$T - T_c = \frac{\rho c_p}{k_f}\frac{dT}{dx}\frac{u_{avg}R^2}{4}\left[\left(\frac{r}{R}\right)^2 - \frac{1}{4}\left(\frac{r}{R}\right)^4\right] \tag{1.11}$$

Heat transfer rates in fluid flow problems are generally given in terms of a dimensionless parameter called Nusslet number which is defined as the ratio of convective heat transfer to the conductive heat transfer (Eq. 1.12).

$$Nu = \frac{hD}{k_f} \tag{1.12}$$

The average value of the Nusselt number for a fully developed flow subjected to a constant heat flux condition is 4.364.

Constant temperature

Under constant wall temperature heating conditions and constant thermophysical properties of the working fluid, the difference between the channel wall temperature and the bulk mean temperature decreases exponentially. The average value of the Nusselt number for a fully developed flow subjected to a constant wall temperature condition is 3.66.

1.3 Two-phase flow

1.3.1 Taylor flow

In Taylor flow, internal recirculation within the slugs leads to an enhanced mixing and the higher velocity of the secondary phase fluid improvise the heat and mass transfer mechanism. Hence, it provides better heat and mass transfer rates. The existence of thin liquid film between the channel wall and secondary phase droplet (or bubble in case of gas-liquid flows) plays a key role during the heat and mass transfer process in Taylor flows. Below a critical Capillary number ($Ca = \mu u_{TP}/\sigma$), thin liquid film does not exist and the two-phase slug flow is known as the sliding slug flow (Bandara et al. 2015b; Abiev 2015). Figure 1.4 shows the properties of a Taylor as well as sliding slug flow.

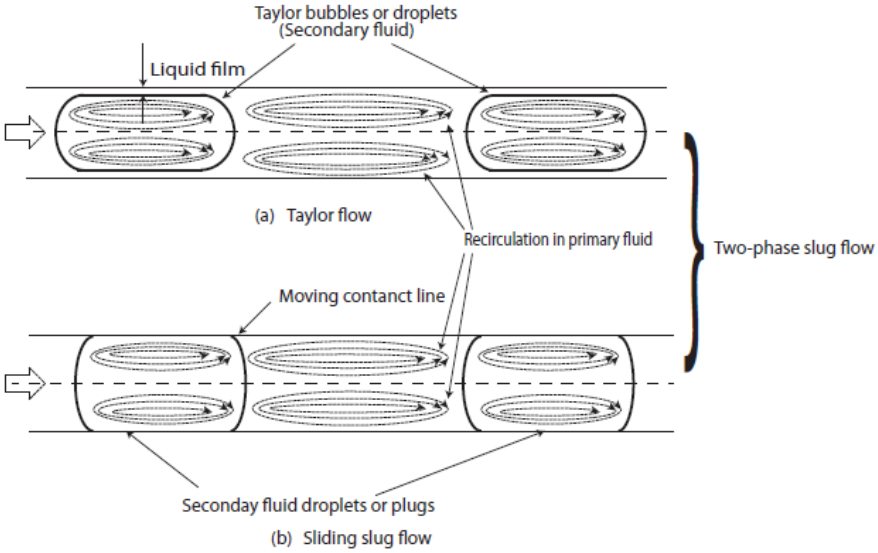

Fig. 1.4. Properties of (a) Taylor flow and (b) Sliding slug flow (Bandara et al. 2015b).

1.3.2 Evaporative cooling

The class of two-phase flow in which the fluids undergo phase change process is known as evaporative cooling or flow boiling. One of its applications is evaporative microchannel cooling, which is used to dissipate thermal fluxes in electronic circuits. It offers a high vaporization energy and surface area to volume ratio of the microchannel or micro chip. In addition, the heat removal is larger than conventional forced air cooling and microchannel liquid cooling due to the involvement of latent heat transfer. Hence, it holds the promise to be an effective way for cooling hot spots.

1.4 Literature review

1.4.1 Hydrodynamics and heat transfer studies of Single-Phase flow in microchannels

In recent years, significant progress has been made in the field of miniaturization. Small surface to volume ratio and superior heat and mass transfer properties are the major key reasons for the rapid demand of microchannel reactors over conventional reactors. Hydrodynamics and thermal characteristics of liquid-only (single-phase) flows in microchannels is extensively studied and reported in the literature. This section reports some of the important works on the flow and heat transfer characteristics of single-phase flows inside microchannels.

The use of single-phase flow for dissipation of heat in electronic chips was first demonstrated by Tuckerman & Pease (1981). Water was used as the working fluid without undergoing a phase change. It was reported in their work that laminar flow in microchannels

provides higher heat transfer rates as compared to that of turbulent flow through macrochannels. Since after their studies, the heat transfer in microchannels received more attention and the studies on convection through microchannels were carried out by various researchers. The experimental studies on single-phase heat transfer in microchannels were conducted by Peng & Peterson (1995) who identified the range of Reynolds number for which the laminar flow, transition and the turbulent flow regimes exist. They reported that for Reynolds number lower than 400, laminar flow exists. For $400 < Re < 1000$, transition from laminar to turbulent flow takes place, and fully developed turbulent flow occurs in the zone with $Re > 1000$. They also determined the effect of fluid flow velocity, thermal boundary conditions and characteristic dimension of the microchannels on the convective heat transfer coefficient. The exhaustive review on the experimental studies reviewed by Morini (2004) lists out important findings on the pressure drop and heat transfer number in liquid-only flows inside microchannels. It was reported that there is a high degree of disagreement in the results of above-mentioned parameters with the conventional theory. Also, it was concluded that more significant studies are required to be conducted to understand the mechanisms of fluid transport and thermal behaviour in single-phase flows inside microchannels.

Lelea et al. (2004) performed numerical and experimental studies to study the fluid flow and thermal behaviour of distilled water inside microtube. The channel diameter in the range 0.1 - 0.5mm and the flow Reynolds number upto 800 were the two major parameters considered in their experiments. They compared their numerical results with the experimental results as well as with the analytical expressions and concluded that the conventional theories of macrochannel were applicable to the single-phase flow of water in microchannels for the channel diameters considered in their study. Cetin (2005) numerically studied the fluid flow and thermal characteristics of single-phase fluid having constant properties in microtubes and micro-parallel plates. Finite difference method was used to discretize the governing equations pertaining to the flow and energy. The effect of rarefaction on the temperature profile and local Nusselt number was also discussed. The single-phase studies of Hestroni (2005) highlight the importance of channel shape and the characteristic length of the channel on the flow and heat transfer characteristics. Similarly, Morini (2006) discussed the role of the channel geometry, entrance effects, coupled heat transfer, fluid viscosity, and viscous dissipation on the heat transfer behaviour for thermally conducting and non-conducting channels. They reported that the average Nusselt number in the laminar regime depends on

the entrance conditions as well as the conjugate effects at low Reynolds number. Rosa et al. (2009) reviewed the numerical and experimental findings on the single-phase heat transfer at the microscale level. They reported the significance of various parameters, viz. entrance effects, viscous dissipation, compressibility effects, coupled wall heat transfer, temperature dependent properties, rarefaction, and surface roughness on the heat transfer performance of microchannels. A thorough experimental study was conducted by Celata et al. (2006) to examine the thermal behavior of the laminar flow of water inside microtubes. The walls of the tube were prescribed with constant heat flux condition. The experiments were performed for four different internal tube diameters, viz. 528 μm, 325 μm, 259 μm and 120 μm, out of which the channel with 528μm diameter provided thermally fully developed flow, whereas, due to a smaller diameter-to-length ratio in the smaller diameter tubes, the thermal development could not be achieved. Also, it was reported that the heat transfer rates were decreasing with a decrease in Reynolds number in contrast to the conventional theory (Nu=4.36), and the measurement errors were highly sensible in the case of the smallest diameter channel which led to an unrealistic evaluation of the mean Nusselt number.

Gawali et al. (2014) investigated the single-phase heat transfer characteristics of water flowing inside a straight rectangular microchannel heat sink having a hydraulic diameter of 507μm. They varied the flow Reynolds number from 200 to 700 to study the heat transfer behavior, overall thermal resistance, temperature distribution, and pressure drop in the microchannel. A close match was observed between their experimental results and the theoretical results for thermal resistances and Nusselt number. Other studies such as the micro-PIV and numerical studies performed by Vocale et al. (2014) and the recent numerical studies of Sahar et al. (2015) on the single-phase flow and heat transfer characteristics inside different microchannels cover a wide range of operating parameters and discuss their significance on heat transfer mechanisms. Morini (2018) provided a detailed review of experimental studies discussing the proposed techniques for the evaluation of local near-wall fluid temperature, the local wall temperature, and the local bulk fluid temperature in single-phase flows. In additions, the pros and cons of the techniques are also discussed so that one can wisely choose the evaluation techniques of the above-mentioned parameters according to the nature of single-phase problems.

Due to increasing loads of high heat fluxes in electronic chips, microprocessors, and computers, the single-phase cooling techniques are reaching their limits and there is the need of the hour to think of other alternate cooling methods which could meet the increased

growth of heat loads in such devices. Two-phase cooling techniques with or without phase change process have been studied by many researchers who reported the potentiality of two-phase flows over single-phase flows. The upcoming sections discuss such important studies introducing the hydrodynamics and heat transfer characteristics of two-phase flows.

1.4.2 Hydrodynamics and heat transfer studies of two-phase flow

Increasing rates of power density associated with miniaturization for development of microelectronic components such as microprocessors have led to the need for moving towards alternate cooling methods. These electronic components produce heat fluxes of the order of 100 W/cm^2 in low-end microprocessors to 300 W/cm^2 in high-end microprocessors. Many researchers have contributed their efforts to the development of technologies for removing high heat fluxes. The prime objective of such technologies is to maintain electronic components under safe operating limits by dissipating high heat loads. So far, single-phase forced air convection cooling techniques have been used to achieve this. However, the rapid increase in power density levels requires higher rates of airflow, which in turn necessitates bigger and more powerful fans. Use of such fans worsens the problems related to profile, vibration and noise control, and hence, forced air convection cooling methods are insufficient to meet the purpose. On the other hand, replacing air with liquid water could provide higher heat transfer rate. However, installation of single-phase liquid cooling device is more complex than single-phase air cooling device. Besides, liquids are more susceptible to leaks which could accelerate the corrosion of metallic parts and damage electronic components. In contrast to single-phase air and liquid cooling techniques, the two-phase flow techniques (either gas-liquid or liquid-liquid without phase change process, and two-phase flow undergoing phase change process) could be used for higher heat removal with low coolant flow rate. The potentiality of these flows over single phase flows has been studied and reported by many researchers (Bandara et al. 2015a; He et al. 2010; Che et al. 2012; Aussillous & Quere 2000; Eain et al. 2015; Eain et al. 2013; Oishi et al. 2009)**.** This section reviews the contributions of some of the researchers who made their efforts in understanding and building the concepts of two-phase flows both experimentally and numerically.

1.4.2.1 Gas-liquid slug flow without phase change process

Taylor flow (also called as bubble-train or slug flow) regime is considered to be the most useful flow regime covering considerable portion in a flow regime map (Triplett, Ghiaasiaan, Abdel-Khalik & Sadowski 1999). Taylor flow is characterized by a sequence of gas bubbles

(or liquid droplets in liquid-liquid flow) filling the entire flow channel with liquid slugs between two consecutive bubbles. In Taylor flows, the presence of recirculation inside the liquid slugs plays a vital role in the heat and mass transfer processes. Particle Image Velocimetry (PIV) technique is often used to visualize the internal circulations within the liquid slugs. Kashid et al. (2005) conducted PIV experiments to examine the effect of mixture velocity in the presence and absence of liquid film on the velocity profile and internal circulations.

Depending upon the flow parameters such as Capillary number, Weber number, and wettability of the channel walls, a thin layer of carrier phase liquid may exist between the channel wall and the two-phase interface. This region of the liquid layer is often known as thin film region and its thickness is termed as thin film thickness. The thin film plays an important role in the heat and mass transfer process. The thin film thickness of the carrier phase film varies with Capillary and Weber numbers. It increases with the increase in flow rate causing the front meniscus of the bubble interface to become sharper in contrast to its tail (Goldsmith & Mason 1963). The prediction of film thickness has been the subject of interest to many researchers. Bretherton (1961) developed the free slip model to evaluate the film thickness with an assumption of $\delta_F << R$. Although, Bretherton's model is applicable for gas-liquid Taylor flows, it can be applied to liquid-liquid Taylor flows with the lower viscosity ratio (Gupta et al. 2013). Aussillous & Quere (A&Q) (2000) proposed their model by relaxing the Bretherton's hypothesis. Irandoust & Andersson (1989) proposed an empirical correlation to predict the film thickness based on the experimental results over a wide range of conditions (9.5×10^{-4}<Ca< 1.90, 0.42 < Re < 860, and 1 < Re/Ca< 140,000). Han & Shikazono (H&S) (2009) and Eain et al. (2013) proposed empirical correlation by incorporating the Capillary, Weber and Reynolds numbers to evaluate the film thickness in visco-capillary and visco-inertial regimes for accounting the capillary and inertial effects. The details of these correlations are shown in Table 1.1.

Table 1.1 Existing empirical and analytical correlations in literature for evaluating film thickness.

Author(s)	Correlation		Parameters
Bretherton (1961)	$\frac{\delta_F}{R} = 1.34Ca^{2/3}$	(1.13)	Circular cross-section, D_h < 1mm, Ca < 0.005, GL Taylor flow.
Aussillous & Quere (2000)	$\frac{\delta_F}{R} = \frac{1.34Ca^{2/3}}{1 + 3.34Ca^{2/3}}$	(1.14)	Circular cross-section, 0.42 <D_h< 1.46 mm, 0.015 < Ca < 1.9, GL

			Taylor flow.
Irandoust & Andersson (1989)	$\frac{\delta_F}{D} = 0.18\left[1 - e^{-3.08Ca^{0.54}}\right]$	(1.15)	9.5×10^{-4} < Ca < 1.90, 0.42 < Re < 860, and 1 < Re/Ca < 140,000.
Han & Shikazono (2009)	$\frac{\delta_F}{D} = \frac{0.670Ca^{2/3}}{(1 + 3.13Ca^{2/3} + 0.504Ca^{0.672}Re^{0.589} - 0.352We^{0.629})}$	(1.16)	Circular cross-section, 0.3 < D_h< 1.3 mm, Ca < 0.40, GL Taylor flow.
Eain et al. (2013)	$\frac{\delta_F}{R} = 0.35(Ca)^{0.354}(We)^{0.097}$	(1.17)	Circular cross-section, D_h = 1.59 mm, 0.002 < Ca < 0.119, 0.047 < We < 0.697 and 14.46 < Re < 100.96, LL Taylor flow.

The effect of channel shape plays an important role in the flow physics of Taylor flows. T-junction microchannels have been acknowledged to be suitable in a wide range of applications, viz., electronic cooling, biomedical, food processing units etc., giving better mixing characteristics as well as hydrodynamics and thermal insights of multiphase flow (Vandu et al. 2005). The effect of contact angle on gas-liquid Taylor flow in a T-junction microchannel was studied by Santos & Kawaji (2010). They observed a change in shape, size, and velocity of the gas and liquid phases due to their interaction with the channel walls (Fig. 1.5). Interface shape was also found to vary due to Laplace pressure, which is a function of the contact angle and velocity. Recently Liu et al. (2016) numerically investigated the effect of inlet orientations on the flow characteristics of gas-liquid Taylor flow in symmetric as well as cross-flow T junction microchannels. Bubble and liquid slug lengths, as well as shear stress in both types of microchannels were studied. It was reported that for same conditions, higher slug lengths could be achieved in the symmetric T-junction microchannels over cross-flow channels. Besides, the shear stress in the cross-flow microchannel was found to be very high at low capillary numbers in contrast to the symmetric T-junction channel under the same operating conditions which indicates the dependency of bubble and slug lengths on the shear stress. The bubble formation process in microchannels of different geometries and cross sections, for example, coaxial-spherical micro-mixers and channels having a square cross-section, have been explained convincingly in the recent studies (Svetlov & Abiev 2018; Lou et al. 2018; Haase 2017).

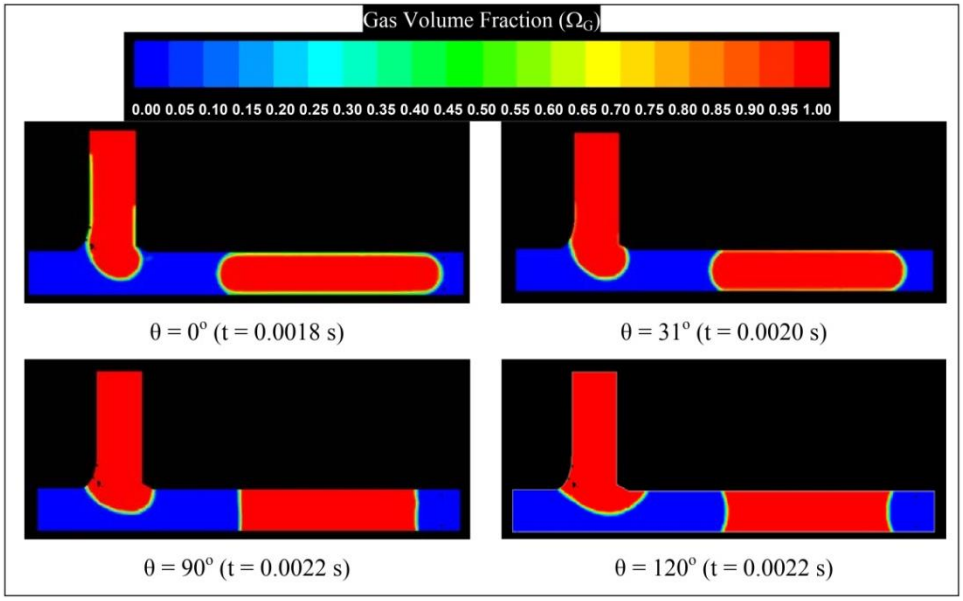

Figure 1.5. Effect of contact angle on bubble shape (Santos & Kawaji 2010).

A numerical study on two-phase slug flow was conducted by Nichita et al. (2010) by implementing dynamic contact angle concept using volume of fluid method where several two-dimensional and three-dimensional tests were performed to demonstrate the accurateness of the numerical model. The effect of surface roughness and hydrophobicity on the fluid flow inside a microchannel was demonstrated in the numerical studies of Kunert & Harting (2008). A three-dimensional lattice Boltzmann model was used for simulating the pressure driven flow between two infinite walls having roughness and wetting /non-wetting properties. They reported that due to nonlinearity between surface roughness and hydrophobicity of channel walls, slip length increases by a factor of three for small interactions.

The effect of channel size on the shape of the dispersed phase gas bubbles in a gas-liquid flow is well explained in the studies of Gupta et al. (2009). They performed numerical investigations on a two-dimensional axisymmetric domain using VOF multiphase method and predicted bubble shapes and validated the bubble formation periods with the experimental results of Salman et al. (2006).

Gupta et al. (2010a) implemented level-set and VOF methods in TransAT and ANSYS Fluent respectively and compared the bubble shape, wall shear stress and the Nusselt number obtained from both the CFD packages. Their operating conditions were Re = 280, Ca = 0.006 with β equal to 0.51. Influence of homogeneous void fraction and mixture velocity on the heat transfer was also studied. They reported that the heat transfer rate increased by approximately 2.5 times for isothermal and isoflux thermal boundary conditions in contrast to

single-phase liquid flow. The hydrodynamics of a single bubble rising in a vertical tube in a two-dimensional axisymmetric domain was examined by Farhangi et al. (2010). They investigated the effect of different parameters such as surface tension, channel height, initial bubble radius and liquid viscosity on the shape and rise velocity of the bubble.

Asadolahi et al. (2012) studied numerically the effect of working fluids (water/nitrogen and ethylene glycol/nitrogen) on bubble shapes, film thickness, pressure drop and bubble velocity in a two-dimensional axisymmetric microchannel (d = 2mm). They performed experimental work for the same combination of fluids and reported that the predicted CFD results were in a close match with the experimental results. Enhancement in heat transfer was also reported in their studies. The effect of plug lengths on the flow field and the recirculation period in Taylor flows was studied analytically by Che et al. (2012). A two-dimensional microchannel having a constant temperature wall boundary condition was used in their studies. They reported that shorter plugs make higher transverse velocity which enhances the heat transfer rate. Talimi et al. (2013) numerically studied the flow and heat transfer characteristics of Taylor flows in a microchannel of square cross-section under isothermal condition. They discussed the effects of slug length, contact angle and Reynolds number on the Nusselt number and validated their results against the experimental data of Betz & Attinger (2010).

1.4.2.2 Liquid-liquid slug flow without phase change process

Despite having a significant impact on the heat transfer performance, gas-liquid flows have certain limitations. The addition of discontinuous gas bubbles into a continuous liquid flow results in lower heat transfer rates in contrast to that of the introduction of the liquid droplet. This happens mainly because of poor heat capacity and thermal conductivity of gas over liquid (Eain et al. 2015). Tuckerman & Pease (1981) were the first to incorporate liquids for the dissipation of high heat fluxes in electronic equipment. Liquid-liquid slug flow finds its use in various applications such as polymerase chain reaction, Nitration of benzene to toluene, micro separation, and electronics cooling (Urbant et al. 2008; Asthana et al. 2011; Ookawara et al. 2007; Song et al. 2006).

In an attempt to take into account liquid/liquid two-phase pressure drop, Gupta et al. (2013) proposed a correlation for the total pressure drop occurring due to three major contributing factors: (a) slug (ΔP_{slug}); (b) film (ΔP_{film}); and (c) the interfacial ($\Delta P_{interface}$)

pressure drops. Slug pressure drop can be evaluated from Hagen-Poiseuille's equation (Eq. 1.18) due to fully developed flow in the primary phase slug.

$$\Delta P_{slug} = \frac{8\mu_c L_s u_{TP}}{R^2} \tag{1.18}$$

Figure 1.6 shows the variation of the wall and axial pressure along the axial length of the channel. It was observed that, in the region of uniform film thickness, the pressure gradients were identical in both the phases. Fouilland et al. (2010) assumed random pressure gradients at the annulus and core, and gave a solution for velocity profile using an analytical, annular, laminar-laminar flow solution for gas-liquid Taylor flows, whereas, Gupta et al. (2013) derived an expression for evaluating the film pressure drop considering equal pressure gradients, unlike arbitrary gradients (Eq. 1.19).

$$\Delta P_{film} = \frac{8\mu_c L_{film} u_{TP}}{R^2(1 + [(R_i{}^4)/(R^4)][(1/\lambda) - 1]} \tag{1.19}$$

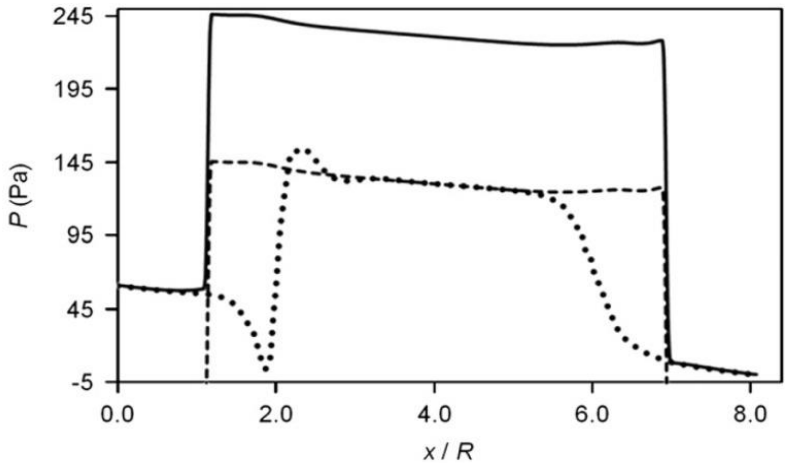

Fig. 1.6. Variation of wall and axial pressure along the axial length of the channel for u_{TP} =0.0566ms^{-1} and β=0.0735 for the dodecane-water system. (The dashed line represents the axial pressure shifted by Laplace pressure difference, which is equal to 75 Pa (approx.)) (Gupta et al. 2013).

For the evaluation of interfacial pressure drop, Bretherton (1961) proposed an expression which is given in Eq. (1.20). The total pressure drop over a unit cell length, given by Eq. (1.21), can be obtained by summating Eq. (1.18), Eq. (1.19), and Eq. (1.20).

$$\Delta P_{interface} = 4.52\frac{\sigma}{R}(3Ca)^{2/3} \tag{1.20}$$

$$\left(\frac{\Delta P}{L}\right)_{UC} = \frac{8\mu_c u_{TP}}{R^2}\frac{L_s}{L_{UC}} + \frac{8\mu_c u_{TP}}{R^2[(1+(R_i{}^4)/(R^4))((1/\lambda)-1)]}\frac{L_{film}}{L_{UC}} + \frac{4.52}{L_{UC}}\frac{\sigma}{R}(3Ca)^{2/3} \tag{1.21}$$

Various flow parameters, for example, size of Taylor droplets/bubbles, channel size, droplet and slug lengths, flow Reynolds number, liquid film thickness etc. significantly affect the flow physics and heat transfer rate of slug flows (Svetlov & Abiev 2018; Gupta et al. 2010a; Sadhana et al. 2018; Abiev 2013).

The numerical studies of Urbant et al. (2008) demonstrated the influence of droplet size on the thermal characteristics of liquid-liquid slug flow inside a circular microchannel under isothermal wall conditions. The reported results give an idea that the performance of microchannel heat sinks could be improved by using liquid-liquid Taylor flows. Che et al. (Che et al. 2013; Che et al. 2015; Che et al. 2011; Che et al. 2012) studied the flow and heat transfer behaviour of plug flows inside microchannels of circular cross-section and reported that the heat transfer rates enhance in the presence of shorter plugs and higher Peclet numbers.

Eain et al. (2015) conducted heat transfer studies in microcapillaries using dodecane, AR20, and Pd5 oils as the carrier phases and water as the dispersed phase in their experiments. They have discussed the impact of film thickness, and slug and droplet lengths on the slug flow heat transfer. The reported results revealed that the two-phase Nusselt number increased when the droplet length was increased. However, the heat transfer rate decreased with increasing liquid film thickness. They have also reported an average enhancement of 600% in the two-phase heat transfer over single-phase flow inside the circular tube subjected to H2 boundary condition. An empirical correlation was also suggested to model the liquid-liquid Taylor flows in thermally developing and fully-developed regions. The use of liquid-liquid Taylor flows for dissipating high heat fluxes results in a higher pressure drop in contrast to single-phase flows. Asthana et al. (2011) incorporated micro-PIV technique in their water-oil Taylor flow studies to experimentally visualize the internal recirculation within the slugs inside a serpentine microchannel. In addition, Laser Induced Fluorescence (LIF) method was used to measure the coolant

temperature. They reported a four-fold increase in the heat transfer rate over liquid-only flows which happened due to increased bulk mean temperature of the liquid slugs present between the droplets.

Fischer et al. (2010) numerically studied the thermal characteristics of water-oil slug flow inside circular channels of diameter 0.1-1mm in the presence of nanofluids. An average enhancement of 400% in Nusselt numbers over single-phase flows was reported in their work. Bandara et al. (2015b) reported an enhancement of 200% in the heat transfer rate using water-oil slug flow inside a 100μm microcapillary at the cost of higher pressure drop on the addition of liquid droplets inside the channel. Che et al. (2015) employed the level set and finite volume methods to compute the flow and heat transfer inside a rectangular microchannel. They reported that the presence of the gutters (space between the droplet menisci and the corners of the microchannel) and vortices decrease the thermal performance of the flow due to the parallel flow behavior, whereas the presence of recirculation inside the droplets and slugs enhance the heat transfer rates due to advection.

Thermal performance of two-phase slug flow inside the microchannel is measured with local Nusselt number which can be obtained using Eq. (1.22). The mean flow, temperature T_{bx} at a plane perpendicular to the axis is computed numerically as a mass-weighted average value and the wall temperature (T_{wx}) is obtained for each point along the channel. The total surface heat flux on the heating wall is uniform along the channel in case of constant wall heat flux condition.

$$Nu_x = \frac{q_w D_h}{k\left(T_{w_x} - T_{b_x}\right)} = \frac{h_x D_h}{k_c} \tag{1.22}$$

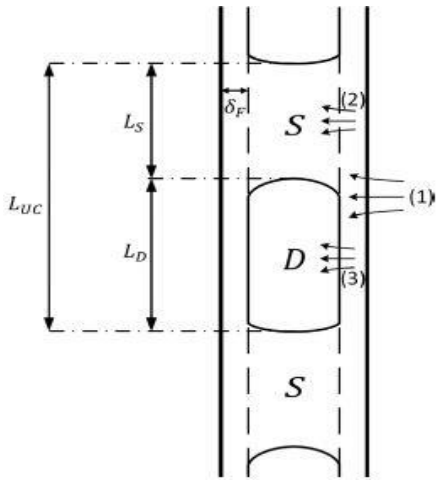

Fig. 1.7. Schematic of the unit cell showing the heat transfer mechanisms from (i) wall to film, (ii) film to slug, and (iii) film to droplet (Dai et al. 2015).

Figure 1.7 shows the schematic diagram of a unit cell comprising one droplet (bubble) zone (denoted by D) and two halves of the liquid slugs (slug zone denoted by S) on either side of the droplet. The total heat transfer process could be divided into three parts, namely: (i) heat transfer from wall to film, (ii) heat transfer from film to slug, and (iii) heat transfer from film to droplet. These three processes are indicated by numbers (1, 2, and 3, respectively) in the figure above. For constant heat flux over the channel wall, the phase temperatures increase at the same rate when the flow is thermally fully-developed. Dai et al. (2015) proposed a unified model (Eq. 1.23) to evaluate the heat transfer coefficients of liquid-liquid as well as gas-liquid Taylor flows. A liquid-liquid Taylor flow with water and hexadecane as the dispersed and continuous working fluids was simulated inside a circular pipe having a diameter of 2mm. The model joins the gas-liquid, and liquid-liquid flow regimes and the applicability of the model has also been validated with their experimental data as well as the data obtained by Leung et al. (2012).

The overall heat transfer resistance for two-phase flow can be given as:

$$\frac{1}{h_{TP}} = \frac{1}{h_w} + \frac{L_{UC}}{L_D}\left(\frac{m}{m+1}\right)^2 \frac{1}{h_{FD}} + \frac{L_{UC}}{L_S}\frac{1}{(m+1)^2}\frac{1}{h_{FS}} \tag{1.23}$$

The effect of homogeneous void fraction (β) on the normalized Nusselt number (Nu*) was discussed in their studies and is depicted in Fig. (1.8). The normalized Nusselt number can be defined as the ratio of the two-phase Nusselt number to that of the Nusselt number in a fully developed liquid-only flow subjected to constant heat flux boundary condition (Nu_0 = 4.364). The following expression gives Nu*:

$$Nu^* = \frac{Nu_{TP}}{Nu_0} \tag{1.24}$$

Shown in Figure 1.8 is statistics of Nu* for the case of different mixture velocities and a given range of L_D/d and L_s/d. The heat transfer rate augments from Nu*=1 (for β=0, i.e. pure hexadecane) to Nu*=6.91, after which the Nu* starts decreasing gradually towards the water-only value. The main reason for this enhancement is that in liquid-liquid flows, an increase in β leads to an elongation of a droplet and contraction in the slug. However, for gas-liquid systems the above-mentioned reason is not valid as the increase in β causes a negative impact on slug and droplet lengths in contrast to the liquid-liquid systems (Leung et al. 2010).

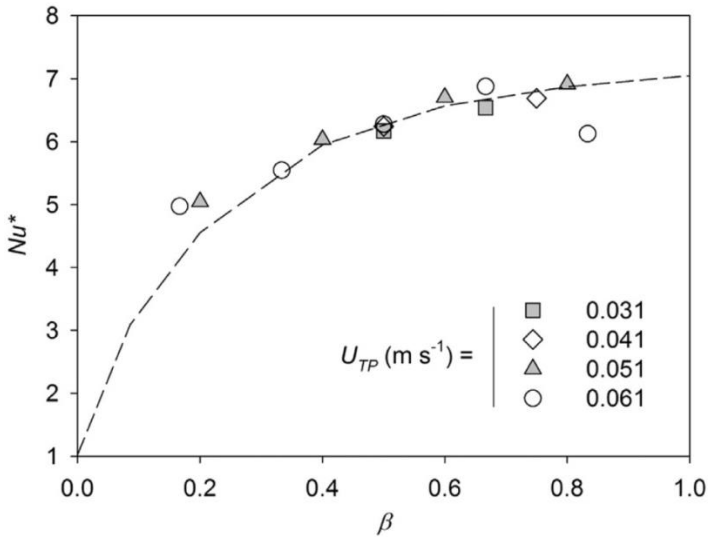

Fig. 1.8. The effect of the homogeneous void fraction (β) on the normalized Nusselt number for different mixture velocities (u_{TP}) with 1.1 < L_D/d < 5.0 and 0.4 < L_S/d < 3.6. The dashed line shows the prediction(u_{TP} = 0.051m/s) of the proposed model (Dai et al. 2015).

The average Nusselt number (Nu_{avg}) for a unit cell obtained from the simulations was calculated using Eq. (1.25).

$$Nu_{avg} = \frac{q_{w_{avg}} D_h}{k_c \left(T_{w_{avg}} - T_{b_{avg}}\right)} = \frac{h_{avg} D_h}{k_c} \tag{1.25}$$

where, $q_{w_{avg}}$, $T_{b_{avg}}$, and $T_{w_{avg}}$ are the average wall heat flux, average bulk mean temperature, and average wall temperature, respectively, given by Eqs.(1.26-1.28):

$$q_{w_{avg}} = \frac{1}{L_{UC}} \int_{x}^{x+L_{UC}} q_{w_x}\, dx \tag{1.26}$$

$$T_{b_{avg}} = \frac{\int_{x}^{x+L_{UC}} \int_{0}^{R} \rho |u_x| c_P T (2\pi r) dr dx}{\int_{x}^{x+L_{UC}} \int_{0}^{R} \rho |u_x| c_P (2\pi r) dr dx} \tag{1.27}$$

$$T_{w_{avg}} = \frac{1}{L_{UC}} \int_{x}^{x+L_{UC}} T_w\, dx \tag{1.28}$$

Other pioneering works (Qian & Lawal 2006; Lim et al. 2014; Lou et al. 2018; Khan et al. 2018; Choi et al. 2018) also add vast information to the available literature on the hydrodynamics and thermal characteristics of Taylor flows in microchannels.

1.4.3 Two-phase flow undergoing phase change process

Two-phase flow undergoing phase changing process is another class of two-phase flows which offer higher heat transfer rates in contrast to single-phase flows. The involvement of latent heat in evaporative cooling provides high heat transfer rates as compared to single phase flows. This section reviews some of the important studies on the heat transfer characteristics of two-phase flows undergoing phase change process.

Flow boiling of water inside a multichannel evaporator consisting of six parallel channels (1×1 mm^2) was examined by Kandlikar (2002). He reported an enhancement in the two-phase heat transfer due to localized flow reversal in some of the channels which occurred from the fluctuations in the pressure drop. Kandlikar (2004) also studied flow boiling in microchannels and proposed two dimensionless groups K1 and K2, where K1 is the ratio of evaporation momentum force to the inertia force and K2 is the ratio of the evaporation momentum force to the surface tension force. He reported that due to the periodic flow of vapour and liquid slugs during a nucleate boiling process, boiling due to convection process diminishes. An exhaustive review on the instabilities of two-phase flow in microchannels was performed by Kuan & Kandlikar (2006) who suggested that heat transfer can be enhanced by providing flow restrictions thereby suppressing the flow instabilities.

The convective boiling heat transfer characteristics of R410A in rectangular microchannels ($1.36 < D_h < 1.44$ mm) were explored by Yun et al. (2006). They suggested an empirical correlation based on their experimental studies to evaluate heat transfer during flow boiling. They reported satisfactory predictions of their results with a mean deviation of 18% against the proposed correlation. Bogojevic et al. (2009) investigated flow boiling instabilities by performing experiments in microchannels with a uniform cross-section. The subcooling conditions of the working fluid, as well as the ratio of heat flux to the mass flux, were acknowledged to be the cause for flow instabilities. Similarly, Mukherjee & Kandlikar (2009) presented a numerical analysis of microchannels with an inlet constriction to suppress flow boiling instability. They observed that the bubble formed due to vapour generation and reported that the bubble has a tendency to move towards the unrestricted end. The experimental studies of Schilder et al. (2010) on the single-phase flow heat transfer of water

and ethanol undergoing a phase change process inside a circular pipe demonstrates the influence of boiling heat transfer on the thermal performance of the channel. They varied the thermal loads and fluid velocity and reported that the existence of thin liquid films at the walls during the bubble growth led to significant augmentation in the heat transfer rates by approximately 3-8 folds in contrast to the single-phase flows. Ganapathy et al. (2013) employed volume of fluid method to study the condensation heat transfer characteristics in microchannels and reported various flow regimes such as annular, transition and intermittent flow during the fluid and heat transfer process. They reported that the numerical pressure drop and Nusselt number were found to be in close agreement with an empirical correlation lying within an average deviation of 8.1 % and 16.6 %. Figure 1.9 shows the flow regimes obtained from the numerical studies of Ganapathy et al. (2013) and that from the several experimental studies available in the literature. Experiments in segmented finned microchannels were conducted by Prajapati et al. (2016) to study the heat transfer characteristics of different coolants. They observed that the mass flux of coolant significantly affects the response time and it is lower in case of flow boiling compared to single-phase fluid flow.

Recently, many experimental and numerical studies of flow boiling heat transfer in small channels have also been carried out by researchers which build a platform for contributing efforts in the direction to achieve high heat dissipation rates which has always remained a challenge (Iqbal & Pandey 2018; Ferrari et al. 2018; Li et al. 2017; Markal et al. 2016; Gao et al. 2018).

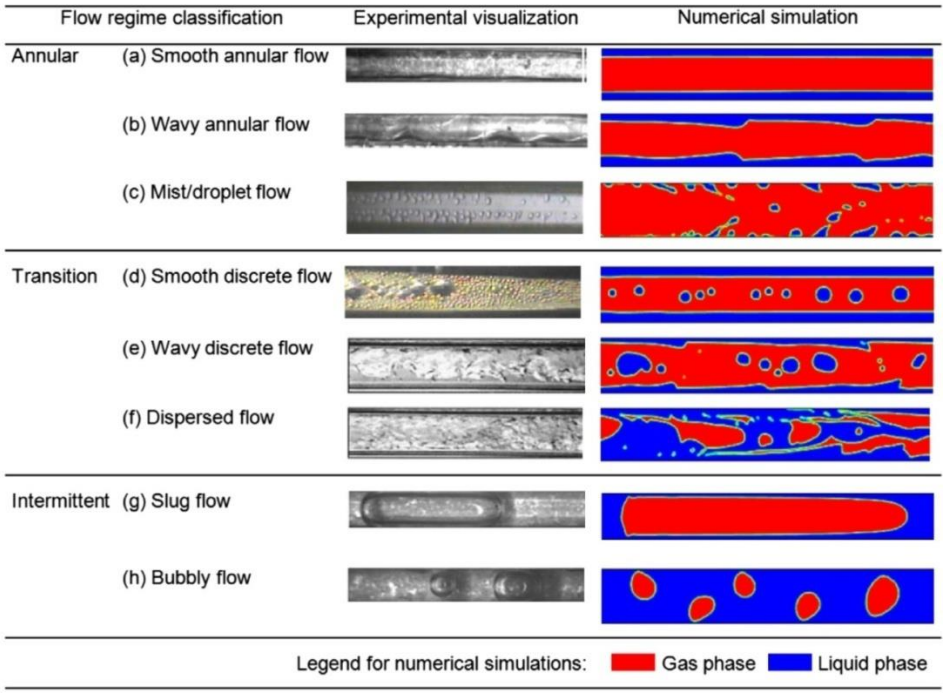

Fig. 1.9. Flow regimes in the microchannel during condensation heat transfer obtained from the CFD simulations of Ganapathy et al. (2013) and experimental studies of: Kim et al. (2012) (Fig. 1.9 a,b,g,h); Wu & Cheng (2005) (Fig. 3c); Hu & Chao (2007) (Fig. 1.9d); Coleman & Garimella (2003) (Fig. 1.9 e,f).

1.5 Shortcomings in the Literature

The above review briefly described the literature on the hydrodynamics and heat transfer characteristics of single-phase flows, two-phase flows without phase change, and two-phase flows undergoing a phase change process inside mini/micro channels. Though the volume of the literature on the hydrodynamics and heat transfer characteristics of the above-mentioned flows are very vast, one can readily identify a number of shortcomings in the existing literature which need attention from the researchers. Few of such gaps in the literature are mentioned below:

i. Several theoretical and experimental investigations were carried out to explore the hydrodynamics of gas-liquid Taylor flow inside the micro channels including T-junction micro channels. Very few studies have been reported on the effect of wall contact angle on the pressure drop and slug lengths of gas-liquid Taylor flows inside a T-junction micro channel having both inlets perpendicular to the horizontal mixing chamber.

ii. Various experimental and numerical studies addressing the heat transfer behavior of liquid-liquid slug flow under constant wall temperature and constant wall heat flux boundary conditions have been reported in the literature. So far, there is no literature available that discusses the effects of modulated thermal wall boundary conditions on the heat transfer characteristics of slug flow inside the micro channels. The slug flow problem with modulated boundary conditions represents a practical situation of day-to-day heat transfer based applications and hence it needs to be addressed.

iii. A very substantial amount of experimental and numerical studies has been conducted on Taylor flows inside micro channels under constant heat flux conditions. In all such studies, the walls of the channels were considered to be stationary. Also, the flow boiling inside a microchannel under modulated wall motion has also been studied separately by some researchers. However, no effort has been made till date to study the heat transfer characteristics of Taylor flows inside the micro channel under modulated wall motion conditions. Taylor flows inside the micro channels with its walls having a small oscillatory motion in the transverse direction of the flow should also be studied.

iv. Several studies have also been carried out in understanding the evaporation heat transfer of two-phase flows inside micro channels due to its benefits over single-phase flows. Nevertheless, systemic studies discussing the effects of (i) varying inlet vapour quality and (ii) gravity on the evaporation heat transfer characteristics of the two-phase flow of water within micro channels are also required to be carried out.

1.6 Objectives and scope of the present research work

The research work discussed in the present thesis is focused on understanding the flow and heat transfer behaviour of two-phase flow, (i) without phase change (gas-liquid or liquid-liquid Taylor flows/slug flows/bubble or droplet-train flows) and (ii) undergoing a phase change (evaporation) inside microchannels. The following investigations are made in the present dissertation to address some of the limitations in available literature:

i. Investigation of the effect of wall contact angle and carrier phase velocity on the flow physics of gas-liquid Taylor flows inside the microchannels.

ii. Investigation of the effects of wall boundary conditions on the heat transfer characteristics of liquid-liquid Taylor flow in a circular microchannel using gradient-adaptation based film capturing technique.
iii. Investigation of the effect of modulated wall temperature boundary conditions on the flow and heat transfer characteristics of liquid-liquid two-phase flow inside a rectangular microchannel.
iv. Investigation of the effect of imparting modulated wall motion on the flow and heat transfer characteristics of liquid-liquid two-phase flow inside a rectangular microchannel.
v. Exploring the effect of channel inclination and inlet vapour quality on the evaporation heat transfer characteristics of water inside the microchannel.

1.7 Organization of the Thesis

The present dissertation is organized into eight chapters:

1. The first chapter gives a brief introduction to the fundamental concepts of single-phase flows, two-phase flows without phase change, and two-phase flows undergoing phase change process. The benefits of two-phase flow over single-phase flow have also been discussed with some of their relevant applications. Exhaustive literature on single-phase flows as well as two-phase flows with and without undergoing phase change process have also been discussed underlining some important works which form the basis of the research discussed in the present thesis. Based on this survey some lacunas in the literature have also been pointed out.
2. The governing equations pertaining to the flow and heat transfer in gas-liquid or liquid-liquid Taylor flows, and evaporative heat transfer have been detailed out in the second chapter of the thesis.

3. Chapter 3 discusses the hydrodynamics of gas-liquid Taylor flow inside a T-junction microchannel, where the volume of fluid interface capturing technique has been employed. The effect of inlet fluid velocity and the wall contact angle on the flow parameters such as gas and liquid slug lengths and pressure drop has been studied. The effect of hydrophilicity or hydrophobicity on the bubble shapes has also been reported.

4. A numerical study of the hydrodynamics and heat transfer characteristics of liquid-liquid Taylor flow in a two-dimensional, axisymmetric circular microchannel has been presented in the fourth chapter. The gardient-adaption technique has been employed for

the capturing of thin liquid films. The wall of the microchannel is subjected to isothermal and constant heat flux boundary conditions in individual cases to determine the influence of thermal wall boundary conditions on the heat transfer rates during the flow.

5. The heat transfer characteristics of liquid-liquid slug flow inside rectangular micro-parallel plates have been discussed in chapter 5. The walls of the microchannel are subjected to modulated temperature boundary conditions and the effects of amplitude and frequency of the sinusoidal wall temperature profile on the time-averaged Nusselt number and transient development of bulk mean temperature are investigated.

6. The thermal behaviour of liquid-liquid Taylor flow inside the micro-parallel plates, where the walls of the channel are given small oscillatory motion in the transverse direction of the fluid flow under constant heat flux boundary condition, has been demonstrated in chapter 6.

7. In chapter 7, the numerical studies on the evaporation heat transfer characteristics of water in inclined rectangular microchannels have been discussed. The effects of channel inclination and inlet vapour quality on the two-phase Nusselt number have been investigated.
8. The last chapter of this thesis, i.e. chapter 8, summarizes the important conclusions of the research work discussed in the thesis and points out the future scope of the present research work.

CHAPTER 2 GOVERNING EQUATIONS

In the present chapter, the governing equations pertaining to the flow and heat transfer in gas-liquid or liquid-liquid Taylor flows, as well as evaporation heat transfer have been explained. In all the numerical studies discussed in the subsequent chapters, the fluids are assumed to be Newtonian fluids. The VOF (Volume of fluid) model (Hirt & Nichols 1981), available in CFD solver ANSYS Fluent, has been used for capturing the interface between the phases. The model solves a single set of governing equations of the flow and energy for individual phases. The volume fraction of a given phase (i.e. α_i) in a computational cell is either 0 or 1 depending on the volume occupied by the phases, whereas its value at the interface is 0.5 and the region $0 < \alpha < 1$ is called as the interfacial region.

2.1 Governing equations of flow and energy

The governing equations of flow and energy which were solved by the solver are given as below,

Continuity equation:

$$\frac{\partial \rho}{\partial t} + \nabla.(\rho \mathbf{V}) = S_{\alpha_i} \tag{2.1}$$

where*t* is time (s), ρ is mixture density (kg.m^{-3}), and $\boldsymbol{V}$ is velocity vector (ms^{-1}).

$$\rho = \rho_L \alpha_L + \rho_G \alpha_G$$

where α_L and α_G are the volume fractions of the liquid and gas phase, respectively. S_{α_i} is the mass source term of phase *i* and is equal to zero for phases undergoing no phase change.

Momentum equation

$$\frac{\partial(\rho \mathbf{V})}{\partial t} + \nabla.(\rho \mathbf{V}\mathbf{V}) = -\nabla P + \nabla.[\mu(\nabla \mathbf{V} + \nabla \mathbf{V}')] + \mathbf{F} \quad (2.2)$$

where μ is the dynamic viscosity of the mixture *(*Pas*)*.

$$\mu = \mu_L \alpha_L + \mu_G \alpha_G$$

Energy equation

$$\frac{\partial(\rho E)}{\partial t} + \nabla.[\mathbf{V}(\rho E + P)] = \nabla.(k_{eff} \nabla T) + S_h \quad (2.3)$$

where E is energy per unit mass (J/kg), P is pressure (Pa), k_{eff} is the effective thermal conductivity of the two-phase system, and S_h is the energy source term (kg/ms^3).

2.2 Surface tension modelling

The body force term '***F***' on the r.h.s of Eq.(2.2) includes the surface tension force (σ) which is modelled by continuum surface force (CSF) model proposed by Brackbill et al. (1992). It is given by Eq. (2.4),

$$F = \sigma k \frac{\rho \nabla \alpha_G}{0.5(\rho_L + \rho_G)} \quad (2.4)$$

where k is interface curvature (m^{-1}).

The interface curvature k was obtained by using Eq. (2.5),

$$k = \nabla.\hat{n} \quad (2.5)$$

where the vector perpendicular to the interface is given by Eq. (2.6).

$$n = \nabla \alpha_l \quad (2.6)$$

and its corresponding unit normal vector is given by Eq. (2.7).

$$\hat{n} = \frac{n}{|n|} \quad (2.7)$$

When the wall contact angle (Θ_w) is introduced, then the unit normal vector adjacent to the walls becomes:

$$\hat{n} = \hat{n}_w \cos \Theta_w + \hat{t}_w \sin \Theta_w \quad (2.8)$$

where $\hat{n}_w$ and $\hat{t}_w$ are the corresponding unit normal and tangential vectors at the wall, and Θ_w is the given static wall contact angle.

2.3 Interfacial phase change modelling

In phase changing problems such as evaporation (or condensation) of water, the liquid-vapour phase change taking place at the two-phase interface is followed by the transport of mass and energy between the phases as well as the absorption (evaporation case) or release (condensation case) of latent heat. These source terms are defined as shown below,

$$S_{\mathrm{l}} = \begin{cases} f_0 \rho_{\mathrm{v}} \alpha_{\mathrm{v}} (T_{\mathrm{s}} - T), & if T < T_{\mathrm{s}} \\ f_0 \rho_{\mathrm{l}} \alpha_{\mathrm{lv}} (T_{\mathrm{s}} - T), & if T > T_{\mathrm{s}} \end{cases}$$

Liquid mass source :

Vapour mass source : (2.9)

$$S_v = \begin{cases} -f_0 \rho_{\mathrm{v}} \alpha_{\mathrm{v}} (T_{\mathrm{s}} - T), & if T < T_{\mathrm{s}} \\ -f_0 \rho_{\mathrm{l}} \alpha_{\mathrm{lv}} (T_{\mathrm{s}} - T), & if T > T_{\mathrm{s}} \end{cases}$$

where T_s is the saturation temperature, f_0 is an adjustable parameter used to reduce the temperature difference between T and T_s to negligibly small values. It should be noted that for the conservation of mass S_l and S_v should sum to zero which indicates that the mass gained/lost by one phase is equal that lost/gained by another phase. The corresponding energy source (S_h) can be evaluated using Eq. (2.10). For a subcooled liquid ($\alpha_l = 1$, $\alpha_v = 0$, $T < T_s$) and a superheated vapor ($\alpha_l = 0$, $\alpha_v = 1$, $T > T_s$), the source terms defined in Eq. (2.9) are zero which indicates no phase change in these two cases. However, in a subcooled vapor ($\alpha_l = 0$, $\alpha_v = 1$, $T < T_s$), superheated liquid ($\alpha_l = 1$, $\alpha_v = 0$, $T > T_s$) or in a thermal non-equilibrium region ($0 < \alpha_l$, $\alpha_v < 1$, $T \neq T_s$), these terms are non-zero at the interface which indicates the possibility of the occurrence of phase change in such conditions.

$$S_{\mathrm{h}} = h_{\mathrm{lv}} S_{\mathrm{l}} \tag{2.10}$$

It should also be noted that the source terms related to the mass and heat transfer at the interface in a phase change process are not part of the solver rather these have been included in the above-mentioned governing equations by writing user-defined C routines and hooking the codes to the solver.

CHAPTER 3 NUMERICAL STUDY OF GAS-LIQUID SLUG FLOW IN T-JUNCTION MICROCHANNEL

3.1 Introduction

Over the last two decades, two-phase slug flow inside microchannels (1 μm < d < 1 mm) has gained significant attention over single-phase flow due to its higher heat and mass transfer capabilities in contrast to liquid-only flow. In general, *T*-junction is used to generate bubbles/droplets inside microchannels. Because of its good mixing characteristics, it finds application in various industries such as electronic cooling, biomedical, and food processing units (Qian and Lawal 2006, Vandu et al. 2005). The lengths of the gas bubbles and liquid slugs in a Taylor flow play an important role in heat and mass transfer processes. The orientations of the fluid inlets of a T-junction microchannel alter the shape and size of bubbles and slugs. Higher slug lengths could be achieved in the symmetric *T*-junction microchannels over cross-flow channels which could aid in heat transfer process (Liu et al. 2016).

The effect of wall wettability on Taylor flow characteristics has been studied by various groups: Kunert and Harting (2008), Talimi et al. (2013), Santos and Kawaji (2010), Abiev (2015), and Nichita et al. (2010). The effect of contact angle hysteresis on the pressure drop in slug flow inside hydrophilic as well as hydrophobic mini- and microcapillaries has been explained convincingly in Abiev (2015).A numerical study on two-phase flow was conducted by Nichita et al. (2010)by implementing dynamic contact angle concept using volume of fluid method where several two-dimensional and three-dimensional tests were performed to demonstrate the accurateness of the numerical model. The effect of surface roughness and hydrophobicity on the fluid flow inside a microchannel was demonstrated in the numerical studies of Kunert & Harting (2008). A three-dimensional lattice Boltzmann model was used for simulating the pressure driven flow between two infinite walls having

roughness and wetting /non-wetting properties. They reported that due to nonlinearity between surface roughness and hydrophobicity of channel walls, slip length increases by a factor of three for small fluid-wall interactions. The concept of slip length was introduced by Navier (1823) who stated that the velocity of the fluid (u) at the wall of a channel is directly proportional to its velocity gradient (i.e., $\frac{\partial u}{\partial x}$). This constant of proportionality is called slip length which measures the slip at the solid/liquid interface. In general, slip length is the distance from the wall where the tangential component of fluid velocity becomes zero.

The pressure drop in fluid flow inside narrow channels affects the efficiency of a fluid flow system. Hence, this area has been of interest to many researchers: Kreutzer et al. 2005, Abiev 2011, Abiev 2013, Roy et al. 2004, Choi et al. 2018, Khan et al. 2018, Lim et al. 2014.The contribution of various pressure losses in a gas-liquid system was discussed by Abiev (2011) and a mathematical model of pressure losses accounting the rearrangement of energy losses and velocity profiles during the continuous formation of gas bubbles was proposed. Abiev(2017) also explained the reasons for the inversion of local pressure gradient and the pressure jumps at the interface of gas-liquid Taylor flow, which was observed in the studies of Kreutzer et al. (2005) and Duran Martinez et al. (2015).

Based on the above literature it is observed that very few studies pertaining to the effect of contact angle on the hydrodynamics of gas-liquid Taylor flow are available in the literature. Hence, an effort has been made in the present chapter to develop better insights into contact angle and its effects on the pressure drop and slug lengths during the two-phase Taylor flow in microchannel.The currentchapter deals with the numerical study on the hydrodynamics of air-water two-phase flow in a T-junction rectangular microchannel. The Volume of Fluid (VOF) multiphase method is used for tracking the two-phase interface using ANSYS Fluent. The influence of input parameters such as inlet liquid velocity and wall contact angle on liquid and gas slug lengths, as well as pressure drophave been investigated.

3.2 Numerical Modeling

3.2.1 *Computational domain*

The physics behind the multiphase flow inside a microchannel is a complex phenomenon. Unlike two-phase fluid flow in conventional channels, where gravity plays a significant role, in microchannels, surface tension plays a vital role (Triplett et al. 1999) because at microscale the surficial effects dominate gravitational effects due to high surface to volume ratio; gravity is therefore neglected in the present study.

In the present numerical study, a 2D planar T-junction microchannel (Fig. 3.1) having a channel width (h) of 0.5 mm is chosen from the work of Qian and Lawal (2006). In the present study, attention has been paid to study the effect of wall contact angle on the pressure drop inside the channel in a gas-liquid Taylor flow which was left out in their studies. The microchannel consists of two vertical inlets, one for gas and the other for liquid, and a horizontal reaction chamber. Air and water enter the channel through the respective inlets and flow through the horizontal part of the microchannel. The vertical portion has a length L_V = 3 mm while the horizontal one has a length L_H = 30 mm. The fluid flow system under consideration was assumed to be at room temperature with atmospheric pressure at the channel outlet. The details of the geometrical parameters of the channel are given in Table 3.1. The liquid velocity varied in the range of 0.05 to 0.25 m/s, whereas gas velocity was kept constant at 0.05 m/s. The contact angle between the walls and fluids was also varied from 0^o to 170^o. Using these conditions Taylor flow was achieved inside the microchannel (Coleman and Garimella 1999; Triplett et al. 1999; Akbar et al. 2003). Axial gas input and two lateral liquid inputs lead to difficulty in the detachment of slugs and provide a smooth stream at the mixing region (Qian and Lawal, 2006), such a manner of introducing phases in the channel was avoided in the present study.

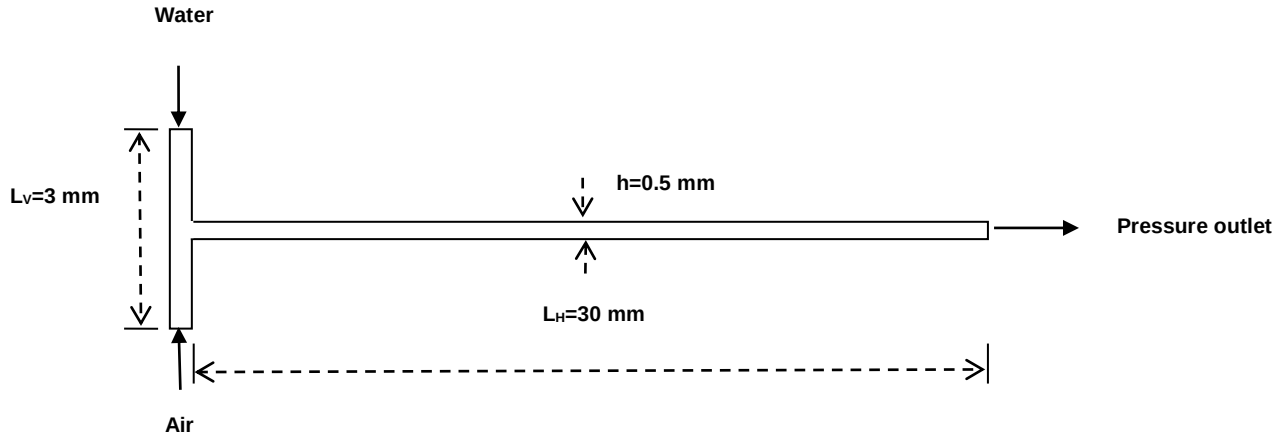

Fig. 3.1 Schematic of the computational domain (Qian et al. 2006).

3.2.2 *Boundary conditions*

Water and air were used as the liquid and gas phases respectively whose physical properties corresponding to an operating pressure of 1 bar are shown in Table 3.1. An incompressible laminar flow at isothermal condition was considered. The inlet velocity of the liquid phase was in the range 0.05 m/s to 0.25 m/s and the incoming gas flow velocity was kept constant at 0.05 m/s throughout the simulations. At walls, a no-slip condition was

specified. The surface tension at the interface was σ = 0.072 N/m. Moreover, the wall contact angle was varied from 0^o to 170^o to study the hydrophilic ($0^o < \Theta_o < 90^o$) and hydrophobic ($90^o<\Theta_o<170^o$) cases respectively. The gravitational effect was neglected due to its negligible impact on the fluid flow in microchannels. The entire computational domain was discretized into quadrilateral structured elements. Grid refinement was achieved by using adaption technique based on gradients of volume fraction as suggested by Mehdizadeh et al. (2011). Though very small elements could be used to track the gas-liquid interface, it would lead to high computational cost. It is advisable to use gradient adaption techniques due to its significant capabilities in tracking the two-phase interface. The wall contact angle was varied to study the influence of contact angle hysteresis on the pressure drop keeping all other conditions the same. All the flow conditions were at room temperature (300 K) during the entire study.

Table 3.1 Physical and geometrical parameters

Parameters	Details
Channel	2D, T-junction rectangular microchannel with both inlets in front of each other
Channel dimensions	L_V=3mm, L_H=30mm, channel width (h) =0.5mm
Flow	Two-phase Taylor flow
Continuous phase	Water (ρ = 998 kg/m^3, μ = 0.001003kg/m s)
Dispersed phase	Air (ρ = 1.125 kg/m^3, μ = 0.000017894 kg/m s)

3.2.3 *Solution strategy*

Governing equations were discretized using finite volume method (FVM) with pressure based solver in ANSYS Fluent. An explicit VOF multiphase method was used to carry out the transient studies. A first-order implicit scheme using non-iterative solver was adopted for the transient formulation. PISO algorithm (Issa 1986) was employed for pressure-velocity coupling. The gradients of various flow parameters were evaluated using the Green-Gauss node based method. A second-order upwind scheme for momentum and PRESTO! scheme for discretization of pressure was used. Geo-Reconstruct algorithm for the

discretization of volume fraction was used. Time step size (Δt) is defined using the CFL condition given by Eq. (3.1) which was first proposed by Courant et al. (1967).

$$C = \frac{u_{cell}\Delta t}{\Delta x_{cell}} \tag{3.1}$$

where C is the Courant number, u_{cell} is the fluid velocity (ms^{-1}) and Δx_{cell} is the cell length (m).

C = 0.25 has been adopted to determine the time-step size in order to have a stable solution of volume fraction equation. The details of the solver parameters are given in Table 3.2.

Table 3.2 Solver parameters

Parameters	Details
Discretization method	Finite volume method
Multiphase method	Volume of fluids
Grid size	30-70 μm
Wall contact angle	0^o - 170^o
Velocity of gas phase	0.05 m/s
Velocity of liquid phase	0.05 - 0.25 m/s
Surface tension	0.072 N/m
Courant number (C)	0.25
Grid refinement	Gradient adaption technique
Solver details	2D Planar, pressure based, absolute velocity formulation, and transient.
Pressure-velocity coupling scheme	PISO scheme
Transient formulation	Non-iterative time advancement (NITA), First order implicit.
Spacialdiscretisation	Green-Gauss node based method for gradient
Pressure discretisation	PRESTO scheme
Momentum discretisation	Upwind
Interface reconstruction	Geo-Reconstruct algorithm
Outlet	Pressure outlet (Atmospheric pressure)
Slip condition	No-slip
Time step size	10^{-7} s
Body force formulation	Implicit body-force formulation
Convergence criteria for x-velocity, y-velocity, and momentum	$1e^{-5}$

3.3 Results and discussion

3.3.1 *Grid Independence Test*

Grid independence study was performed to select the optimal mesh size in the present CFD modeling of slug flow. A structured square mesh (in case of a 2-D study) minimizes spurious currents in the region of the gas-liquid interface. Gupta et al. (2009) suggested the use of uniform structured grid for modeling Taylor flows. The mesh is automatically refined around the vicinity of the interface which adapts itself based on the gradient method. The threshold values for the refinement and coarsening of the mesh near the interface are 0.15 and 0.1, respectively. The gradient adaption method is computationally less expensive as it refines the mesh near the interface and maintains the base mesh elements elsewhere. Figure 3.2 shows the refined mesh elements near the interface obtained dynamically using the grid adaption method. Studies of Ganapathy et al. (2013) suggests that in two-phase flow numerical studies using VOF interface capturing technique, mesh size of around D/50 (D is hydraulic diameter) serves good for capturing the flow physics at the interface. However, in the present study, the current grid size of 50 microns resulted in grid independent velocity profiles (Fig. 3.3) and bubble profiles (Fig. 3.4(a-c)). Figure 3.3 shows the variation of the axial velocity of the continuous phase, lying between two bubbles at an instant, for 0° wall contact angle for different mesh sizes in the range of 70 microns to 30 microns. Similar velocity profiles are obtained for 30, 40 and 50 micron element size. The bubble profiles for a given contact angle (0°, 60°, and 150°) at different mesh sizes (40, 50, and 60 microns) are depicted in Fig. 3.4(a-c). Bubble profiles were found to be similar for 40 and 50 microns element size. In order to save computational cost, 50 micron element size was chosen for the present study. Equal fluid velocities (u_G = u_L = 0.05 m/s) at their respective inlets were set during the grid independence test.

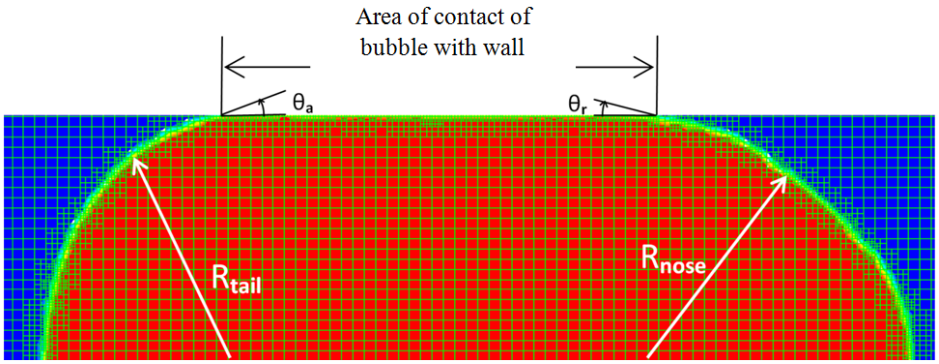

Fig. 3.2 Grid refinement near the interface based on the gradient adaption technique (base mesh element size: 50 microns). The air bubble is shown in red and the liquid water slug is shown in blue.

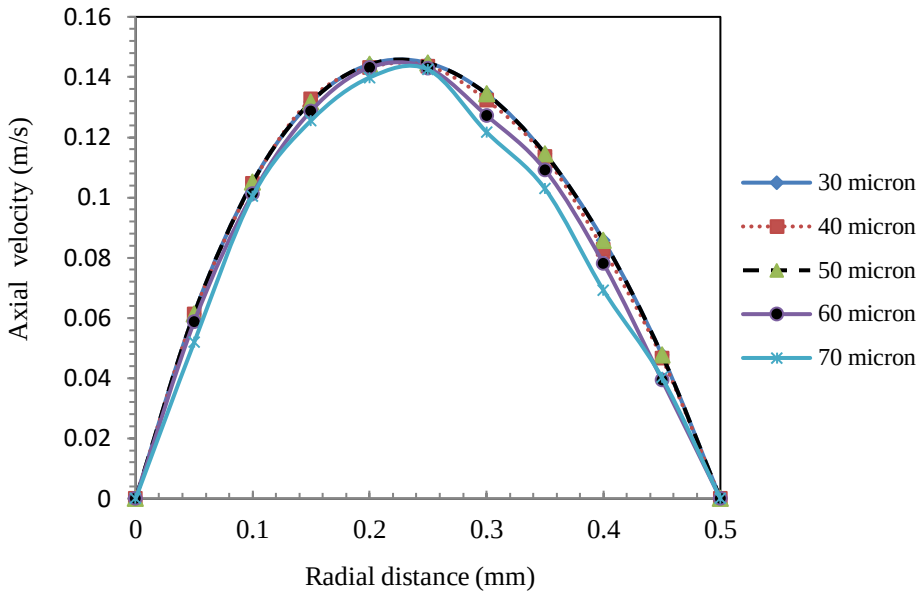

Fig. 3.3 Variation of axial velocity along the radial length for different mesh sizes (u_G= u_L = 0.05 m/s, Θ_w = 0°).

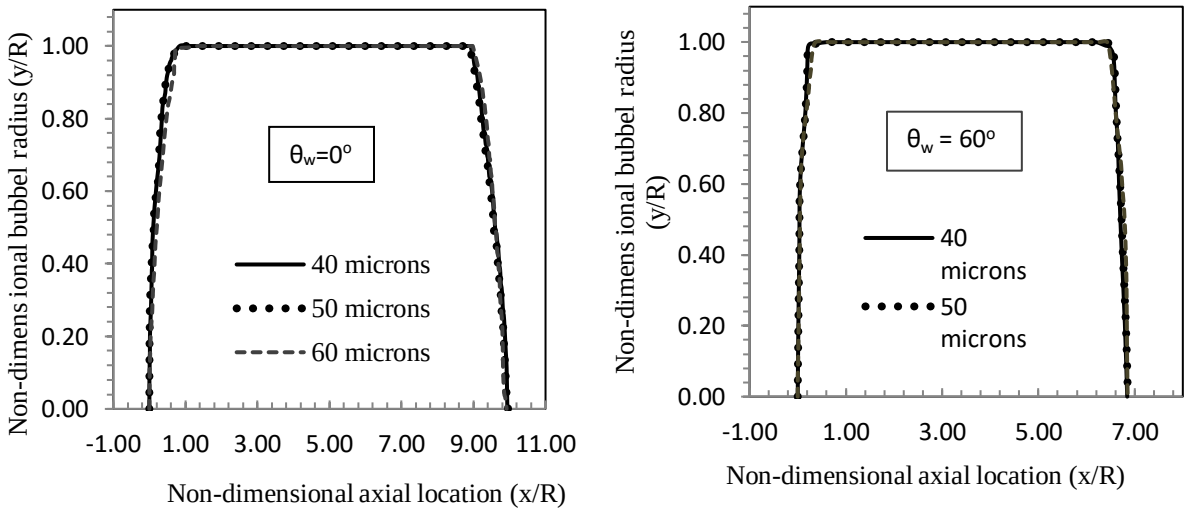

(a) (b)

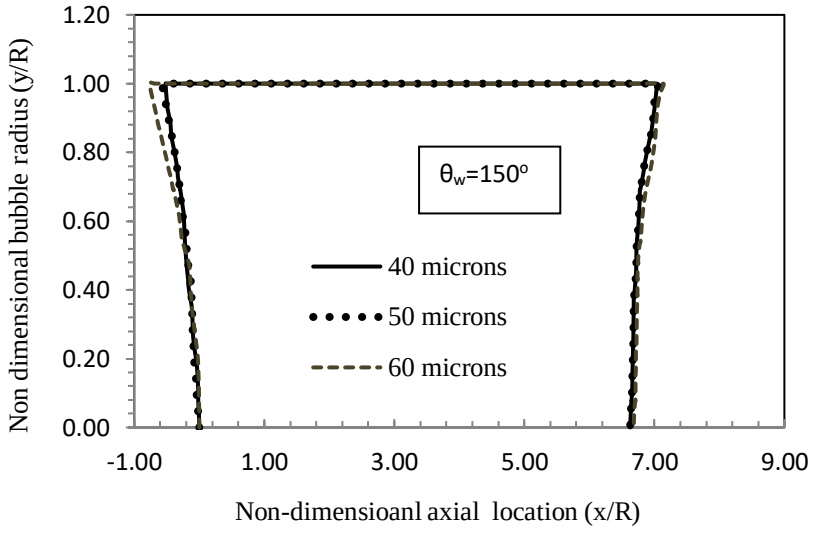

(c)

Fig. 3.4 Variation of bubble shape at different grid sizes for a given contact angle; (a) $\theta_o = 0^o$, (b) $\theta_o = 60^o$, and (c) $\theta_o = 150^o$. Here *R* is half the height of the channel.

3.3.2 *Validation*

Although many researchers have studied the flow characteristics of the gas-liquid two-phase slug flow inside microchannels and demonstrated the Taylor flow regime maps, most of their work were limited to flow patterns (Triplett et al. 1999). Experimental studies inside capillaries gave little information on liquid and gas slug lengths when the air was injected into water through a permeable media (Laborie et al. 1999). A thorough experimental study was conducted by Kreutzer et al. (2005) to study the hydrodynamics of two-phase gas-liquid flow inside a capillary. They proposed a correlation to measure the apparent friction factor (*f*) as given in Eq. (3.2).

$$f = \frac{16}{Re}\left[1 + 0.07\frac{D}{L_L}\left(\frac{Re}{Ca}\right)^{1/3}\right], \qquad Re = \frac{\rho_L U_{TP} D}{\mu_L} \tag{3.2}$$

where, *Re* is Reynolds number.

The constant 0.17 was suggested in place of 0.07 to avoid any experimental impurities which would generate surface tension gradient causing Marangoni effect. The present numerical code was validated against the benchmark experimental results of Kreutzer et al. (2005). The variation of apparent friction factor with the dimensionless slug length using air-water fluid systems is depicted in Fig. 3.5, and also tabulated in Table 3.3. It can be seen that the apparent friction factor diminishes with liquid slug length. This happens because the two-phase flow tends to behave like single-phase when the liquid slug length increases.

Overall, the results obtained from the present study are found to be in close agreement with the experimental data of Kreutzer et al. (2005) with a maximum deviation of less than 10%.

Table 3.3 Comparison between the results of the present numerical study and experiments of Kreutzer et al. (2005).

U_L (m/s)	L_S (mm) (Experiment)	L_S (mm) (CFD)	f*Re (Experiment)	f*Re (CFD)	Absolute difference (CFD- Experiment)	Absolute relative difference (CFD- Experiment)/ (Experiment)× 100%
0.005	1.24	1.20	51.00	52.22	1.22	2.39
0.007	1.30	1.25	49.45	50.61	1.16	2.34
0.009	1.33	1.29	48.60	49.65	1.05	2.16
0.01	1.49	1.53	45.05	44.26	0.79	1.75
0.02	1.63	1.67	42.65	41.93	0.72	1.68
0.03	1.69	1.76	41.58	40.58	1.00	2.41
0.04	1.87	2.00	39.21	37.67	1.54	3.93
0.05	2.19	2.49	35.81	33.40	2.41	6.73
0.1	2.94	3.25	30.75	29.32	1.43	4.65
0.15	4.13	3.96	26.50	26.95	0.45	1.69
0.2	4.12	5.19	26.52	24.35	2.17	8.18
0.25	6.09	5.52	23.12	23.85	0.73	3.16

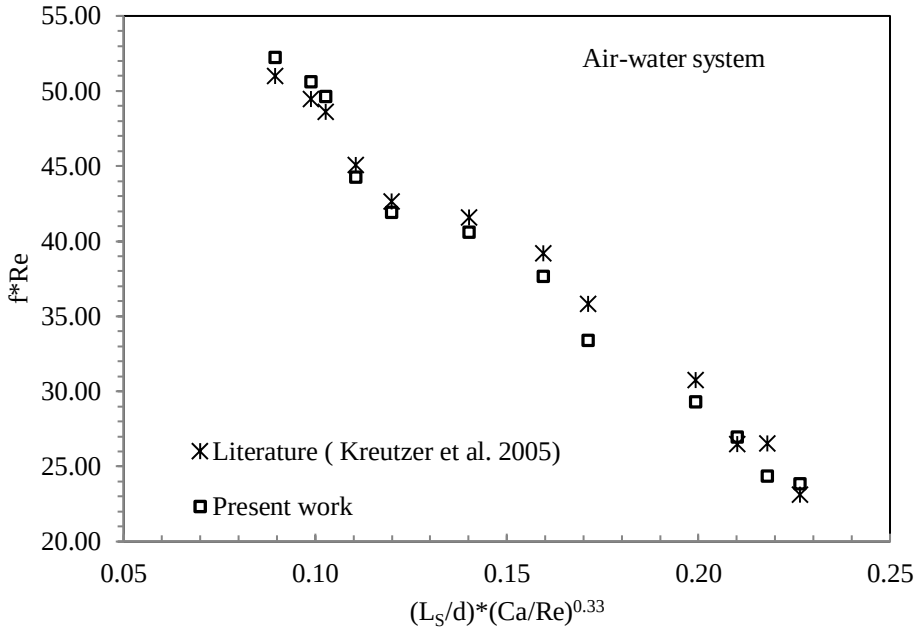

Fig. 3.5 Comparison of numerical data with experimental results of Kreutzer et al. (2005), (f*Re) vs. dimensionless slug length $(L_S/d)*(Ca/Re)^{0.33}$.

3.3.3 *Slug flow development with time*

This section describes the development of gas and liquid slugs inside the T-junction microchannel. Initially, the whole domain was filled with water and the two working fluids were allowed to enter from their respective inlets with uniform velocities. Figure 3.6(a-f) shows the transient development of bubble and liquid slugs inside the T-junction microchannel. It is observed that the bubble and liquid slugs are formed either at the intersection of the T-junction or at the beginning of the horizontal mixing zone of the microchannel. The incoming gas phase meets the incoming liquid phase at the junction of the microchannel where the onset of bubble formation takes place, Fig. 3.6(a).

Further, the growing bubble acquires the channel diameter and blocks the incoming liquid phase due to which the pressure builds. This causes an increase in the flow velocity of the continuous phase between the wall and bubble leading to the shearing action on the dispersed phase. It can be seen in the figure that the squeezing process in gas bubble occurs at the junction of the microchannel. At the inlet of the mixing zone, the two-phase interface moves downstream causing the elongation of the dispersed phase. With time the neck of the bubble gets thinner and the squeezing process begins due to high-pressure buildup. Later, depending on the flow conditions, the gas bubble of the required shape and size is formed after the squeezing process, Fig. 3.6(b). This way a continuous bubble-train flow (Taylor flow or slug flow) is developed and travels along the channel, Fig. 3.6(a-f). A similar transient development of bubbles was reported in the numerical work of Qian and Lawal (2006) which validates the numerical code used in the present study. It should be noted that the size of slugs depends on various parameters, such as inlet velocities of liquid and gas phase, viscosity and wall contact angle (Pohorecki and Kula, 2008).

(a) t = 0.052 s

(b) t = 0.071 s

(c) t = 0.094 s

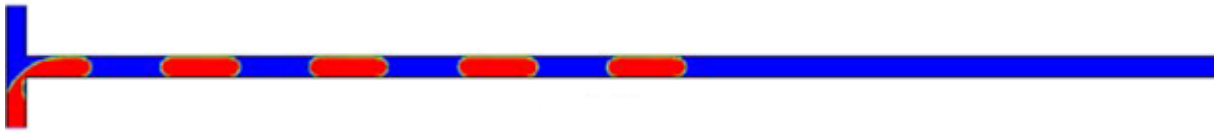

(d) t = 0.13 s

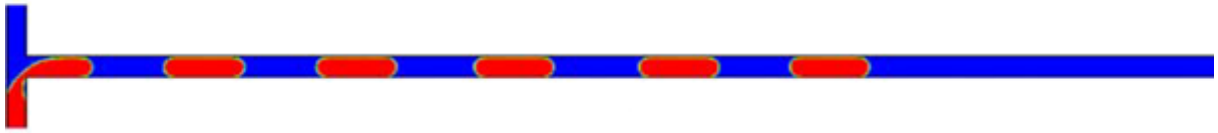

(e) t = 0.17 s

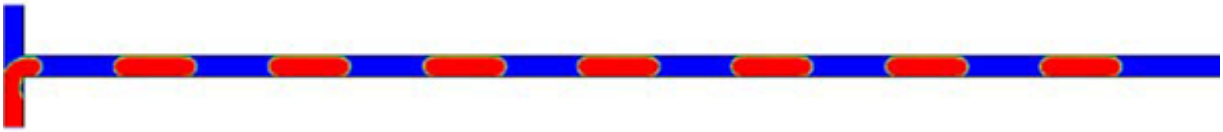

(f) t = 0.2 s

Fig. 3.6(a-f) Transient development of Slug-train flow ($u_G = u_L$ = 0.05 m/s, $\theta_o = 0^o$). The air bubble is shown in red and the water slug is shown in blue.

3.3.4 *Variation of slug and bubble length with the liquid flow rate*

From the literature currently available, it is observed that liquid and gas slug lengths are affected by various parameters like channel cross-sections, superficial velocities of working fluids, fluid properties, and film thickness. In addition, the gas and liquid slug lengths play a key role in heat and mass transfer processes. Liu and Wang (2011) proposed the film theory and reported that the presence of primary phase film between the bubble and channel wall greatly affects the mass transfer coefficients and has a directly proportional relationship.

In the present work, simulations were carried out by varying the inlet liquid velocity ($0.05 < u_L < 0.25$ m/s) to study the relationship of inlet liquid velocity with the bubble and liquid slug lengths. Figure 3.7 shows the terminology used in the present study for the convenience of the readers. Figure 3.8 represents graphically how the liquid slug length increases when the inlet velocity of the liquid phase is increased. Further, the variation in bubble length with liquid flow rate is also studied, as shown in Fig. 3.8. It is found that the bubble length decreases when the velocity of the incoming liquid phase is increased.

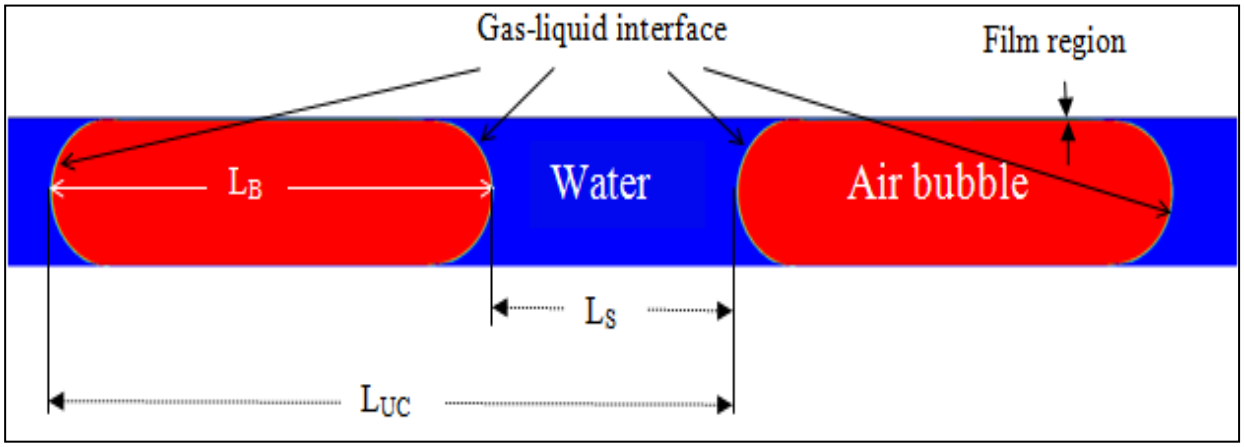

Fig. 3.7 Terminology used in the present two-phase flow.

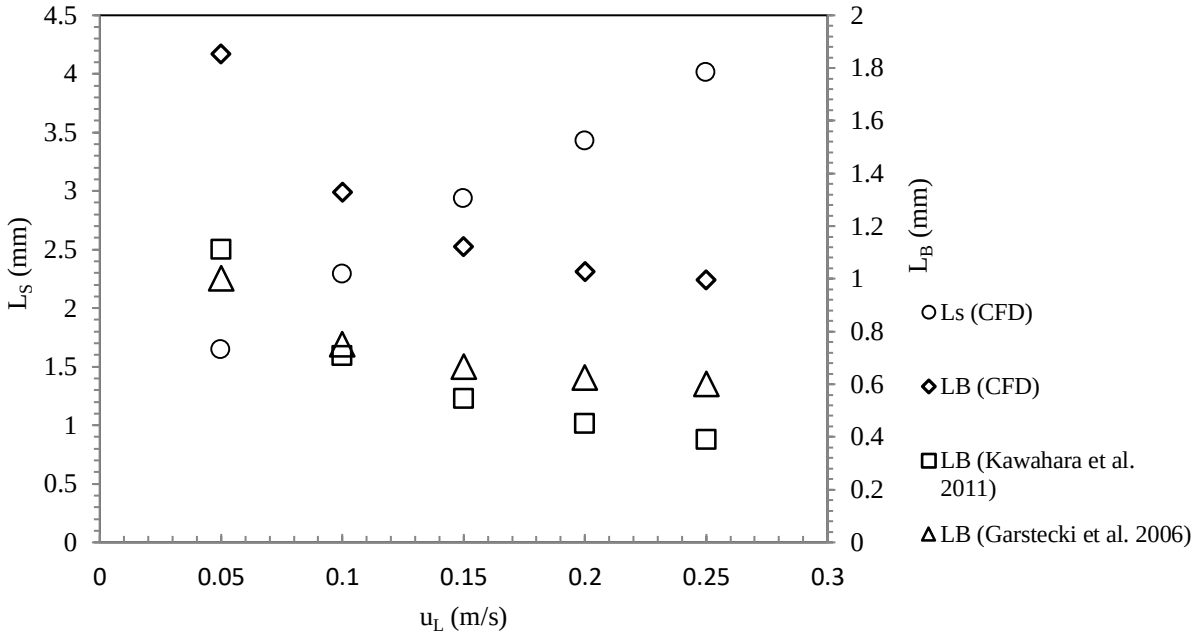

Fig. 3.8 Influence of inlet liquid velocity on liquid and gas slug lengths (u_G = 0.05 m/s, Θ_o= 0°).

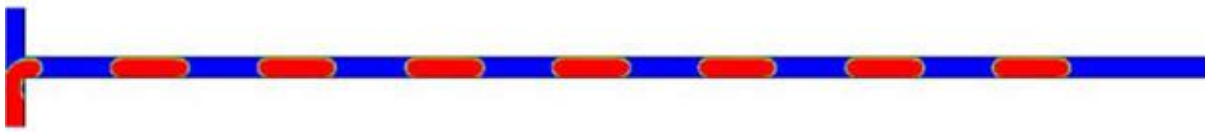

(a) u_L = 0.05 m/s and u_G = 0.05 m/s

(b) u_L = 0.1 m/s and u_G = 0.05m/s

(c) u_L = 0.15m/s and u_G = 0.05m/s

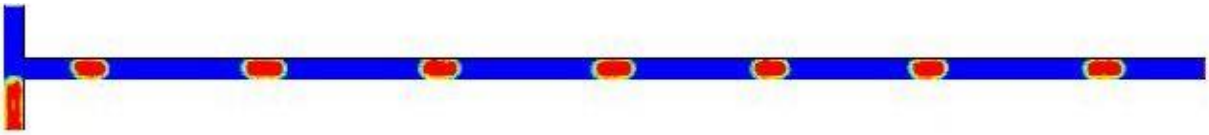

(d) u_L = 0.20 m/s and u_G = 0.05m/s

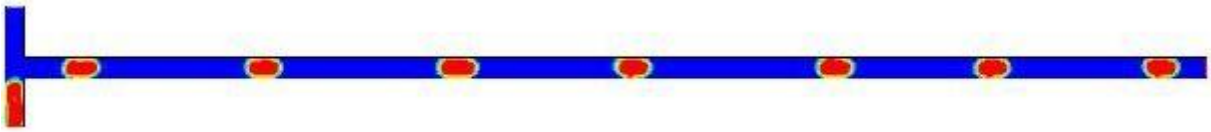

(e) u_L = 0.25 m/s and u_G = 0.05m/s

Fig. 3.9(a-e) Contours of the volume fraction of air in a T-junction microchannel at different liquid velocities (θ_o =0^o). The air bubble is shown in red and the water slug is shown in blue.

The results obtained from numerical simulations are compared with the correlations of Kawahara et al. (2011) and the scaling law proposed by Garstecki et al. (2006). It is found that the trends obtained from the CFD study are in close agreement with the literature correlations, as shown in Fig. 3.8. Studies of Garstecki et al. (2006) and Kawahara et al. (2011) were based on T-junction microchannels having inlets perpendicular to each other, whereas in the present studies, the inlets of the T-junction mixer were facing each other. This could be the main reason for the double difference in the present numerical results and the results of Garstecki et al., 2006 and Kawahara, 2011. Similar differences in the slug and bubble lengths for different orientation of the T-junction microchannel could be observed in the studies of Qian and Lawal (2006). Figure 3.9(a-e) illustrates the above-mentioned relationship pictorially. Laborie et al. (1999) have reported similar relationships of the slug and bubble lengths with the liquid flow velocity in their experimental work. Similar trends could also be observed in cases where gas velocities are varied keeping a fixed liquid velocity at the inlet. In such a case, the bubble length would increase and the liquid slug length would decrease with the gas velocity.

3.3.5 *Centerline pressure variation along the horizontal mixing zone*

This section presents the variation of centerline pressure along the length of the mixing zone of the microchannel. Unlike single-phase flows, in two-phase flows, the

pressure drop comprises two terms, namely, viscous term arising from friction at the channel walls and Laplace term associated with the surface tension at the gas-liquid interface.

The difference in pressure between the adjacent liquid and gas slugs is called as Laplace pressure. Figure 3.10 shows the variation of pressure at the centerline of the T-junction microchannel. In this figure, the upper horizontal lines represent the gas slug regions whereas the lower lines represent the liquid slug regions. Once each bubble is formed in the horizontal mixing zone after the elongation and squeezing process, it occupies the channel cross-section and flows downstream. The curvature of the nose and tail of the bubble are stronger (higher) and weaker (smaller), respectively and hence, the nose has a smaller radius of curvature and the tail has a bigger radius of curvature (Fig. 3.2). This leads to a lower pressure drop at the tail unlike higher pressure drop at the nose (Eqs. 13-19 in Abiev, 2017).

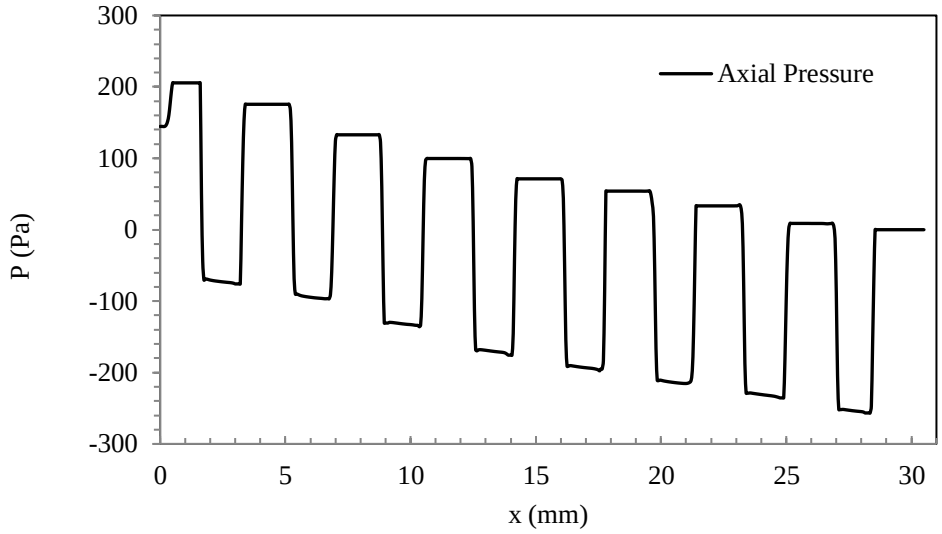

Fig. 3.10. Variation of axial pressure ($u_G = u_L = 0.05$ m/s and $\theta_o = 0^o$).

3.3.6 *Variation in pressure drop, slug length, and bubble length with the contact angle*

Wall Contact angle (θ_w) plays a key role in two-phase flow as long as both the fluids are in contact with the wall of the microchannel. Once the two-phase interface gets detached from the wall, the contact angle will have no influence on the fluid flow. In this study, the influence of contact angle on the pressure drop inside the T-junction microchannel was studied by varying the contact angle in the range 0^o–170^o (hydrophilic and hydrophobic) keeping all other conditions fixed. Inlet velocities of both the phases were assumed to be equal and constant ($u_G = u_L = 0.05$ m/s) and only the wall contact angle was varied.

Jovanovic et al. (2011) studied the hydrodynamics and pressure drop of liquid-liquid slug flow inside microcapillaries of circular cross-section ($248 < d < 498$ μm) using two

system of fluids, viz. water-toluene, and ethylene glycol/water-toluene. They proposed two different models namely, stagnant film model (Eq. 3.4) and moving film model (Eq. 3.5), for modeling the pressure drop in the two-phase flow. The liquid film of the carrier phase between the channel and the dispersed phase is assumed to be stagnant in the stagnant film model, whereas in the moving film model the thin liquid film between the wall and the dispersed phase is under motion. A close match was obtained between the two models with an average relative deviation of less than 5% which showed a negligible influence of film velocity on the pressure drop. In addition, with an increase in inertia, they observed that the curvature parameter in Bretherton's interface pressure drop equation (Eq. 3.3), which assumes negligible inertia, starts decreasing due to deformations in the menisci of the droplet. This signifies the importance of the curvature parameter in the modeling of pressure drop models.

Bretherton's interface pressure drop model

$$\Delta P_{interface} = C(3Ca)^{2/3}\frac{\sigma}{D} \tag{3.3}$$

where, C is the curvature parameter For semi-spherical ends of droplets, it is equal to 7.16 (Bretherton, 1961).

Stagnant film (SF) model (Jovanovic et al. 2011)

$$\Delta P_{SF} = \frac{8\mu_d u_b \alpha L}{(R-\delta)^2} + \frac{8\mu_c u_{TP}(1-\alpha)L}{(R)^2} + \frac{L}{L_{UC}}7.16(3Ca)^{2/3}\frac{\sigma}{d} \tag{3.4}$$

where R is radius of the capillary (m), L is length of the capillary, L_{UC} is the length of the unit cell (m), δ is the carrier phase film thickness (m), d is the diameter of capillary (m), σ is the interfacial tension (N/m), Ca is the capillary number.

Moving film model (Jovanovic et al. 2011)

$$\Delta P_{MF} = \frac{4u_d \alpha L}{(R^2-(R-\delta)^2)/\mu_c + (0.5(R-\delta)^2)/\mu_d} + \frac{8\mu_c u_{TP}(1-\alpha)L}{(R)^2} + \frac{L}{L_{UC}}7.16(3Ca)^{2/3}\frac{\sigma}{d} \tag{3.5}$$

Abiev (2011) reported in his gas-liquid studies that the total pressure drop inside a microchannel should be attributed to the following major factors: (i) the pressure drop due to

the rearrangement of the velocity profiles inside the liquid slug (ΔP_{trans}, Eq. 3.6) and (ii) the pressure drop during the motion of bubbles arising due to the formation of gas-liquid interface and its renewal ($\Delta P_{\Delta F}$, Eq. 3.7). They proposed a correlation signifying the importance of the number of unit cells in the formulation of the total pressure drop model by considering the above-mentioned factors, given by Eq. (3.8).

$$\Delta P_{trans} = -aN_{UC}L_S\left\{1 + \frac{1}{2bL_S}[1 - \exp(-bL_S)]\right\} \tag{3.6}$$

where, $a=8\mu U_S/R^2$, and $b=\mu\lambda_m^2/\rho U_S R^2$. Here, λ_m indicates the roots of second order Bessel function (Slezkin 1955).

$$\Delta P_{\Delta F} = \frac{2R_b}{R^2}\frac{w}{U_s}\frac{L_C}{L_{UC}}\sigma \tag{3.7}$$

where, R_b is the bubble radius (m), R is channel radius (m), *w* is relative velocity (m/s) of the bubble with respect to liquid slug ($w=U_b-U_S$), and L_C and L_{UC} are the lengths of the capillary and unit cell (m), respectively.

The total pressure drop inside a microchannel is obtained by the following equation:

$$\Delta P_{total} = \Delta P_{trans} + \Delta P_{\Delta F} \tag{3.8}$$

It should be noted that, in the above equation, the effect of contact angle on the overall pressure drop is not considered. In sliding slug flows, contact angle hysteresis plays a key role and affects the bubble shape as well as pressure drop. Hence, in subsequent studies, Abiev (2015) studied the effect of contact angle on the pressure drop inside a capillary and proposed another correlation for overall pressure by including a new term accounting for the contact angle hysteresis, as given in Eq. (12)

$$\Delta P_{CA} = \frac{4\sigma}{d}(\cos\theta_r - \cos\theta_a)N_{UC} \tag{3.9}$$

where θ_r and θ_a are receding and advancing contact angles, respectively given by:

$$\cos\theta_r = \cos\theta_o + 2(1 + \cos\theta_o)Ca^{0.5} \tag{3.10}$$

$$\cos\theta_a = \cos\theta_o - 2(1 + \cos\theta_o)Ca^{0.5} \tag{3.11}$$

where, θ_o is the static wall contact angle (refer Abiev (2015) for more details).

Hence, the overall pressure drop inside the microchannel including the effects of the contact angle is given by,

$$\Delta P_{overall} = \Delta P_{total} + \Delta P_{CA} = \Delta P_{trans} + \Delta P_{\Delta F} + \Delta P_{CA} \tag{3.12}$$

The results of the overall pressure drop obtained from the present numerical study are compared with the standard correlations of Jovanovic et al. and Abiev (2015), as shown in Fig. 3.11. The figure shows that the pressure drop decreases with the contact angle in hydrophilic cases, whereas in hydrophobic cases it increases significantly. The difference in the results between the CFD study and correlation of Jovanovic can be attributed to the effect of contact angle hysteresis which was not considered in the correlation proposed by Jovanovic et al. However, the CFD results are in close agreement with Abiev, who considered the effect of contact angle in the formulation of the pressure drop model**.** In hydrophilic cases, smaller area of contact between the wall and liquid slugs exists unlike in hydrophobic cases. This is due to the rise in total liquid slug length and a fall in the total bubble length inside the microchannel with contact angle. Also, the viscosity of the liquid phase is higher than that of the gas phase; hence lower frictional pressure drop could be expected in the hydrophilic microchannels over hydrophobic microchannels.

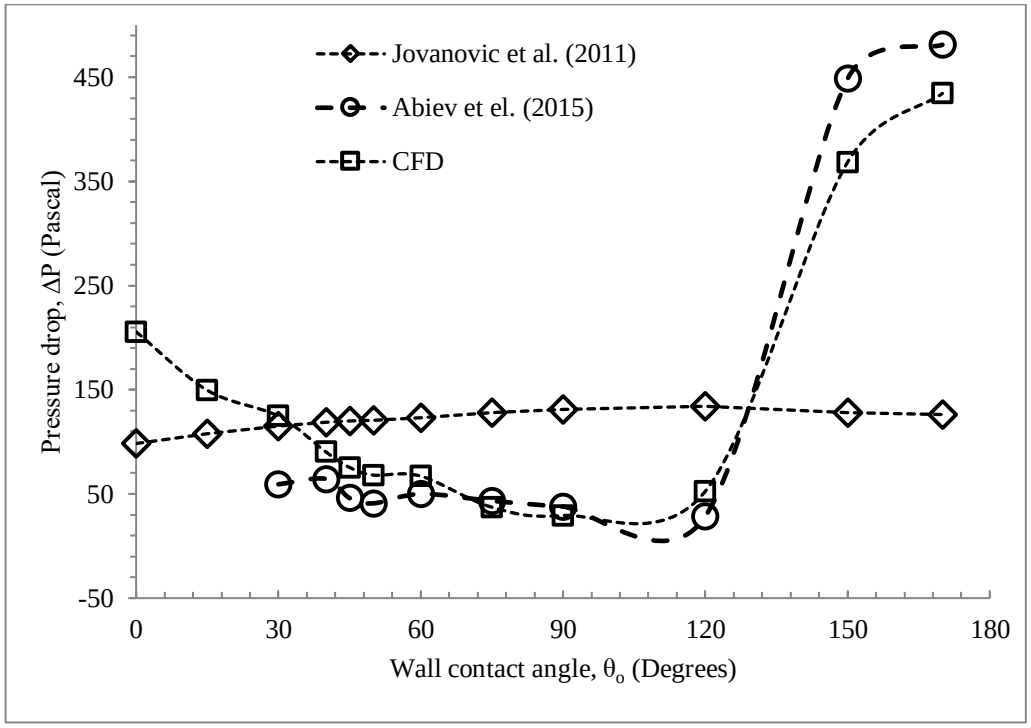

Fig. 3.11 Influence of contact angle on pressure drop ($u_G = u_L = 0.05$ m/s).

Figure 3.12 depicts the variation of the bubble and liquid slug lengths with the wall contact angle. It is observed that the liquid slug length as well as the bubble length decrease with the increase in contact angle for hydrophilic cases; however, on further increase in contact angle, the slug length starts to increase with the contact angle for hydrophobic cases. This can be attributed to the fact that the shape of the front and rear menisci of the gas bubble, in hydrophilic cases, are of convex and concave nature respectively, whereas the

reverse is noticed in hydrophobic cases where the shapes of the front and rear menisci are concave and convex respectively, as shown in Fig. 3.13(b). In hydrophobic cases, the continuous phase fluid lying between two consecutive bubbles pushes the front and rear interfaces towards the center of the bubble, which in turn provides more area of contact of bubble with the wall. However, the vice-versa is true for hydrophilic cases, where limited area of contact of the bubble with the channel wall is available.

The two-phase interface in the hydrophobic channels loses its symmetry with respect to the channel centerline due to interfacial instabilities. In the present numerical studies, asymmetry in the bubble shape along the channel centerline is observed. Similar asymmetric behavior in the bubble shapes was also observed in the experimental studies of Cubad et al. (2006). The liquid film flow is not observed for any of the test cases in the present study (Santos and Kawaji 2012). Figure 3.13(a) shows the variation of dispersed phase volume with contact angle inside the microchannel. The volume fraction of the dispersed phase decreases in hydrophilic channels because of the reduction in contact length of the bubble with channel wall arising from the changing shape of the interface. On the other hand, in hydrophobic cases, the volume fraction of the dispersed phase increases with contact angle as the length of contact of the bubble with the wall increases. Figure 3.13(c) is shown for the comparison of the contact length of the bubble with the channel wall between a hydrophilic and hydrophobic case having nearly equal volume fraction. It is clear from the figure that for the same volume fraction of the dispersed phase, the length of contact is higher for the hydrophobic case over the hydrophilic case.

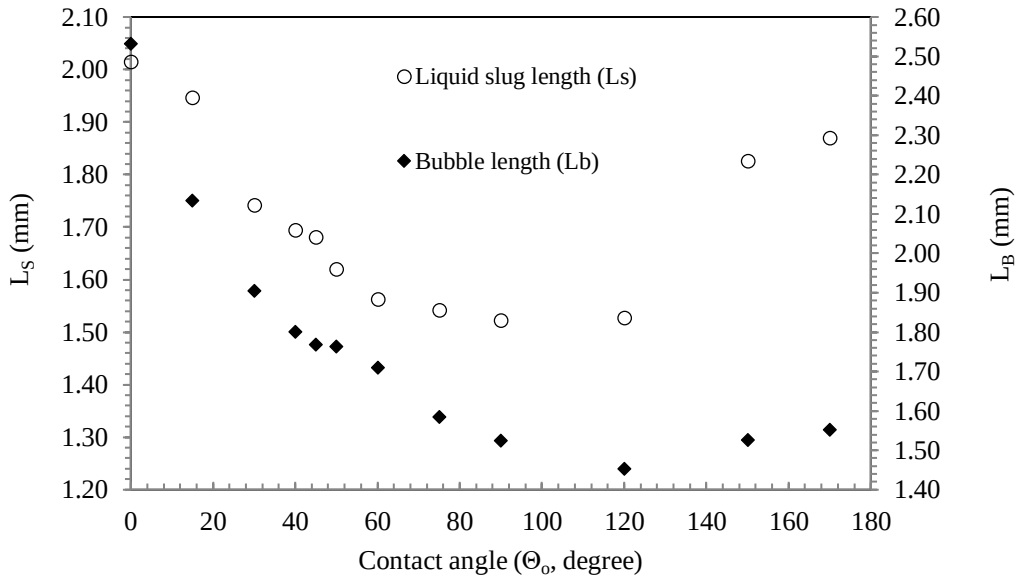

Fig. 3.12 Influence of contact angle on gas and liquid slug lengths (u_G = u_L = 0.05 m/s).

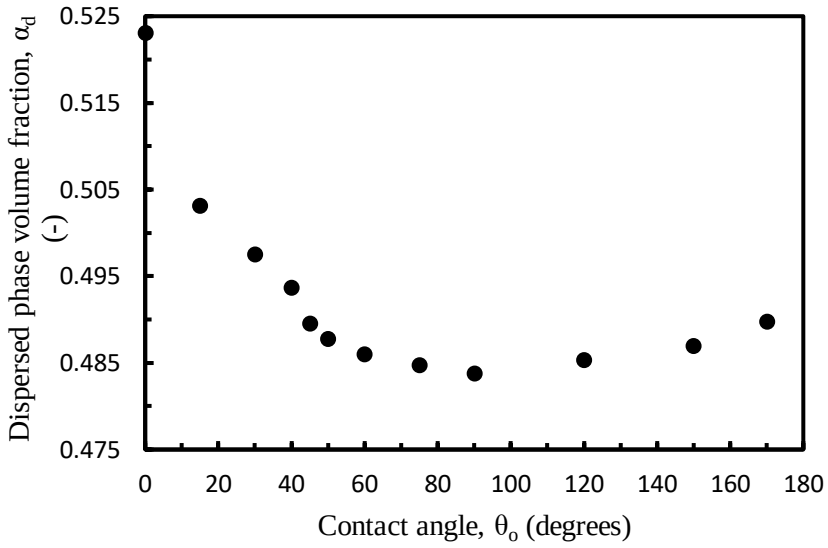

(a)

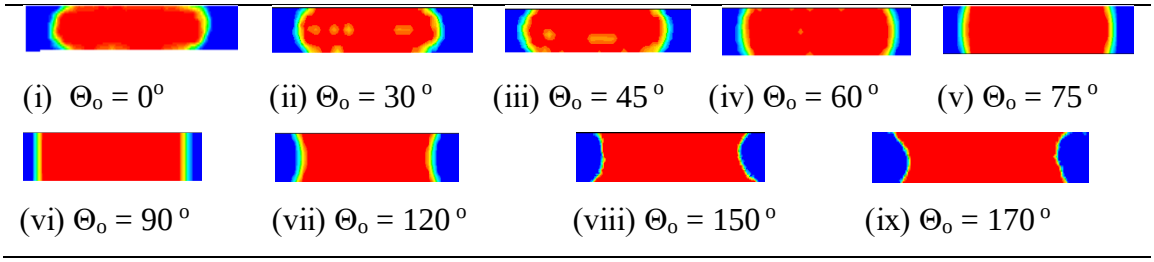

(b)

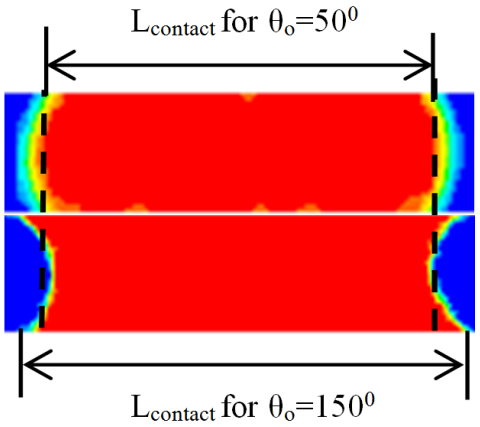

(c)

Fig. 3.13 (a) Variation of dispersed phase volume fraction(α_d) with static contact angle (θ_o); (b) shapes of gas-liquid interface at different contact angles; and (c) Length of contact in hydrophilic and hydrophobic cases having similar volume fraction ($u_G = u_L = 0.05$ m/s). The air bubble is shown in red and the water slug is shown in blue.

3.4 Summary

In this chapter, the hydrodynamics of a two-dimensional, incompressible, and laminar air-water two-phase Taylor flow inside a T-junction microchannel having a characteristic dimension of 0.5 mm was discussed. The effect of carrier phase liquid velocity on the bubble and liquid slug length was reported. The increase in liquid velocity has led to an increase in the liquid slug lengths and a decrease in the bubble lengths. The trends of the bubble and liquid slug lengths, for different inlet liquid velocity, were found to be in close agreement with the trends obtained from standard models. The effect of wall wettability on the bubble and liquid slug lengths in hydrophilic and hydrophobic channels was also discussed. The bubble and liquid slug lengths decreased with wall contact angle in hydrophilic channels, whereas these lengths increased with the contact angle in hydrophobic channels. In addition, the bubble shapes were observed to be asymmetric in hydrophobic cases which can be attributed to the effect of contact angle hysteresis and higher drag forces in the non-wetting walls. It was also observed that the length of contact (or the area of contact) between the bubble and channel wall, for approximately same volume fraction of the gas phase, was higher in the hydrophobic case than the hydrophilic case. The effect of contact angle on the gas volume fraction was also discussed where the values of volume fraction decreased in wetting channels and increased in non-wetting channels. The numerical results of the pressure drop inside the microchannel for different contact angles were compared with the phenomenological models available in literature and a close match was observed between them. The analysis of pressure drop results revealed that the fluid flow in hydrophobic channels could lead to higher pressure drops. It happens due to an overall increase in the liquid slug length and a decrease in the overall bubble length with the contact angle which raises the frictional pressure drop inside the channel. It is strongly advised to consider the effect of contact angle hysteresis in the evaluation of pressure drop across the microchannel when the thin liquid film between the channel wall and the gas-liquid interface is absent. In addition, it is recommended to use hydrophilic channels for two-phase slug flow problems when the pressure drop is a point of concern.

CHAPTER 4

NUMERICAL STUDY OF THE HYDRODYNAMICS AND HEAT TRANSFER CHARACTERISTICS OF LIQUID-LIQUID TAYLOR FLOW IN MICROCHANNEL

4.1 Introduction

Numerous researchers have contributed their efforts in extensively studying the flow physics, heat, and mass transfer behavior of Taylor flow and convincingly explained its potentiality over single-phase flow (Talimi et al. 2013, Muzychka et al. 2010, Fukagata et al. 2007, Gupta et al. 2010a, Sadhana et al. 2019, Zhang et al. 2016). Extensive reviews on the Taylor flow can also be found in the studies of Abiev (2012), Bandara et al. (2015a), Talimi et al. (2012), Gupta et al. (2010b). However, these works were mostly limited to the gas-liquid (GL) Taylor flow. Despite having a significant impact on the heat transfer performance, GL flow has certain drawbacks. Since gas has lower thermal conductivity than liquid, the role of the gas phase in the two phase heat transfer is often neglected in GL slug flow. On the other hand, replacing the gas bubble with a liquid droplet offers higher rates of heat transfer due to its comparable heat capacity with that of the carrier phase liquid. Liquid-liquid (LL) slug flow is capable of dissipating high heat transfer rates and provide enhanced mass transfer rates. From the available literature it can be easily noticed that very little work emphasizing the characteristics of liquid-liquid slug flow has been reported (Dai et al. 2015, Asthana et al. 2011, Vivekanand et al. 2018, Gupta et al. 2013, Bandara et al. 2015b). In the present chapter the numerical studies of a two-phase slug flow and heat transfer in a LL slug flow regime inside a microcapillary have been discussed. The numerical code is validated against the benchmark results available in literature. In addition, pressure drop and the effect of isothermal and constant wall heat flux boundary condition on the heat transfer characteristics of LL Taylor flow have also been discussed.

4.2 Methodology

The objective of this study is to explore the flow and heat transfer characteristics of two-phase liquid-liquid slug flow in the circular microchannel. This is accomplished by passing two immiscible fluids (mineral oil and water) inside a heated microchannel. Oil droplets are patched at the upstream of a vertical circular microchannel. The thermal and flow fields within the channel and the local variations of the heat transfer coefficient at the heated wall are investigated for water and mineral oil as the carrier and dispersed phase fluids respectively. CFD solver ANSYS Fluent (version 15) is used to carry out the simulations. Due to the symmetry of the problem, a two-dimensional axisymmetric formulation is considered to reduce the computational cost. VOF multiphase algorithm is adapted to capture the interface. To overcome VOF issues on poor interface reconstruction, the geometric reconstruction algorithm is implemented to calculate the surface tension.

4.3 Numerical framework

4.3.1 Computational domain and boundary conditions

The numerical model consists of a circular microchannel having length 3000μm with an internal diameter of 100μm. In general, the walls of microchannel are assumed to be made of silicon (Fig.4.1). The properties of water (primary fluid) and light mineral oil (secondary fluid) are shown in Table 4.1 below. The interfacial tension of oil with water is 0.04925 N/m, and its viscosity is 0.023 kg/ms.

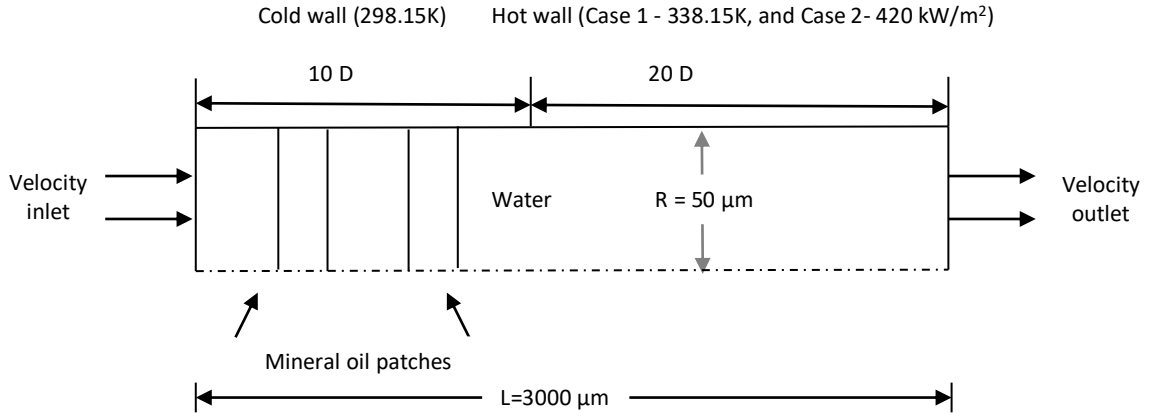

Fig. 4.1 Schematic diagram of the fluid flow model.

Table 4.1 Properties of the working fluids.

Material	Density [kg/m^3]	Specific heat [J/kg K]	Thermal conductivity [W/m K]	Viscosity [kg/m s]
Water	998	4182	0.6	0.001003
Light mineral oil	838	1670	0.17	0.023
Silicon	2330	710	149	----------

For the development of slug flow, a length of 1000µm which is bigger than the hydrodynamic entrance length is allocated with a wall temperature of 23^{o}C (equal to the incoming liquid water temperature) before entering the heating section. The rest of the channel wall (20D, i.e. 2000µm) is supplied with (a) constant temperature (338.3K), and (b) uniform heat flux of 420kW/m^2 respectively. A uniform velocity of 0.22 m/s with 0 *Pa* pressure outlet is given as the inlet and outlet boundary conditions respectively. A comparison has been made between the present two-phase flow and the single-phase fluid flow, and important conclusions have been reported in the present work.

4.3.2 Flow solver

The simulations were carried out in ANSYS Fluent 15.0 using finite volumes in 2D axisymmetric space. Interface reconstruction was done by using the geometric reconstruction scheme which represents the interface by a piecewise linear approach. Fractional step method along with variable time step strategy and global Courant number of 0.25 was used for momentum, pressure and energy equations. First order non-iterative fractional step method was used for the transient formulation of continuity and momentum equation in the simulation. Time steps of the order of 10^{-7} were used as the elements for simulations were around 2µm. For spatial discretisation, Green-Gauss node based gradient was adopted along with QUICK scheme for momentum and energy equations, and body force weighted scheme for pressure terms.

4.4 Results and discussions

4.4.1 Grid convergence and Validation

The entire domain was discretized with a homogeneous structured grid consisting of quadrilateral elements with a size of 2 µm (D/50) as shown in figure 4.2. The use of a locally

refined grid near the channel wall was considered for capturing thin liquid film during the slug flow. The main reason was to maintain a constant resolution of the liquid–oil interface throughout the computational domain.

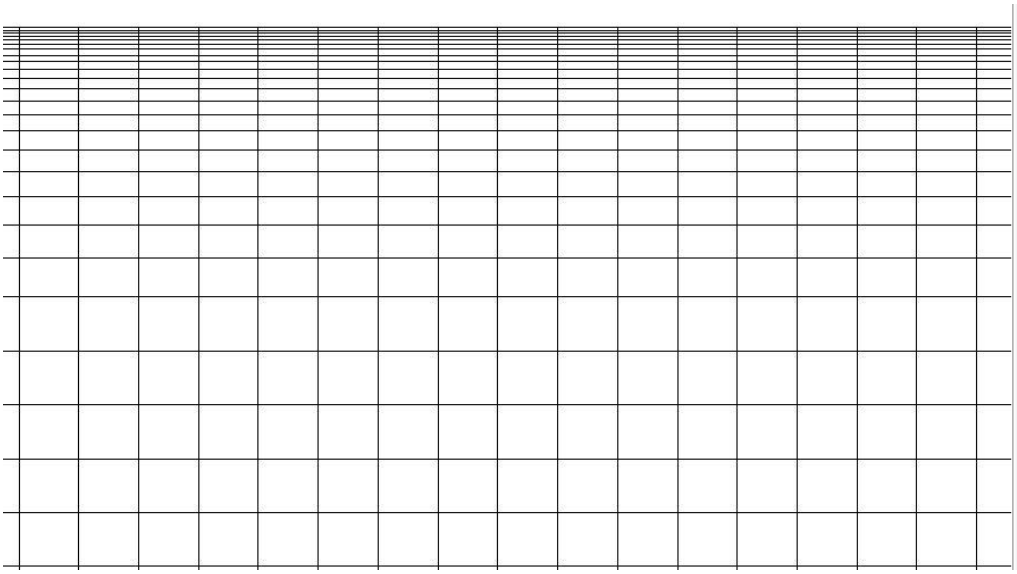

Fig. 4.2. Computational mesh.

Figures 4.3(a-b) shows the variation of volume fraction of oil and temperature variation along the radius and axis of the channel, respectively for 1, 2, and 4µm mesh sizes.

The volume fraction across the channel in presence of oil plugs is an important parameter as it indicates the existence of thin liquid film.

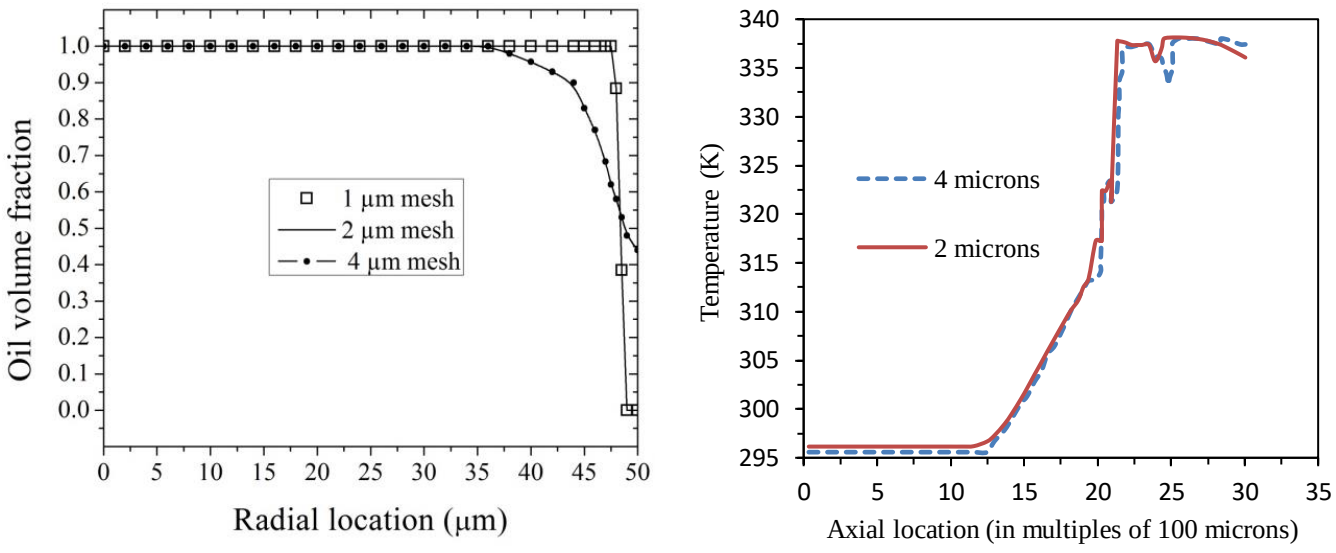

(a) (b)

Fig. 4.3 (a) Oil volume fraction distribution along the radial axis in the mid of an oil slug, and (b) Temperature variation along the axis for different mesh sizes.

As shown in Figure 4.3 (a), there is considerable variation of volume fraction close to the channel wall. The volume fraction of the oil droplet falls down sharply from α = 1 at the vicinity of the wall to α = 0 at the wall which indicates the presence of the thin film of the carrier phase fluid between the channel wall and the two-phase interface. The oil volume fraction was found be similar for finer meshes having 1μm and 2 μm mesh sizes. In addition, the axial variation of the temperature was also found to be similar for 2 and 4μm size.

The axial velocity along the radius, as obtained from literature (Bandara et al. 2015b) and present CFD studies, respectively has also been depicted in Fig. 4.4(a-b) for validation of the present numerical code. The data was selected when oil droplets were at a similar distance away from the inlet under the same initial and boundary conditions as that of the literature.

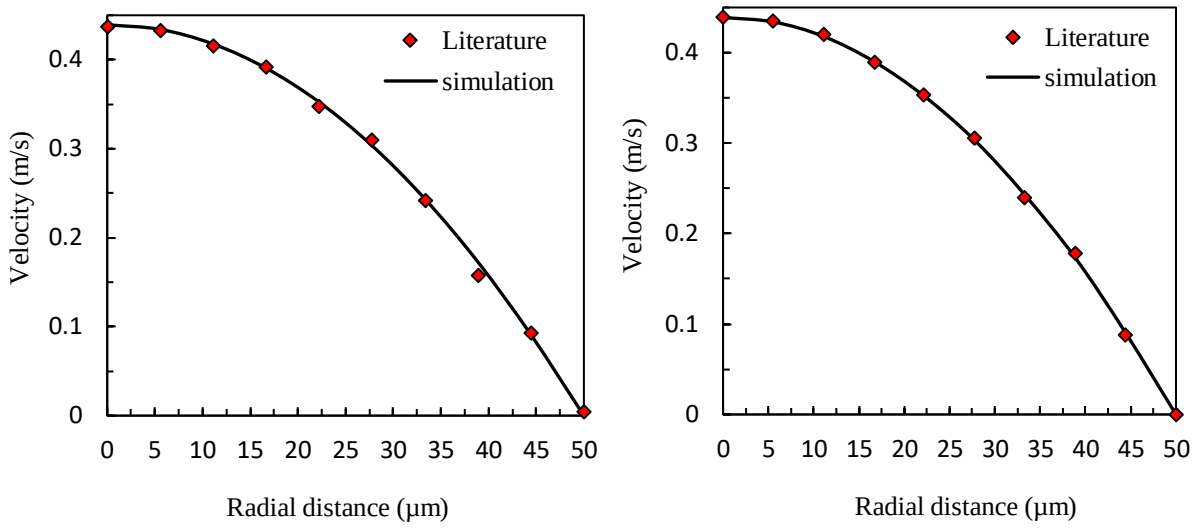

(a) (b)

Fig. 4.4 Velocity distribution along: (a) a plane at 9D away from the inlet (before the oil slugs), and (b) a plane at 15D away from the inlet (between the oil slugs).

4.4.2 Pressure drop

Pressure drop is one of the critical parameters in the design of fluid flow systems. Hence, accurate prediction of pressure drop is of prime importance. For single phase flow, the pressure drop is estimated by using Darcy–Weisbach equation which relates the pressure loss or head loss due to friction along the length of a channel. Unlike single phase flow, in two phase flow, the pressure drop comprises of two terms, namely, viscous term arising from friction at channel walls and Laplace term associated with surface tension at the interface.

The difference in pressure between the adjacent liquid and gas slugs is called as Laplace pressure. Pressure drop in two phase flow is estimated by using wide range of accepted empirical equations (Lockhart and Martinelli 1949).

Figure 4.5 shows the variation of axial and wall pressure at the centerline of the circular microchannel. In the axial pressure profile, the upper lines represent the droplet regions, whereas, the lower lines represent the liquid water slug regions. The slope of the pressure line in the continuous liquid slug zone reveals the magnitude of pressure drop due to friction. In the droplet zone, axial pressure increases so as to satisfy the required force to counterbalance the surface tension force at the interface. Smaller curvature can be expected at the bubble tail as compared to its nose due to lower pressure drop at the rear interface in contrast to the front interface.

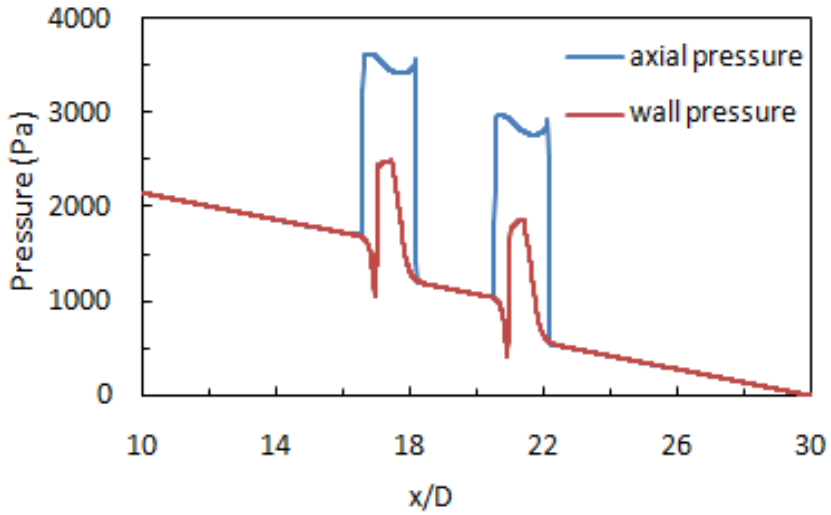

Fig. 4.5 Variation of axial and wall pressure along the microchannel.

4.4.3 Recirculation zone

One of the important characteristics of two phase slug flows over single phase flows is improved mixing and heat transfer rates due to recirculation inside the two phases. Figure 4.6 shows the streamlines in the slug and liquid droplet. The dispersed phase droplet has three recirculation zones which enhances heat transfer in the slug flows. Lac and Sherwood (2009) also observed three recirculation zones, similar to those observed in our studies. In earlier studies on gas-liquid Taylor flows similar recirculation zones were observed which have insignificant effect on heat transfer rates, whereas, in the present liquid-liquid slug flow case, the recirculation plays a vital role because of higher thermal conductivity of liquid droplet in contrast to gas bubble in a gas-liquid Taylor flow.

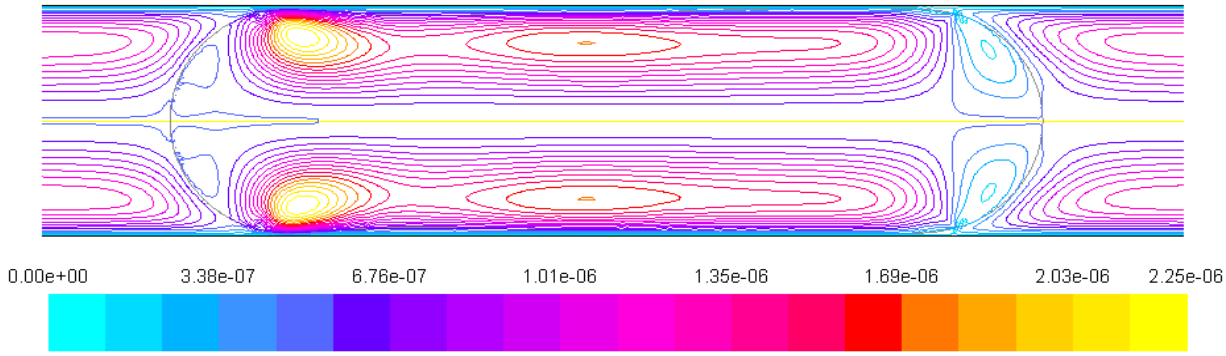

Fig. 4.6 Contours of stream function (kg/s) in the droplet and slug regions.

4.4.4 Heat transfer

4.4.4.1 Effect of isothermal wall boundary condition

Heat transfer performance in the flow channel with an isothermal wall is measured using Nusselt number which is calculated from Eq. 4.1 (Dai et al. 2015). The mean flow temperature T_{mx} at a plane perpendicular to the axis is computed as a mass weighted average value and the wall temperature, T_{wx} is uniform along the channel for isothermal wall condition. Total surface heat flux on the heating wall gives q_x value for each point along the channel. The calculated Nusselt number along the channel for isothermal walls is shown in Figure 4.7. According to Figure 4.7, the Nusselt number of the water only flow asymptotes towards 3.67 which is the theoretical value for single-phase flow in circular channels under constant wall temperature. The figure shows a significant increase in Nusselt numbers with slug flow having an average Nu of ~187% over single-phase flow. The presence of recirculation inside the liquid slugs and droplets plays the key role in the enhancement of heat transfer rate. Thus, having a train of droplets along the channel will lead to higher heat removal rates. There is a large spatial variation of the local Nu in the slug region.

$$Nu_x = \frac{q_x D_h}{k\left(T_w - T_{m_x}\right)} = \frac{h_x D_h}{k} \tag{4.1}$$

Similar work has been reported by Bandara et al. (2015b) using gradient adaption meshing technique. In their study, they have reported an augmentation of approximately 200% over single-phase flow. Whereas, the present study has been carried out by employing near-wall mesh treatment given by Gupta et al. (2009). Gupta el al. (2009) have extensively validated their meshing method and carried out a series of works based on the proposed meshing method. According to their method, there must be at least five cells in the film region to

successfully capture the flow physics involved in the two-phase study. In the current study, capturing of thin liquid film surrounding the droplets was achieved by placing more than ten cells in the film region (Fig. 4.2). It is found that there is considerable difference in the local Nusselt number obtained from the present numerical study and that of the work of Bandara et al (2015b). These deviations could be attributed to the adopted meshing methodology.

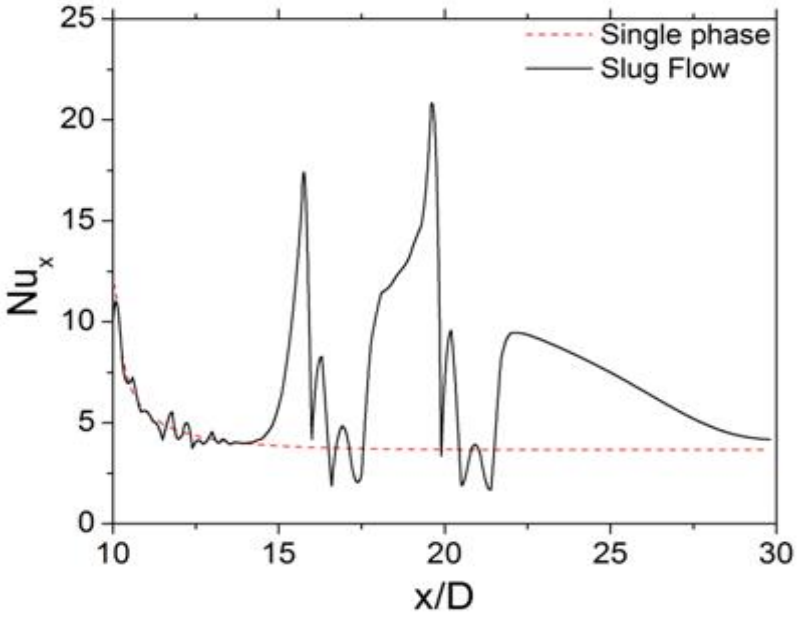

Fig. 4.7 Variation of local Nusselt number for constant temperature wall boundary condition.

4.4.4.2 Effect of constant wall heat flux boundary condition

Heat transfer under constant wall heat flux has also been numerically studied for both single-phase and slug flow. A constant heat flux of 420kW/m^2, which is approximately equal to the average value of heat flux obtained from the isothermal study, was prescribed over the wall in this case. For constant heat flux condition, the Nusselt number is measured using Eq. 4.2. Total surface heat flux on the heating wall is uniform along the channel for constant heat flux condition. T_{wx} on the heating wall gives the local wall temperature value for each point along the channel. T_{mx} is estimated using the same method as was used for the isothermal case. As shown in figure 4.8, the Nusselt number of the water only flow asymptotes towards 4.36 which shows a good agreement with the theoretical value of Nusselt number for constant wall heat flux boundary condition. A significant increase of average Nu (up to 210%) has been achieved using constant heat flux boundary condition at the channel wall. It is recommended to consider constant flux at wall rather than isothermal wall for practical purpose.

$$Nu_x = \frac{qD_h}{k\left(T_{w_x} - T_{m_x}\right)} = \frac{h_x D_h}{k} \tag{4.2}$$

Due to strong dependence of heat transfer rates on slug and droplet lengths, the work could be extended to investigate the effects of flow parameters along with void fraction, capillary number, and film thickness on the hydrodynamics and the heat transfer characteristics of the slug flow.

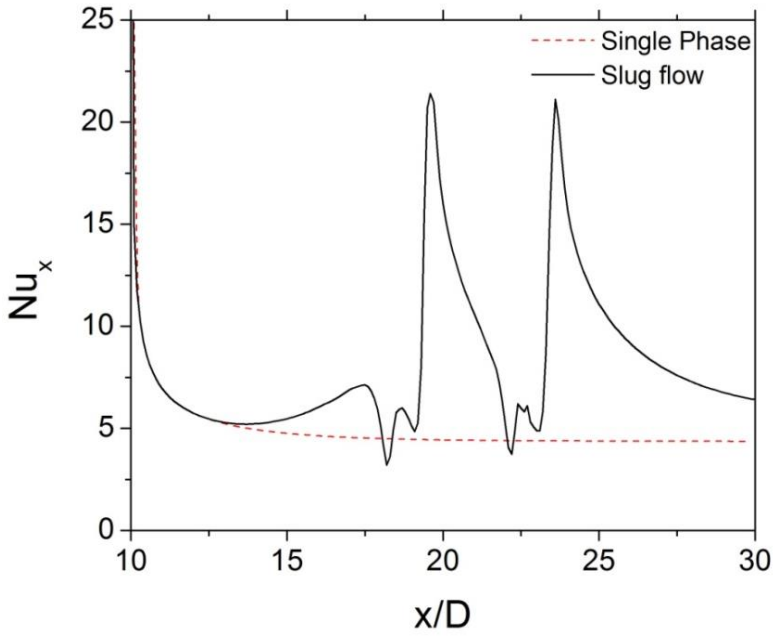

Fig. 4.8 Variation of local Nusselt number for constant heat flux boundary condition.

4.5 Summary

The hydrodynamics and heat transfer characteristics of liquid–liquid Taylor flow have been studied using CFD techniques in a vertical circular microchannel of 100 microns diameter using light mineral oil and water as the dispersed and carrier phases, respectively. The slug velocities obtained from CFD simulations were found to be in close agreement with the literature. Due to higher pressure drop at the frontal interface, the nose of the droplets has higher curvature as compared to their tail. Heat transfer characteristics of the LL Taylor flow in the microchannel have also been studied. Two different thermal wall boundary conditions viz. isothermal and constant heat flux respectively were prescribed over the channel wall. It was observed that, for the same operating conditions as well as identical properties of fluids, constant heat flux provides higher Nusselt number in contrast to isothermal boundary condition provided the average temperature of the surface in case of constant heat flux should be equal to the wall temperature of the isothermal BC, or else, the average heat flux in

isothermal BC should be equal to the heat flux in the constant heat flux BC. An increase of approximately 187% in average Nusselt number during the slug flow was observed over single phase (3.67) flow for isothermal wall conditions. However, for constant wall heat flux condition, a significant increase of average Nusselt number during the slug flow (up to 210%) over single phase flow (4.36) under the same operating conditions was observed. One of the possible reasons for this enhancement in heat transfer during the slug flow is because of the three recirculation zones in the slug region between two consecutive droplets which play a vital role in the heat transfer process since the conductivity of liquid droplet is higher in contrast to gas bubble in a gas-liquid flow.

CHAPTER 5 EFFECT OF WALL TEMPERATURE MODULATION ON THE HEAT TRANSFER CHARACTERISTICS OF DROPLET-TRAIN FLOW INSIDE A RECTANGULAR MICROCHANNEL

5.1. Introduction

Although experimental studies on heat transfer in Taylor flow regime inside microchannel are limited in literature, abundant numerical studies have been carried out by various groups who addressed the influence of several parameters such as droplet size (Urbant et al. 2008, Che et al. (2011, 2012, 2013)), nanofluids (Fischer et al. 2010), Peclet number (Che et al. (2011, 2012, 2013)), Reynolds number (Bandara et al. 2015b) on the thermal performance of microchannels in Taylor flow regime under isothermal and constant heat flux boundary conditions. An approximate enhancement of 200% - 600% in the heat transfer rates with respect to single-phase flow was reported in these works. Mehdizadeh *et al*. (2011) employed volume of fluid (VOF) method to track the liquid film during a water-air slug flow inside a circular microchannel. The results of their numerical studies showed a considerable improvement in thermal performance (610%) in contrast to single-phase flow. Bandara*et al*. (2015a) performed an exhaustive review of the numerical and experimental works of the two-phase flow inside mini and microchannels undergoing no phase change process.

The thermal behaviour of fluid flow inside a channel depends on several parameters including the nature of wall boundary conditions to which the channel is subjected. The experimental studies of Mantle et al. (1994) reveal the effect of wall temperature modulation on the natural convection of a horizontal layer of fluid which was heated from below. An electrical circuit consisting of a timer, a variable resistor, and a variac was used to provide the modulated temperature to the bottom wall in their experiments. They reported an increase in the heat transfer rate by 12% using the modulated wall temperature condition in contrast to

that without having temperature modulation. It is observed that the fluid flow heat transfer studies in microchannels under modulated heating conditions are very limited in the literature. Nikkhah et al. (2015) discussed the effect of periodic heat flux heating condition on forced convective heat transfer of water/functionalized multi-walled carbon nanotube (FMWCNT) nanofluid in a two-dimensional microchannel. They reported that the periodic heating causes a periodic change for both dimensionless temperature along the centerline and local Nusselt number along the length of the microchannel. Cole (2010) performed numerical simulations for thermal sensing of steady laminar flow in a parallel-plate microchannel to which steady-periodic heating was introduced at the channel wall. They reported an increase in the amplitude of heater temperature followed by a decrease in its amplitude with an increase in fluid flow. This finding was acknowledged to the heat transfer progression which was dominated by axial conduction at upstream and convection at downstream. The studies of Nikkhah et al. (2015) and Cole (2010) reveal the importance of periodic heating on the thermal performance of the microchannels.

Till date, there is no literature available which discusses the influence of modulated temperature boundary conditions on heat transfer characteristics of slug flow inside microchannels. In the present chapter, the flow and thermal behaviour of LL Taylor flow inside a parallel plate microchannel under sinusoidal wall temperature boundary conditions have been discussed with a special emphasis on the effects of amplitude and frequency of the modulated wall temperature on the two-phase heat transfer rates.

5.2. Numerical framework

5.2.1. Computational domain, Initial and Boundary conditions for the single-phase study

Figure 5.1 shows the computational domain used for the single-phase study which represents a problem similar to Graetz problem. The computational domain consists of a two-dimensional rectangular microchannel having a length of 3000µm with a depth (h) of 100µm. In this study, a planar (x-y), incompressible, laminar flow of water at a uniform velocity of 0.22 m/s inside the microchannel has been considered. A uniform velocity inlet and pressure outlet boundary conditions were applied at both ends of the channel with no-slip condition at the channel walls. At the beginning of each simulation, the solution domain was initialized with a fluid temperature equal to that of the incoming fluid temperature (296.15K) and an initial fluid velocity of 0.22 m/s which is equal to the incoming velocity of water. The upper

and lower walls of the domain were divided into two regions, viz. (a) lower temperature walls (L_{cL} = L_{cU} = 10h) having a wall temperature equal to that of the incoming liquid (296.15K) for allowing the flow to become hydrodynamically developed, and (b) higher temperature walls (L_{hL} = L_{hU} = 20h) with wall temperature of 338.3K.

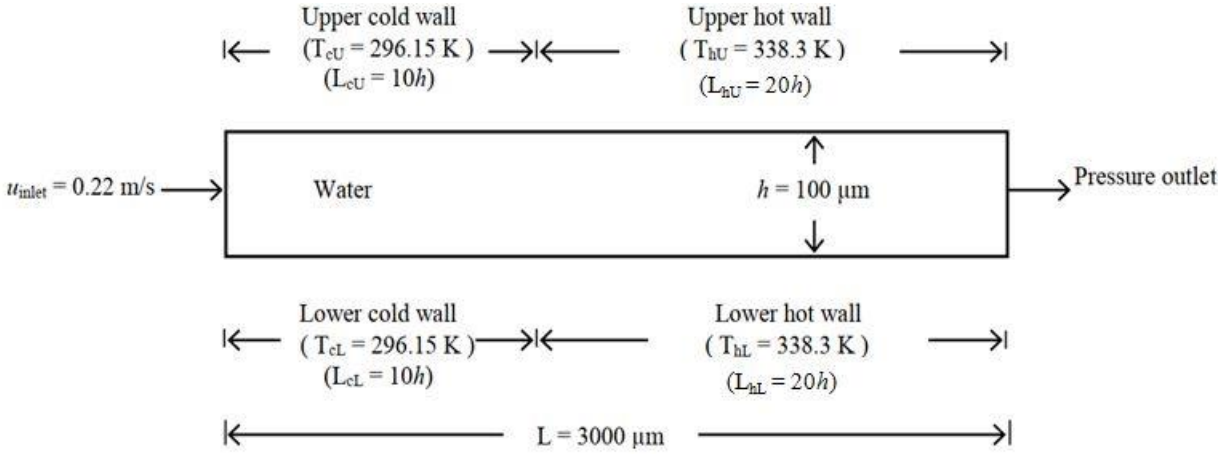

Fig. 5.1. Schematic of the computational domain for the studies on single-phase flow of water in the microchannel.

5.2.2. Computational domain, Initial and Boundary conditions for the two-phase study

In the two-phase studies, a two-dimensional, planar (x-y), laminar, incompressible liquid-liquid slug flow (or droplet-train flow) inside a rectangular microchannel has been considered. Water and oil are used as the primary and secondary phase fluids, respectively. Figure 5.2 shows the schematic of the computational domain used in the two-phase studies which is identical in shape and size as that of Fig. 5.1. A uniform velocity inlet condition and a pressure outlet boundary condition has been applied at both ends with no-slip condition at the channel walls. The continuous phase liquid enters at a uniform velocity which was varied in simulations in the range 0.049 < u_{TP} < 1.10 m/s having an inlet temperature of 296.15 K. At the beginning of each simulation, the solution domain has two secondary phase oil droplets having a size equal to 115µm with a liquid slug of length 280µm between the droplets. The entire flow channel is initialized with a uniform pressure of zero Pascal, an initial temperature equal to the incoming fluid temperature (i.e. 296.15 K), and an initial mixture velocity u_{TP} equal to the velocity of the incoming fluid. A constant temperature of 296.15K, same as that of the incoming fluid temperature, has been prescribed to the upper and lower cold walls of the microchannel up to the length until the fluid becomes hydrodynamically fully developed. However, the temperature conditions specified over the hot walls of the channel are different for different cases as shown in Table. 5.1. It should be

noted that the width of the microchannel in the third dimension is assumed to be very large as compared to the height of the microchannel; hence, the microchannel can be treated as micro parallel plates in the present study. The properties of the working fluids used in the present study are tabulated in Table 5.2. The viscosity of the oil is 0.023 kg/ms and the surface tension coefficient for the oil-water combination is 0.04925 N/m.

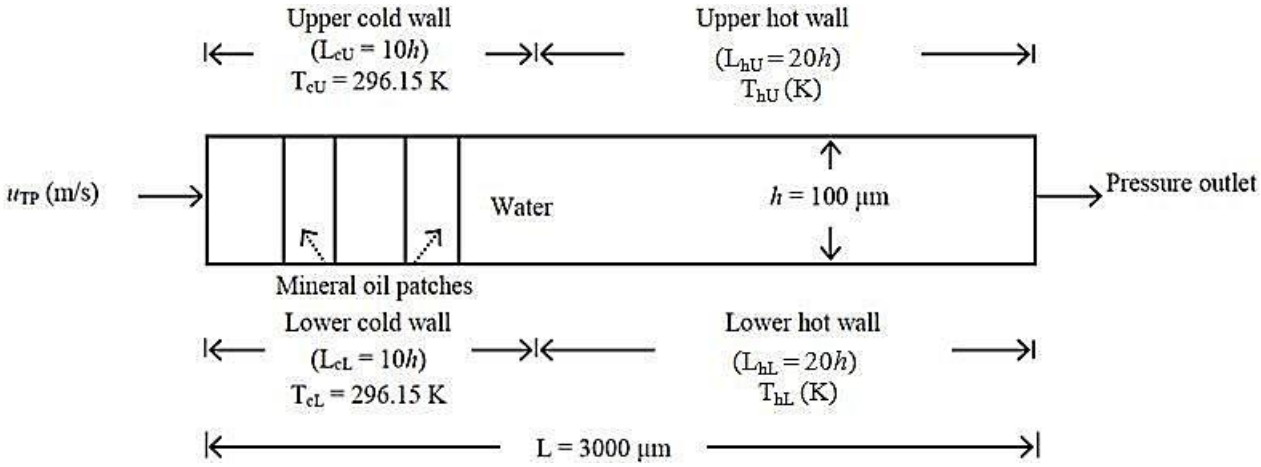

Fig. 5.2. Schematic diagram of the computational domain for the oil-water slug flow studies.

Table 5.1. Details of different temperature boundary conditions applied on the hot walls of the microchannel for the two-phase flow and heat transfer studies.

Case no.	*Boundary Condition*	*Temperature value / equation*
1	Walls without temperature modulation	T_{hU}= T_{hL}=338.3K
2	Both hot walls with in-phase modulated temperature	T_{hU}= T_{hL}=338.3(1+ε sin(ωt))
3	Upper hot wall without temperature modulation and lower hot wall with temperature modulation.	T_{hU}= 338.3K, T_{hL}=338.3(1+ε sin(ωt))
4	Both hot walls with anti-phase modulated temperature	T_{hU}= 338.3(1+ε sin(ωt)), T_{hL}=338.3(1-ε sin(ωt))

Table 5.2. Properties of working fluids.

Material	Density [kg/m^3]	Specific heat [J/kg K]	Thermal conductivity [W/m K]	Viscosity [kg/m s]
Water	998	4182	0.6	0.001003

Mineral oil	838	1670	0.17	0.023
Silicon	2330	710	149	----------

5.2.3. Numerical schemes

The commercial code ANSYS Fluent 15.0. has been employed to carry out the numerical studies. VOF technique was used to track the LL interface between the phases. Non-iterative fractional step method has been employed for the unsteady formulation of the flow equations. An explicit piecewise linear approach based geometric reconstruction scheme was used for interface reconstruction. A maximum Courant number of 0.25 was used for the volume fraction equation. Variable time-stepping strategy with minimum and maximum time-step size of 10^{-9} and 10^{-6}s along with a global Courant number of 0.25 for flow and energy equations has been used. Spatial discretization was done using Green-Gauss node based gradient method. The body force weighted scheme has been employed to solve the pressure equation. The convective terms of the momentum and energy equations have been solved using QUICK scheme.

5.3. Results and discussion

5.3.1. Meshing methodology

Figure 5.3(a) shows a part of the computational mesh used in the simulations which consist of 390000 square elements with an aspect ratio closer to one. Near-wall mesh treatment has been performed by following the guidelines of Gupta et al. (2009)[21] to capture the thin liquid film between the wall and droplet. Bretherton (1961)[40] proposed a correlation to estimate the thickness of the continuous phase film existing between the dispersed phase droplet and the channel wall as a function of the Capillary number based on the mixture velocity. The film thickness obtained from Bretherton's equation could be considered as the first approximation while meshing to capture the liquid film. Figure 5.3(b) shows the variation of the dimensionless temperature profile along the transverse direction in the liquid slug during slug flow without wall temperature modulation. Show in the figure are the temperature profiles for three different mesh sizes having 330000, 390000, and 500000 elements. It can be seen from the figure that for the mesh sizes of 390000 and 500000, the temperature profiles are almost similar. Hence, a mesh having 390000 elements has been used for all further simulations including the single-phase study.

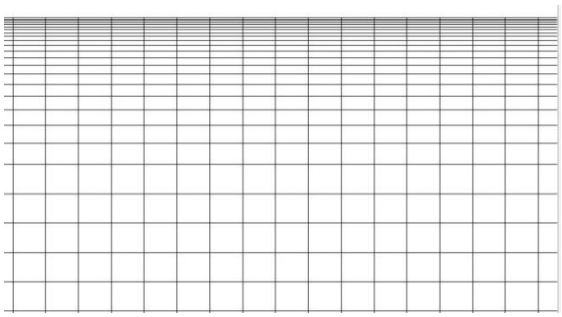

(a)

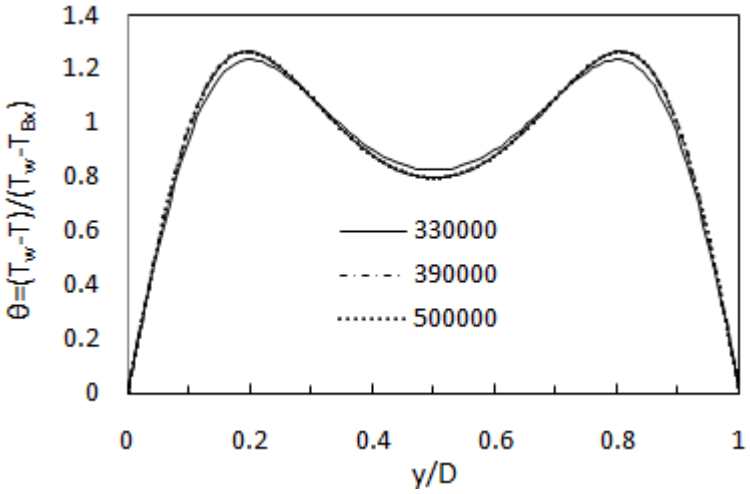

(b)

Fig. 5.3. (a) Computational mesh; (b) Temperature profiles in the liquid slug region for different grid sizes.

5.3.2. Single phase flow and heat transfer study of water inside the microchannel

Analytically, fully developed axial velocity profile of a single phase flow of a fluid between parallel plates is given by Eq. 5.1 which could be obtained by solving the plane Poiseuille flow equation. The present computational fluid dynamics (CFD) source code has been validated against the benchmark analytical equation for the centerline velocity profile of the single-phase flow of water flowing at a uniform velocity of 0.22 m/s inside the channel. Figure 5.4 compares the variation of the fully developed dimensionless velocity profile obtained from the present numerical study with the velocity profile obtained from Eq. 5.1. It can be seen that a reasonable agreement is observed between the two velocity profiles. Figure 5.5(a) shows the temporal variation of wall and bulk temperature of the single-phase flow. The bulk temperature has been evaluated using Eq. 5.2 which could be obtained by performing the energy balance of the flow channel. The temperature difference between the wall and bulk fluid becomes constant after reaching the steady state, as shown in Fig. 5.5(a). Figure 5.5(b) depicts the transient development of heat transfer in non-dimensional form, i.e. Nusselt number. For a fluid flow between parallel plates, whose walls are subjected to the constant wall temperature boundary condition, the average value of the Nusselt number of a thermally developed flow takes the value of 7.55 (Shah, 1975)[58]. It can be seen from Fig. 5.5(b) that the flow becomes thermally fully developed after a certain time and achieves a thermally developed value of Nusselt number approximately equal to 7.50, which shows a

close match with the analytical value of the single-phase Nusselt number. The Nusselt numbers for single-phase and two-phase flows have been evaluated using Eq. 5.3.

$$u_x = 6u_{TP}\frac{y}{h}\left(1-\frac{y}{h}\right) \quad (5.1), \qquad T_{b_m} = \frac{\int_{L_{hyd}}^{L}\int_0^h \rho|u_x|c_P T\, dydx}{\int_{L_{hyd}}^{L}\int_0^h \rho|u_x|c_P\, dydx} \quad (5.2),$$

$$Nu_{avg} = \frac{h_{avg}D_h}{k} \quad (5.3), \qquad \text{where, } h_{avg} = \frac{q_w}{\left(T_w - T_{b_m}\right)} \quad (5.4)$$

Non-circular channels are widely used in fluid recirculation based applications like heating and cooling of buildings. Reynolds number for a flow through a non-circular channel/pipe/duct is evaluated on the basis of hydraulic diameter (D_h) which is defined as the ratio of four times of the cross-sectional area to the wetted perimeter of the channel/pipe/duct (Eq. 5.5).

$$D_h = \frac{4A_c}{P} \quad (5.5)$$

where A_c is the cross-sectional area of the pipe, and P is its wetted perimeter.

In Eqs. (5.3 and 5.4), $D_h = 2h$, q_w is the area-weighted average of wall heat flux obtained by averaging the upper and lower wall surface heat flux of the higher temperature regions individually. Similarly, T_{bm} is the bulk mean temperature of the two-phase fluid present in the higher temperature zone. The use of custom field function in ANSYS Fluent made it convenient to evaluate the bulk mean temperature using the volume-integral method.

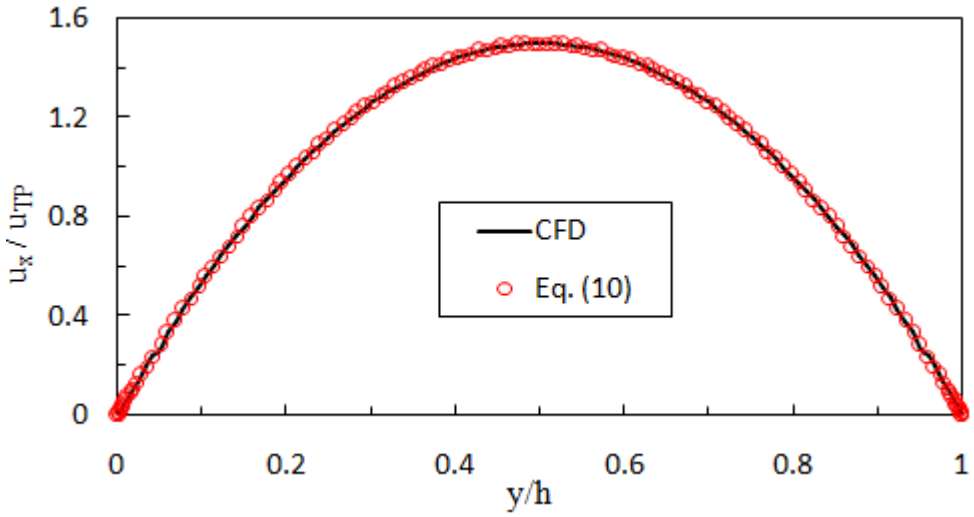

Fig. 5.4. Comparison of the centerline velocity profile of the single-phase flow obtained from CFD and Eq. 10 (at a plane perpendicular to the flow direction).

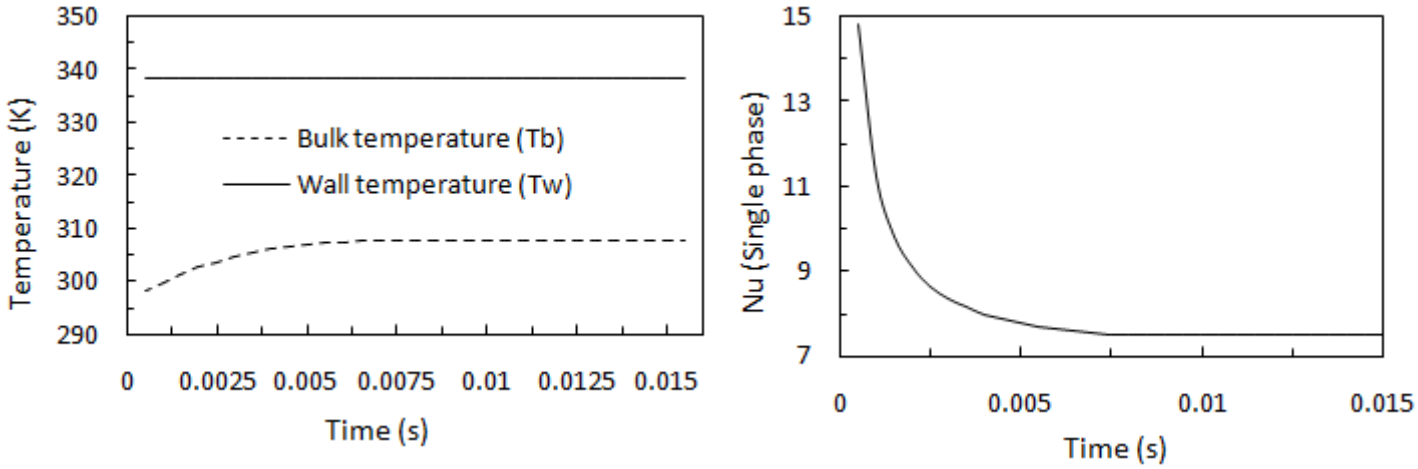

(a) (b)

Fig. 5.5. Transient development of (a) Wall and bulk mean temperatures, and (b) Nusselt number in single-phase liquid-only flow.

5.3.3. Two-phase flow and heat transfer studies of water-oil slug flow inside the microchannel

5.3.3.1. Droplet shape

The flow becomes hydrodynamically fully developed at approximately 0.4 ms and the shape of the droplet becomes independent of the dispersed phase volume. Figure 5.6 shows the transient development of droplet profile. Initially, the shape of the droplet is assumed to be rectangular at time t = 0s, then the flow starts developing and the shape of the droplet changes with time, later it achieves a fully developed profile once the flow becomes fully developed. For the present flow conditions, i.e. for a mixture velocity of 0.22 m/s at the inlet, and surface tension coefficient of 0.04925 N/m, a ripple (waves or undulations) at the rear end of the droplet was witnessed. These ripples indicate the zones of sharp pressure jumps which arise due to a barrage on the liquid-liquid interface (Fukagata et al. 2007, Asadolahi et al. 2011, Gupta et al. 2013, Bretherton 1961)[13,15,22,40].

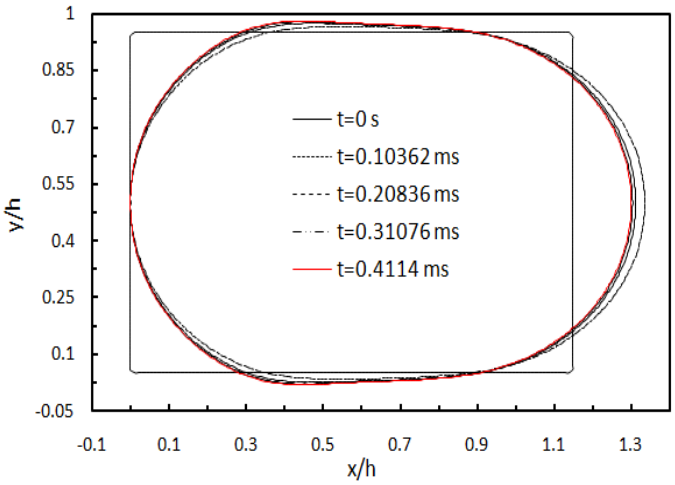

Fig. 5.6. Transient development of the dispersed phase droplet.

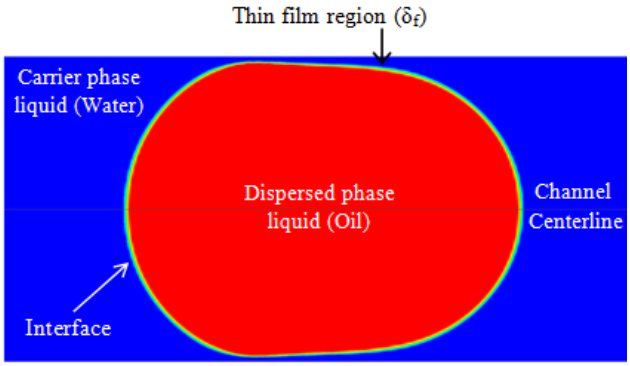

Fig. 5.7. The contours of oil volume fraction with the thin film region at Re = 44.6 and Ca = 0.0044.

5.3.3.2. Film thickness

In the present work, a non-uniform thin film of the continuous phase between the liquid-liquid interface and the channel wall has been observed (Fig. 5.7). Bretherton (1961)[40] developed a model to evaluate the film thickness with an assumption of δ_F << R (radius of the microchannel) (Eq. 5.7), whereas, Aussillous and Quere (A&Q) (2000)[56] proposed an empirical model (Eq. 5.9) by relaxing Bretherton's hypothesis. Han and Shikanzono (H&S) (2009)[57] and Eain et al.(2013)[65] proposed empirical correlation by incorporating the Weber and Reynolds numbers to evaluate the film thickness in visco-capillary and visco-inertial regimes for accounting the capillary and inertial effects (Eqs. 5.8 and 5.6). The details of these correlations are shown in Table 5.3. Figure 5.8 compares the film thickness obtained from the present numerical study and that by using correlations for estimating the film thickness. The film thickness has been found to increase with the Capillary number (0.0009 < Ca < 0.022) (Fig. 5.8). At higher mixture velocities, the nose of the droplet became sharp with its tail being flatter. This behavior in the thin film region has also been noticed by Goldsmith and Mason (1963)[61] and Olbricht and Kung (1992)[62] who reported the presence of non-uniform film region due to smaller droplet size (L_D / D = 1.15). The fim thickness predicted in the present study was found to be in good agreement with Bretherton's model for all Capillary numbers; however, it was in close match with H&S and A&Q models at lower Capillary numbers and with Eain et al. model at higher Capillary numbers only. A little deviation was found between the CFD results and the correlations with a maximum mean

absolute deviation (MAD) of 5%, 20%, 23%, and 25% with respect to Bretherton, H&S, A&Q, and Eain et al. models, respectively. These deviations could be attributed to the choice of location for the measurement of film thickness based on which the correlations were proposed. For example, H&S and Eain et al. measured the film thickness at the flatter section of the film region between the wall and interface in their experiments. It should be noted that the characteristic film thickness has been obtained in the present studies by averaging the film thickness between the channel wall and the two-phase interface in the non-uniform film region.

Table 5.3. Existing empirical and analytical correlations in literature for evaluating film thickness.

Author(s)	Correlation		Parameters
Eain et al. (2013)[65]	$\frac{\delta_F}{R} = 0.35(Ca)^{0.354}(We)^{0.097}$	(5.6)	Circular cross-section, D_h = 1.59 mm, 0.002 < Ca < 0.119, 0.047 < We < 0.697 and 14.46 < Re < 100.96, LL Taylor flow.
Bretherton (1961)[40]	$\frac{\delta_F}{R} = 1.34Ca^{2/3}$	(5.7)	Circular cross-section, D_h < 1mm, Ca < 0.005, GL Taylor flow.
Han and Shikazono (H&S) (2009)[57]	$\frac{\delta_F}{D} = \frac{0.670Ca^{2/3}}{1 + 3.13Ca^{2/3} + 0.504Ca^{0.672}Re^{0.589} - 0.352We^{0.629}}$	(5.8)	Circular cross-section, 0.3 < D_h < 1.3 mm, Ca < 0.40, GL Taylor flow.
Aussillous and Quere (A&Q) (2000)[56]	$\frac{\delta_F}{R} = \frac{1.34Ca^{2/3}}{1 + 3.34Ca^{2/3}}$	(5.9)	Circular cross-section, 0.42 < D_h < 1.46 mm, 0.015 < Ca < 1.9, GL Taylor flow.

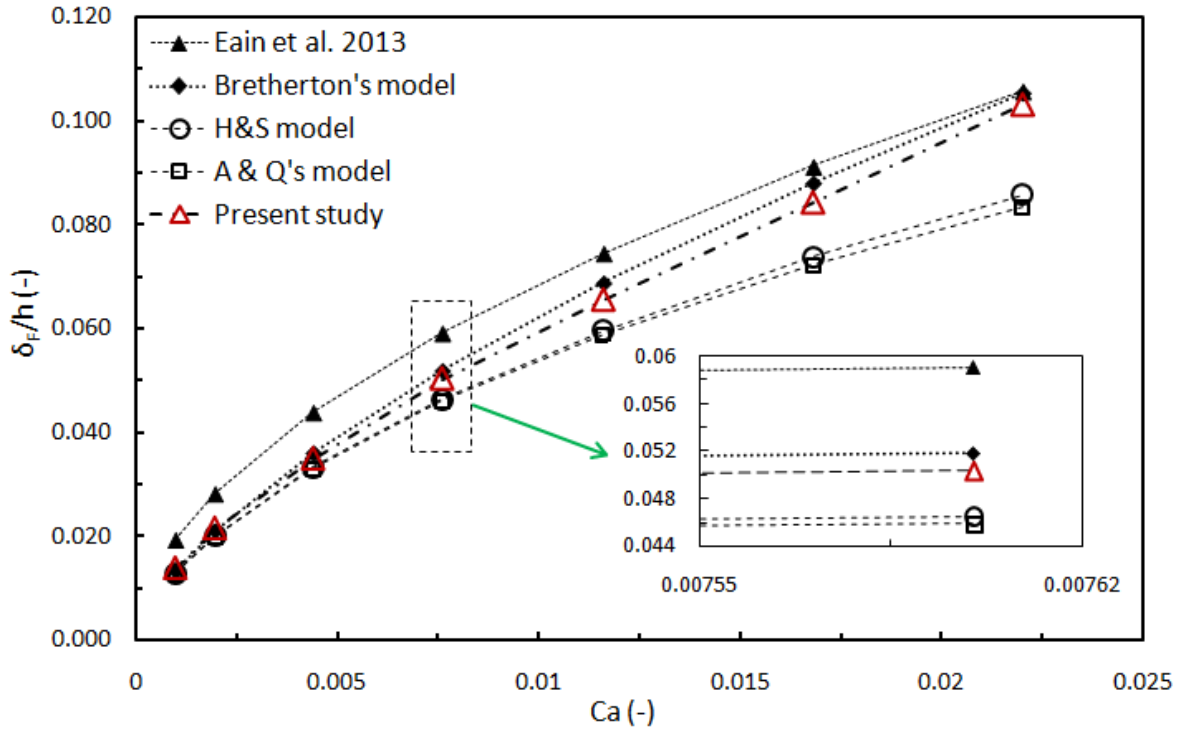

Fig. 5.8. Comparison of continuous phase film thickness w.r.t Capillary number (0.0009 < Ca < 0.022) as obtained from present CFD studies and phenomenological models available in the literature. The inset shows the enlarged view of the variation of film thickness at Ca = 0.0076 (The dashed lines are used only to guide the eyes of the reader).

5.3.3.3. Comparison of heat transfer results between two-phase flow and single phase flow studies

Before conducting the two-phase studies, a single phase study has been performed along with a two-phase study with water and oil as the working fluids (without modulation, i.e. Case 1 of Table 5.1). The objective behind this was to confirm the heat transfer augmentation in two-phase flow over single-phase flow. Shown in Fig. 5.9 are the transient development of Nusselt numbers for single-phase flow of water and two-phase flow of water-oil Taylor flow without temperature modulation at higher temperature region. It is observed that the introduction of secondary phase oil droplets to the flow enhances the heat transfer rate in contrast to the single-phase flow. An average Nusselt number of approximately 10.66 was obtained using two-phase flow without wall temperature modulation, whereas, the average Nusselt number obtained in the single-phase study was 7.55. This augmentation in heat transfer could be attributed to the fluid recirculation which occurs in the liquid slugs. In addition, the comparable thermal conductivity of secondary phase liquid with that of the primary phase liquid could be another reason for such enhancement in heat transfer rate.

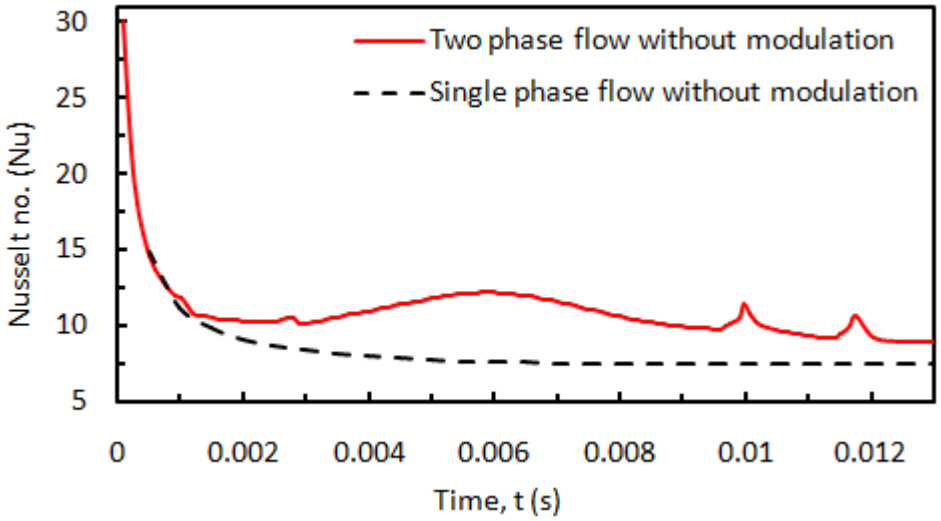

Fig. 5.9. Transient development of Nusselt number in two-phase and single-phase flows without wall temperature modulation.

5.3.3.4. Validation of present heat transfer results with a heat transfer model based on experimental findings

Table 5.4 compares the numerical value of the Nusselt number under no wall temperature modulation (338.3K) with the Nusselt number calculated from the correlation proposed by Dai et al. (2015)[4]. The correlation proposed by Dai et al. for evaluating two-phase Nusselt number in the slug flow regime under constant heat flux boundary condition was modelled for the following range of parameters $0.001 < Ca < 0.18$, $10 < Re < 1100$, characteristic dimension (D) = 2mm, $2.1\times10^{-5} < \mu < 0.017$ kg/ms. However, it was also reported in their work that the model suits well for isothermal wall boundary condition for the above range of parameters. In the present study, for the chosen value of parameters (i.e. Re = 44.6, Ca = 0.0044, and D = 200µm), the two-phase Nusselt number has been found to be in close match with that evaluated using the model (mean absolute deviation (MAD) ~ 7.56%) which suggests the suitability of the model for the present study.

Table 5.4. Comparison of Nusselt number between the present study and correlation of Dai et al (2015).

Calculation method		**Nu_{TP}**
$\frac{1}{Nu_{TP}} = \frac{1}{Nu_w} + \frac{L_{UC}}{L_D}\left(\frac{m}{m+1}\right)^2 \frac{1}{Nu_{FD}}\frac{k_C}{k_D} + \frac{L_{UC}}{L_S}\frac{1}{(m+1)^2}\frac{1}{Nu_{FS}}$	(5.10)	9.91
Present study		10.66
		MAD = 7.56%

5.3.3.5. Selection of optimal combination of thermal wall boundary conditions for two-phase study under modulated wall temperature conditions

This section describes the heat transfer characteristics of liquid-liquid slug flows inside the microchannel whose higher temperature walls have been prescribed with four different combinations of temperature boundary conditions, as mentioned in Table 5.1. In all the cases, except for the first case, the frequency and amplitude of modulated temperature were set to 500π rad/s and 0.02, respectively. The time-averaged Nusselt numbers obtained from the wall temperature modulations have been found to be comparatively higher than the Nusselt number of the single-phase flow. However, the maximum value of the time-averaged Nusselt number, equal to 11.19, was obtained by using the boundary conditions mentioned in case 3 in contrast to the other three cases, as shown in Fig. 5.10. The temporal variation of the fluctuation in Nusselt number for the case of in-phase wall temperature modulation showed higher peaks in contrast to the anti-phase modulation (Fig. 5.11). However, the time-averaged value of the Nusselt number for in-phase modulation turned out to be lesser than anti-phase modulation. It happened because the increase in the Nusselt number for the first half cycle was equal to the decrement in Nusselt number in the second half of the cycle. Although in case of anti-phase modulation the fluctuations in the Nusselt number have lower peaks, since both the walls behave thermally opposite to each other, the shoot-up in the Nusselt number remains under control unlike in in-phase modulation. As compared to in-phase and anti-phase wall temperature modulations, the case with upper hot wall having an isothermal condition and the lower hot wall having modulated wall temperature condition showed highest peaks in the temporal variation of the Nusselt number as well as time-averaged Nusselt number. This happened due to the unmodulated temperature condition at the upper hot wall which does not restrict the heat flow from the lower modulated wall, unlike other cases. Hence, this combination of boundary conditions (i.e., upper wall of higher temperature region at constant temperature 338K, and the lower wall of higher temperature region at modulated temperature condition) has been considered in further studies to explore the effects of amplitude and frequency on the two-phase heat transfer coefficients under slug flow conditions.

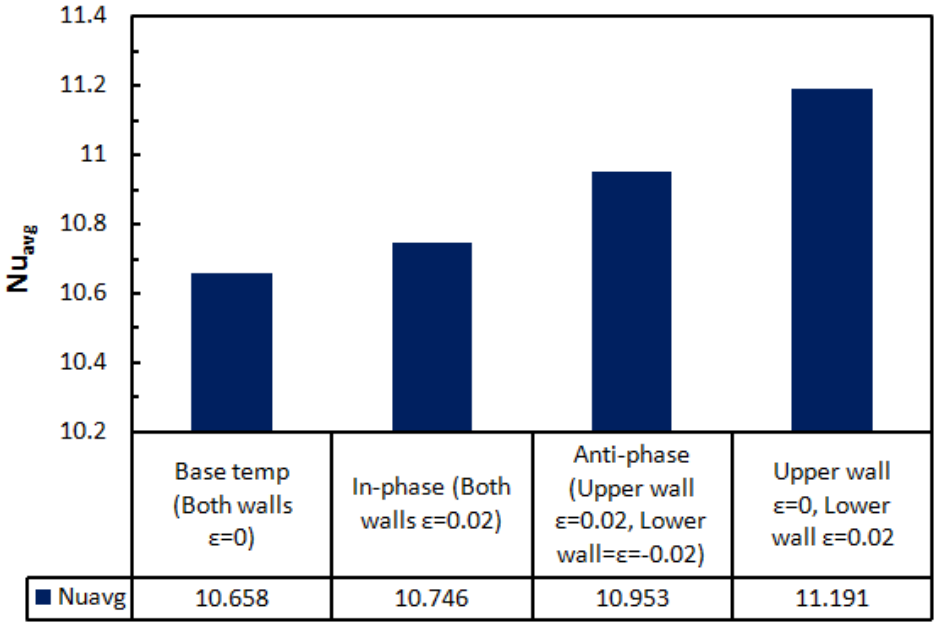

Fig. 5.10. The time-averaged Nusselt number for different thermal wall boundary conditions at the higher temperature region.

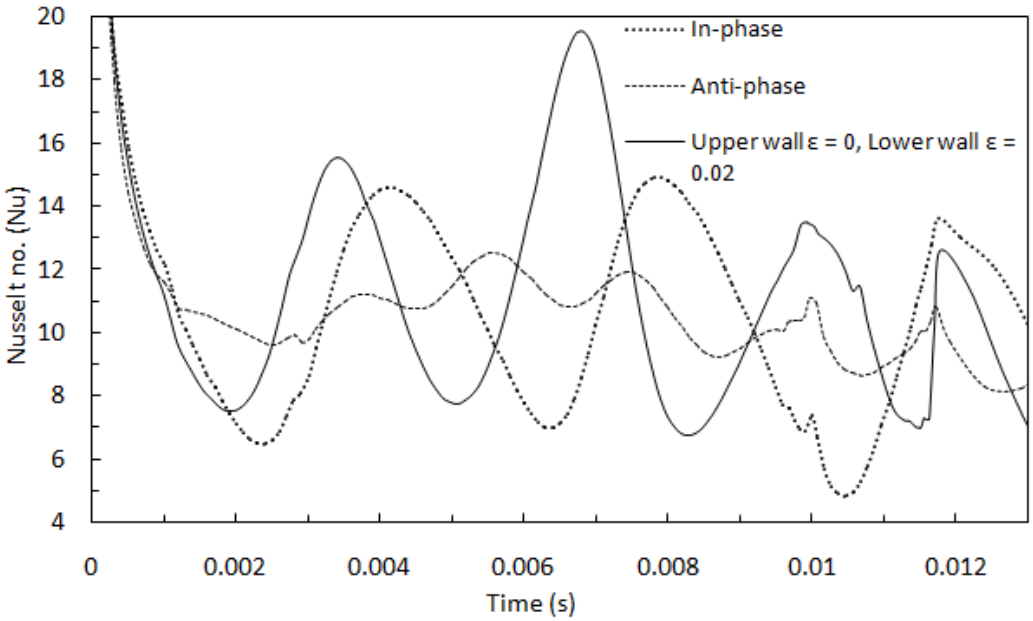

Fig. 5.11. Temporal variation of Nusselt number for different types of wall temperature modulation considered in the studies.

5.3.3.6. Effect of varying amplitude and frequency on the time-averaged two-phase Nusselt number

This section describes the effect of amplitude and frequency on the two-phase time-averaged Nusselt number of the liquid-liquid slug flow in the microchannel. The amplitude of the sinusoidal temperature profile at the upper and lower walls of the higher temperature region

of the channel has been varied in the range 0 to 0.03, keeping its frequency fixed at a value of 500π rad/s. The average Nusselt number was found to increase with an increase in amplitude, then attain a maximum value of 11.19 at ε = 0.02 after which it decreased on further increase in the amplitude, as shown in Fig. 5.12.

In another set of studies, the frequency of the sinusoidal temperature profile at the upper and lower walls of the higher temperature region of the channel has been varied in the range 0−750π rad/s, keeping its amplitude fixed at a value of 0.02. The average Nusselt number was found to increase with an increase in the frequency from 0 < ω < 500π rad/s), then attain a maximum value of 11.19 at ω = 500π rad/s and later it decreased on further increase in the frequency, as shown in Fig. 5.13. From the above two studies, it has been noticed that for an amplitude of 0.02 and a frequency of 500π rad/s, an optimum value of heat transfer coefficient is obtained, which signifies the importance of these two parameters in the heat transfer process during slug flows.

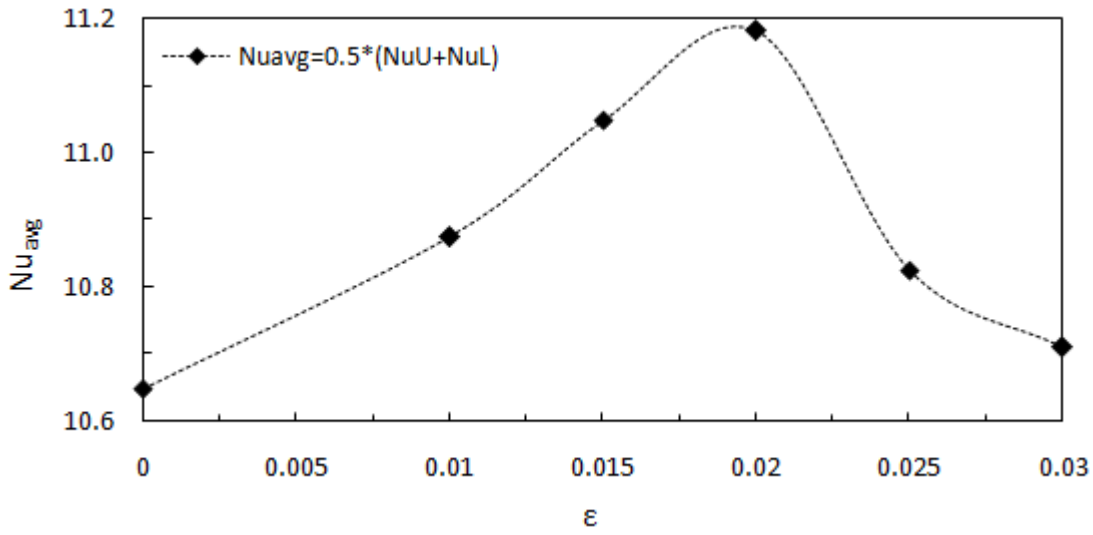

Fig. 5.12. The time-averaged Nusselt number at different values of amplitude (ε) for a given value of frequency (ω=500π rad/s) for case 3. (The dashed lines are used only to guide the eyes of the reader).

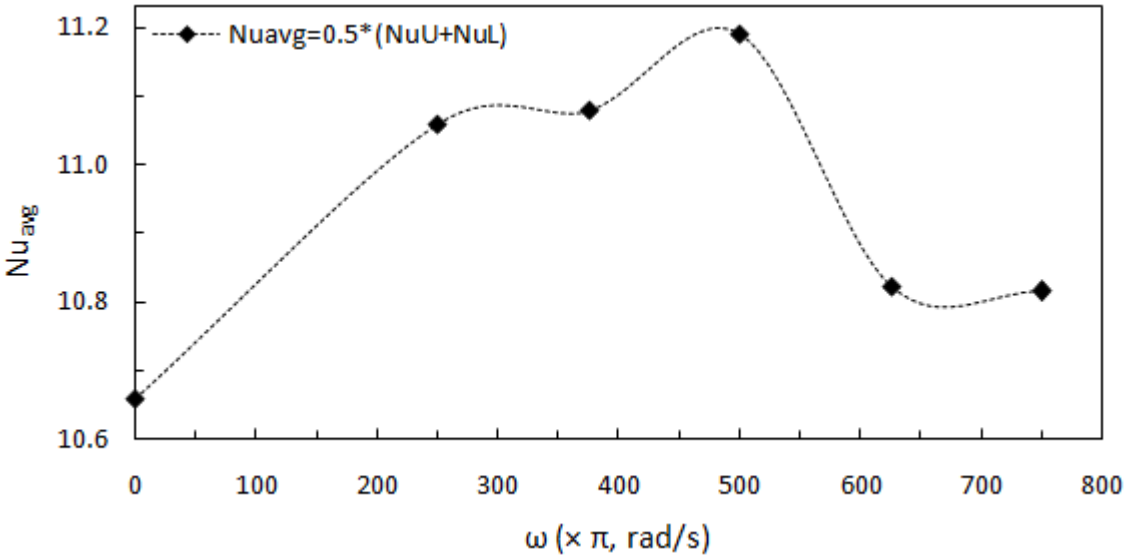

Fig. 5.13. The time-averaged Nusselt number at different values of frequency (ω) for a given value of amplitude (ε =0.02) for case 3. (The dashed lines are used only to guide the eyes of the reader).

Figure 5.14 shows the comparison of dimensionless temperature profiles in the middle of the oil droplet along the transverse direction of the flow for different values of amplitude at a given frequency of 500π rad/s. It can be seen that the slope of the temperature profile near the lower wall for an amplitude of 0.02 is higher in contrast to other values of amplitude, which in turn emphasizes higher temperature gradient in case of ε = 0.02 with respect to other values. Because of this reason, the heat transfer rate is expected to be higher as compared to other cases. On the other hand, the slope of the temperature profiles near the upper wall is more or less same due to isothermal condition at the upper wall of the microchannel. Similar conclusions can be drawn from Fig. 5.15 which compares the dimensionless temperature profiles in the middle of the oil droplet along the transverse direction of the flow for different values of frequency at a given amplitude of 0.02. These findings can be understood in detail with the help of dimensionless temperature contours for either of the above cases as discussed in the subsequent paragraphs.

Figure 5.16 shows the contours of the dimensionless temperature around the downstream droplet for different values of amplitude at a fixed frequency of 500π rad/s. It can be seen that the curvature of the iso-contour lines becomes stronger when the amplitude of the wall temperature varies from 0.015 to 0.02. This ensures higher gradients of temperature for ε = 0.02 in contrast to ε = 0.015. On further increase in the amplitude from 0.02 to 0.025, the curvature of the iso-contour lines becomes weaker which ensures a

decrement in the temperature gradient. In general, the normal temperature gradient of a temperature contour near the wall, i.e. $(\theta_w - \theta_i) / (y_w - y_i)$, gives the heat transfer rate or Nusselt number. Here, θ stands for the non-dimensional temperature, *y* stands for the transverse location of a point at a given axial location and the subscripts 'w' and 'i' stand for wall and any interior location of the computational domain. It was analyzed that the difference $(y_w - y_i)$ was lesser for an amplitude of 0.02 in contrast to the difference in *y* for an amplitude of 0.025. This implies that an iso-contour line with higher gradient would be closer to the wall and vice-versa for lower temperature gradient. However, this variation is not constant throughout the length of the domain, hence, an averaging of the Nusselt number has been carried out and the same has been shown in Fig. 5.11 which depicts the temporal variation of Nusselt number for different boundary condition including the present case (i.e upper wall without temperature modulation and lower wall with temperature modulation having ε = 0.02 and 500π rad/s). Figure 5.17 shows the contours of dimensionless temperature around the downstream droplet for different values of frequency at a fixed amplitude of 0.02. It can be seen that the curvature of the iso-contour lines becomes stronger when the frequency of the wall temperature varies from 375π rad/s to 500π rad/s. This again ensures higher gradients of temperature for the case of 500π rad/s in contrast to 375π rad/s. On further increase in the amplitude from 500π rad/s to 625π rad/s, the curvature of the iso-contour lines becomes weaker which ensures decrement in the temperature gradient. The same reason as mentioned above for the case of varying amplitude at a fixed frequency holds good in this finding as well.

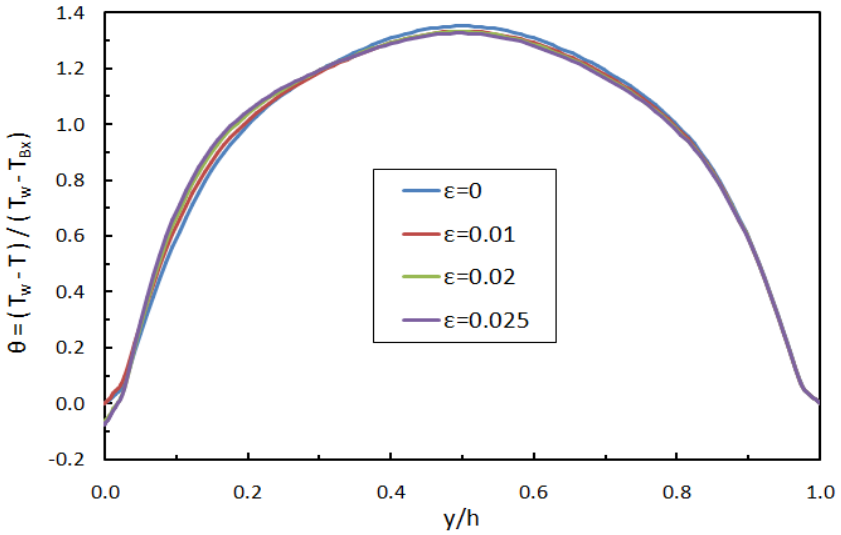

Fig. 5.14.Variation of dimensionless temperature along the transverse direction of flow at the center of the oil droplet with the amplitude at a fixed frequency (ω = 500π rad/s).

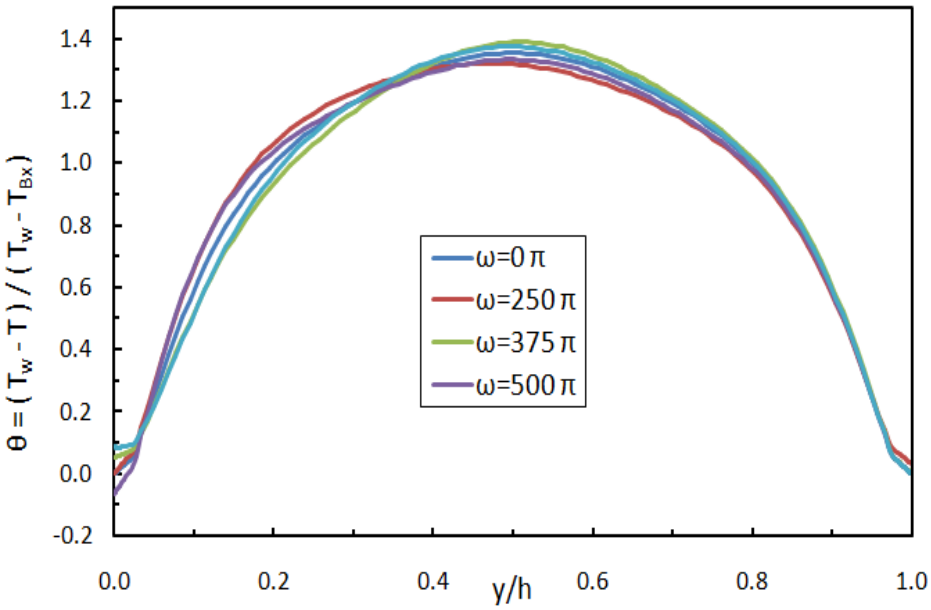

Fig. 5.15.Variation of dimensionless temperature along the transverse direction of flow at the center of the oil droplet with frequency at a fixed amplitude (ε = 0.02).

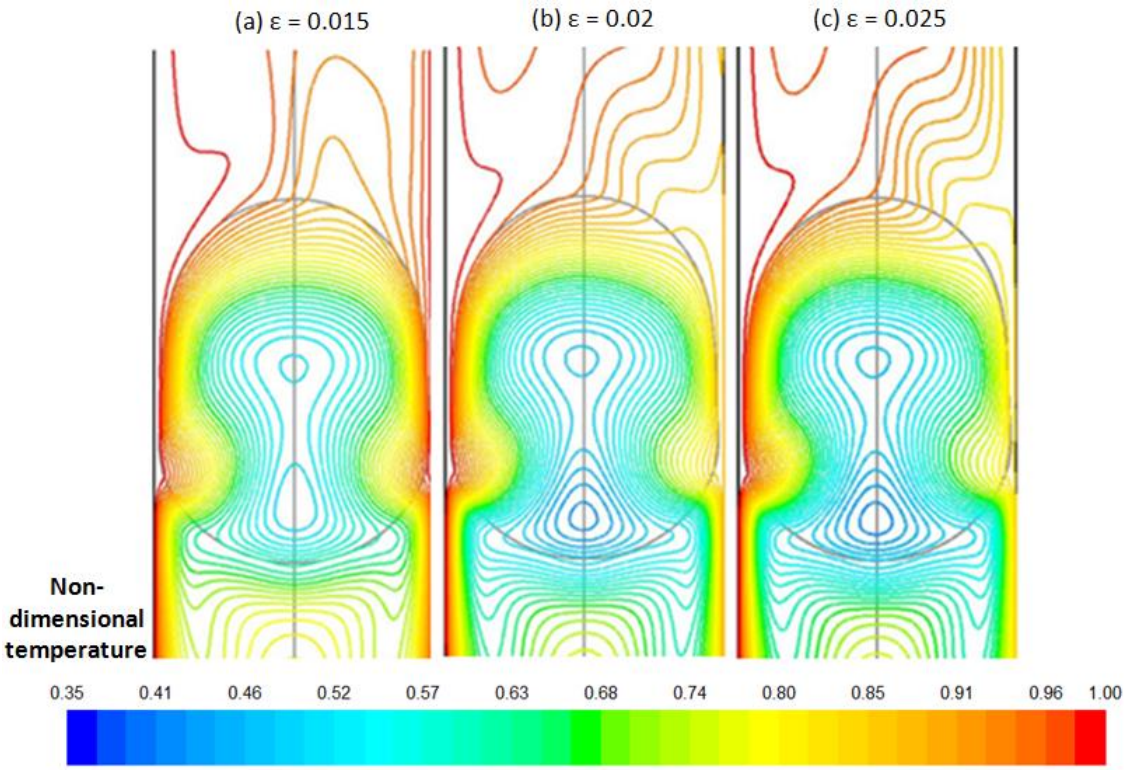

Fig. 5.16. Non-dimensional temperature contours for different amplitude at a fixed frequency of 500π rad/s.

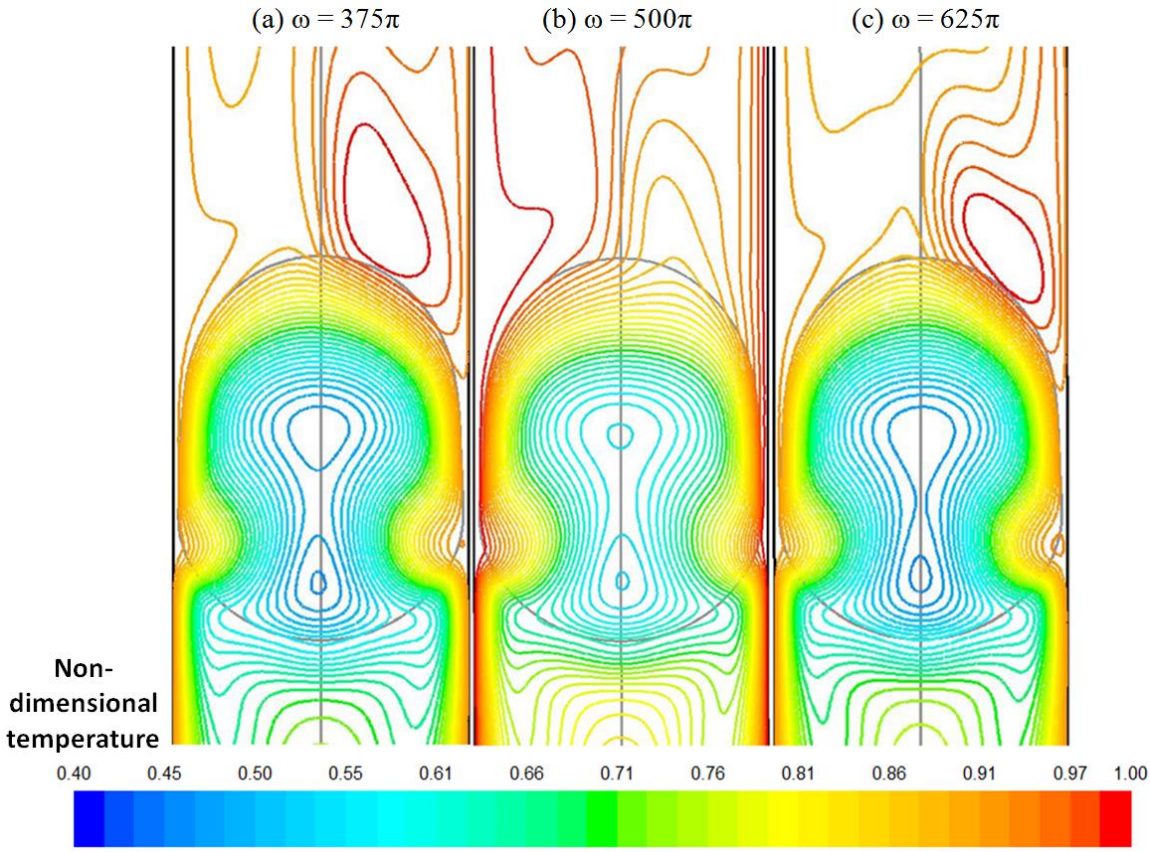

Fig. 5.17. Non-dimensional temperature contours for the different frequencies at a fixed amplitude of 0.02.

5.3.3.7. Effect of Capillary number on the slug flow heat transfer

Figure 5.18 shows the variation of Nusselt number as a function of Capillary number for the case where the upper hot wall of the channel was prescribed with isothermal condition (T_{hU} = 338.3K) and the lower hot wall with modulated temperature condition having amplitude and frequency of temperature modulation 0.02 and 500π rad/s, respectively. For the water-oil system, Nusselt number increases progressively with an increase in Capillary number. Although film thickness increases with the Capillary number as explained in section 5.3.3.2 and depicted in Fig. 5.8, the Nusselt number was found to increase with an increase in the Capillary number which could be attributed to the dominance of convective heat transfer in contrast to conductive heat transfer. Capillary number and film thickness along with the dependence of slug and droplet length on mixture velocities for a given homogeneous void fraction have a combined effect on Nusselt number which was also explained in the experimental studies of liquid-liquid slug flow heat transfer performed by Bandara et al. (2015b).

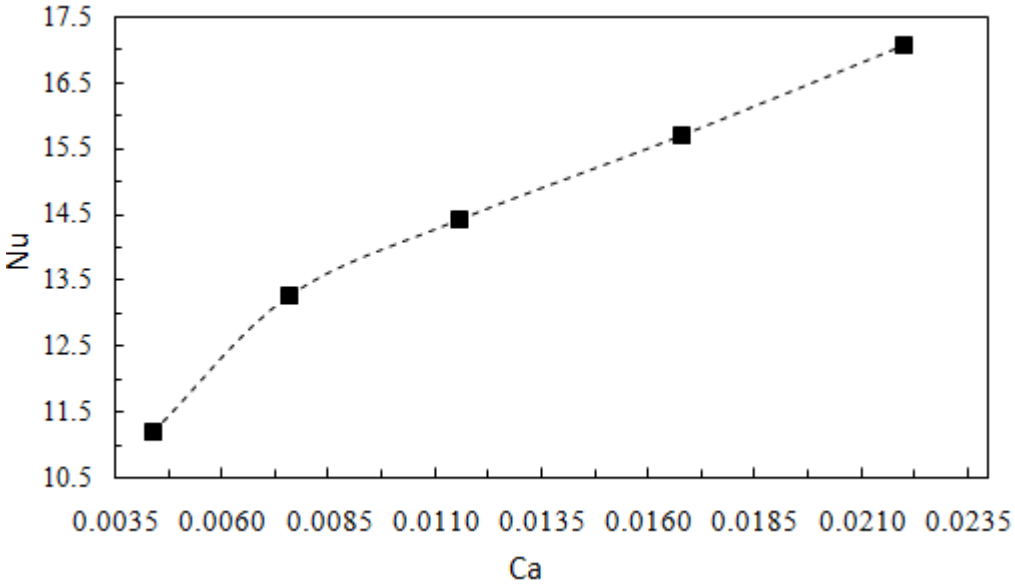

Fig. 5.18. Effect of Capillary number on the Nusselt number (ε = 0.02, ω = 500 π rad/s).

5.4. Summary

This chapter discussed the flow physics and heat transfer characteristics of a two-dimensional, planar, incompressible, laminar water-oil Taylor flow in a rectangular microchannel subjected to modulated thermal boundary conditions. The hotter walls of the channel were subjected to different modulated boundary conditions with a base temperature of 338.3K. VOF technique was employed to capture the interface of the two-phase flow. Initially, the single phase flow of water under isothermal wall boundary conditions with an inlet velocity of 0.22 m/s was studied. The single phase flow and heat transfer results obtained from the study were validated with benchmark analytical results. Later, two immiscible dispersed phase oil droplets were introduced into the flow domain under the same boundary conditions as that of single-phase flow. A significant increase in the heat transfer rate (~ 42%) over single-phase flow was observed in the two-phase flow without modulation. The two-phase Nusselt number without wall temperature modulation was compared with an empirical model for evaluating two-phase Nusselt number. A close match was obtained between the two values with a mean absolute deviation of approximately 7.56%.

Later, the higher temperature walls of the channels were prescribed with different modulated temperature conditions and the combination of boundary conditions resulting in optimum heat transfer rate was chosen as the base case for further two-phase heat transfer studies. The effect of amplitude ($0 < \varepsilon < 0.03$) and frequency ($0 << 750\pi$ rad/s) of the sinusoidal wall temperature profiles on the heat transfer rate was also studied. The heat

transfer rate was found to be highest for an amplitude of 0.02 and a frequency of 500π rad/s. The key reason for such an increase was due to a higher temperature gradient at the middle of the droplet along the transverse direction for an amplitude of 0.02 and frequency of 500π rad/s in contrast to other cases. The results of the numerical study using modulated temperature conditions on channel walls showed a significant improvement in the heat transfer by approximately 50% over liquid-only flow for a mixture velocity of 0.22 m/s. Besides, the transient development of droplet shape, variation of the carrier phase film thickness and heat transfer rates for a range of Capillary numbers ($0.0009 < Ca < 0.022$) were also discussed. The film thickness and the heat transfer rates were found to increase with the Capillary number which indicates the dominance of convective heat transfer over conduction heat transfer. An approximate enhancement of 50% to 126% in the average heat transfer rates was achieved for the chosen range of Capillary numbers ($0.0044 < Ca < 0.022$) under modulated wall temperature condition (i.e. $\varepsilon = 0.02$ and $\omega = 500\pi$ rad/s) in contrast to liquid-only flow. This concludes the present work which has significant implications for heat transfer applications based on slug flow inside microchannels.

CHAPTER 6 EFFECT OF MODULATED WALL MOTION ON FLOW AND HEAT TRANSFER IN THE TAYLOR FLOW REGIME IN A RECTANGULAR MICROCHANNEL

6.1 Introduction

Liquid-liquid (LL) Taylor flow in microchannels has drawn significant attention of researchers in the last few years for the removal of high heat fluxes in microstructured devices. However, in almost all the previous studies, the heat transfer studies have been carried out for stationary channel walls (Bandara et al. 2015a). In general, the heat transfer behaviour of a fluid flowing inside a channel depends also on the motion of the channel wall (Reynolds 2014). Few studies on single-phase flow inside conventional channels and two-phase flow inside microchannel give an idea about how a small modulated motion to the channel walls could lead to an enhancement in the heat transfer rates. Zheng et al.(2017) discussed the effect of modulated wall motion on the boiling heat transfer coefficient of liquid hydrogen inside a tube in their three-dimensional numerical studies. They reported the influence of amplitude and frequency of the modulated wall motion on the evaporative heat transfer rate. Their results indicate that the heat transfer augments in the presence of modulated wall motion. Similarly, the experimental studies of Hosseinian et al. (2018)indicate that the performance of the double pipe heat exchanger significantly augments when its surface is subjected to modulation. It was reported that the rate of heat transfer increased with an increase in modulation level. These modulations were provided at the surface of the heat exchanger with the help of electro-dynamic vibrators. The numerical studies of Sowayan (2013) describe the influence of the modulation frequency of the bottom plate of a square cavity with insulated vertical walls on the heat transfer rate. It was reported that the rate of heat transfer augmented with an increase in the frequency of the modulated bottom wall due to an increase in the flow Reynolds number. The experimental studies of Shariff (2011) demonstrate the enhancement in flow boiling heat transfer in microchannels

when the walls were subjected to acoustic vibrations. The experimental setup comprised of heating elements for heat flux variations and excitation elements to provide the vibrations. The frequency of the vibration was varied with frequencies of 5, 10, and 15 kHz. They reported an enhancement in flow boiling heat transfer by 21% using acoustic vibration in contrast to flow convective boiling under no vibration. Although flow boiling inside a channel is highly unstable, no system failure was reported in their work. The experimental studies of Whitehill et al. (2010) demonstrate the droplet behaviour under high intensity acoustic vibration. They investigated the influence of low frequency (60 to 200 Hz) vibration of droplets in the direction normal to the glass slide on which they sit. Low frequency oscillations could be acoustically as well as mechanically provided to the heating section used in the studies of Eain et al. (2015), Dai et al. (2015) and Bandara et al. (2015b). This could be achieved using excitation elements and electromagnetic micro shakers, respectively. Micro shakers with different range of operating frequencies are easily available in the market which consumes very less power in the range 40-60W.

Based on these studies it can be anticipated that the thermal performance of a microchannel with slug flow conditions could also be improved by providing modulated motion to the channel walls. Since such an idea has never been implemented on slug flow studies earlier, an effort has been made in the present work to study computationally the influence of modulated wall motion in the transverse direction of the fluid flow on the hydrodynamics and thermal characteristics of oil-water Taylor flow in a rectangular microchannel under constant heat flux boundary condition. The effects of frequency and amplitude of the modulated wall motion on the droplet shape, film thickness, pressure drop, and Nusselt number have been investigated.

6.2 Numerical modelling

6.2.1 *Computational domain*

The periodic behaviour of Taylor flows allows us the modeling of the present flow problem using a fully developed unit cell. Figure 6.1 shows the schematic diagram of the computational unit cell used in this study. The unit cell comprises of a single oil droplet at its center with two halves of the primary phase liquid slug surrounding the oil droplet. A two-dimensional rectangular microchannel having periodic inlet and outlet was modeled in the design modeler of ANSYS workbench. Light mineral oil and water have been used as the dispersed and carrier phase fluids, respectively by assuming them as Newtonian fluids. The

periodic unit cell has been assumed to be moving with the speed of the droplet (U_D) and remained steady in the droplet frame of reference. It should be noted that the width of the microchannel in the third dimension is assumed to be very large as compared to the height of the channel; hence, the microchannel can be treated as micro parallel plates in the present study. The details of the physical properties and geometrical parameters of the flow and the computational domain are respectively given in Table 6.1.

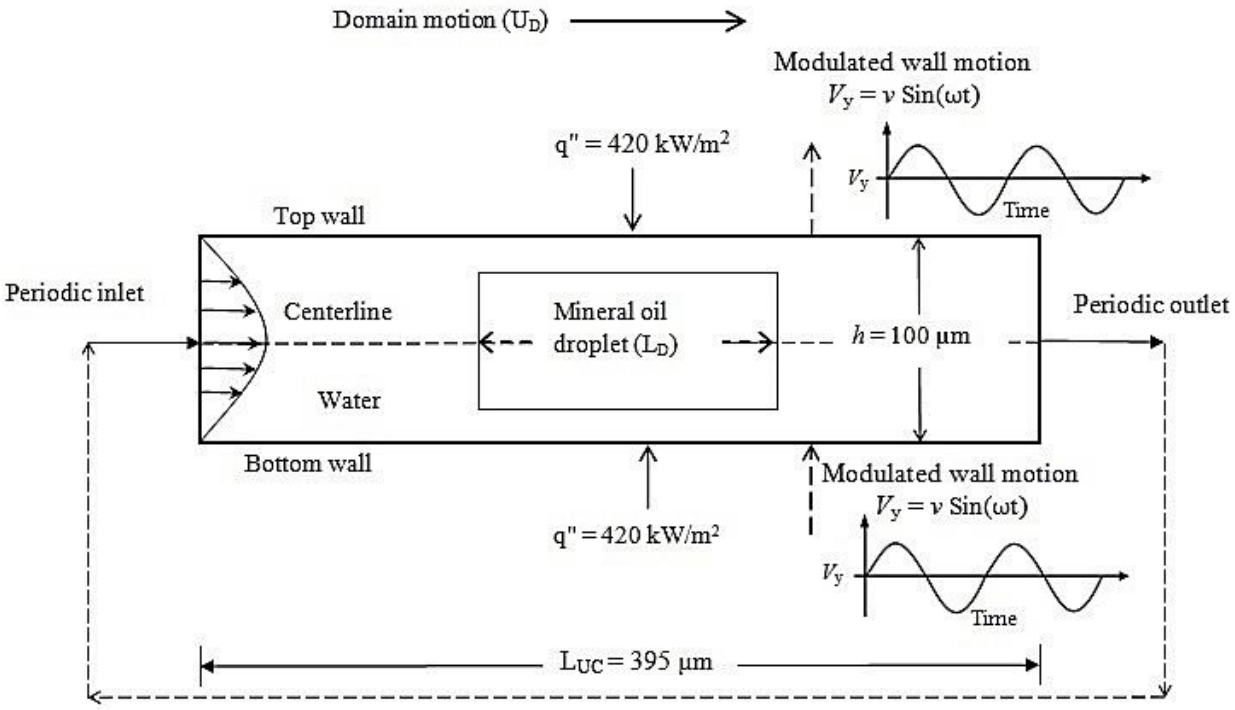

Fig. 6.1. Schematic diagram of the computational domain used in the present numerical studies.

Table 6.1 Physical parameters of the flow and computational unit cell.

Parameters	Details
Channel	2D, Planar, rectangular microchannel
Channel dimensions	h = 100 µm, L_{UC} = 395 µm, 100 < L_S < 310 µm, 85 < L_D < 295 µm
Flow type	Liquid-liquid Taylor flow
Carrier phase	Water (ρ = 998 kg/m^3, μ = 0.000985 kg/ms, c_p = 4182, k = 0.6 W/mK)
Discontinuous phase	Light mineral oil (ρ = 838 kg/m^3, μ = 0.023 kg/ms, c_p = 1670, k = 0.17 W/mK)
Surface tension coefficient	σ = 0.04925 N/m

6.2.2 *Numerical method*

The moving domain method (MDM) available in ANSYS Fluent has been incorporated to model the two-phase flow because of its lower computational cost as compared to the stationary domain method (SDM). The dynamic mesh method has been employed as the flow domain moves with the droplet velocity, and hence the shape of the domain also changes over time. Rigid body treatment has been used since both the domain as well as the incoming stream move in the same direction. In addition, the dynamic layering technique has been adopted to update the mesh at each time step. It should be noted that at the beginning of each time-step the droplet velocity has been calculated using Eq. (6.1) and was supplied to the solver by user-defined C routines. The detailed description of the MDM including the application of periodic velocity and temperature conditions at the boundaries for solving Taylor flow problems can be found in the studies of Asadolahi et al. (2011).

$$U_D = \frac{\int_x^{x+L_{UC}} \int_0^h \alpha_D u_x dy dx}{\int_x^{x+L_{UC}} \int_0^h \alpha_D dy dx} \tag{6.1}$$

The homogeneous void fraction (β) is given by the following expression:

$$\alpha_D U_D = \beta u_{TP} \tag{6.2}$$

6.2.3 *Initial and boundary conditions*

A two-dimensional, planar, incompressible, and laminar LL slug flow inside a rectangular microchannel has been modeled in the present study. A no-slip wall condition with a constant wall heat flux of 420 W/m^2 has been prescribed at the top and bottom walls of the channel. The upper and lower walls of the microchannel were subjected to modulated motion in the transverse direction of the flow. The modulated wall velocity has been defined with the help of user-defined functions and is given as:

$$V_y = vSin(\omega t) \tag{6.3}$$

where *v* is the amplitude of the modulated velocity given by,

$$v = av_o \tag{6.4}$$

In Eq. (6.4) v_o is the velocity of any fluid element passing through a cell at a given instant of time, given by;

$$v_o = \frac{\Delta x}{\Delta t} \tag{6.5}$$

where Δx is the size of the smallest cell in the computational domain, and Δt is the maximum time step size of the variable time step range. For sake of convenience, v_o will be called as base velocity hereafter. In Eq. (6.4), a stands for the amplification factor w.r.t. the base velocity.

Periodic temperature, periodic velocity inlet, as well as pressure outlet conditions, were prescribed at both the ends of the channel. The initial temperature of the fluid at the inlet was set to 296.15K and the operating pressure was atmospheric pressure. The continuous phase liquid was allowed to enter the domain at a constant velocity. At the beginning of each simulation, the solution domain contains a cylindrical liquid droplet having a size equal to the required volume fraction. The entire flow channel was initialized with a uniform pressure of zero Pascal and a fully-developed parabolic velocity profile having an average mixture velocity equal to the velocity of the incoming primary (continuous) phase fluid. The transverse ($v_{x,y}$) and centerline velocity ($u_{x,y}$) components, as well as the inlet and outlet temperatures, have been transformed to the upstream boundary from the downstream boundary by invoking user-defined C routines in the solver:

$$u_{x,y} = u_{x+L_{UC},y} \tag{6.6}$$

$$v_{x,y} = v_{x+L_{UC},y} \tag{6.7}$$

$$\left.\frac{\partial T}{\partial x}\right|_{x=0} = \left.\frac{\partial T}{\partial x}\right|_{x=L_{UC}} \tag{6.8}$$

While solving the above equation, an unknown temperature 'T_u' arises which is given by,

$$T(x,y,t) = T_a(x,y,t) + T_u(t) \tag{6.9}$$

The actual inlet temperature could be computed by obtaining the value of T_u using global energy balance technique. However, only the temperature shift, given by Eq. (6.20), is of interest in this study; hence, the temperature has been treated as a passive scalar. The detailed derivation of Eq. (6.10) can be found in Asadolahi et al. (2011). In order to achieve this

periodic temperature boundary condition, the faces of the domain having fluid outflow and inflow at the boundaries have to be identified first. This has been done by observing the computational domain in droplet frame of reference. Once the inflow and outflow faces were identified, these were treated as inlet and outlet cells, respectively in droplet frame of reference. Later, the modified temperature fields were wrapped to the inlet cells from the respective outlet cells. Figure 6.2 pictorially describes the above-mentioned procedure. The presence of recirculation inside the continuous phase slug causes the fluid inflow and outflow at the boundaries.

$$T_{x+L_{UC,y}} - T_{x,y} = \Delta T_{UC} = \frac{q_w A_{w_{UC}}}{\left[(1-\beta)\rho_c c_{p_c} + \beta \rho_D c_{p_D}\right] u_{TP} A_{XS}} \tag{6.10}$$

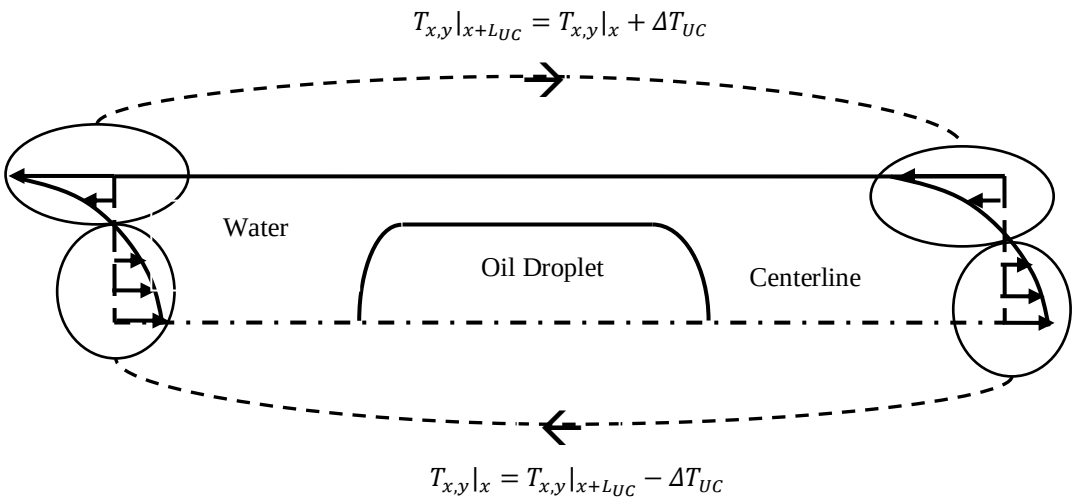

Fig. 6.2. The direction of temperature wrapping and the velocity and temperature profiles at the periodic boundaries in the droplet frame of reference.

6.2.4 *Numerical schemes*

The commercial code ANSYS Fluent 15.0 has been employed to perform this study. VOF method has been adopted to capture the LL interface. First order implicit with non-iterative fractional step method has been employed for the unsteady formulation of the flow equations. The piecewise linear approach based explicit geometric reconstruction scheme has been used for the interface reconstruction. A maximum Courant number of 0.25 was used for the volume fraction equation. Variable time-stepping strategy with minimum and maximum time-step size of 10^{-9} and 10^{-6}s and a global Courant number of 0.25 for flow and energy equations have been used. Green-Gauss node based gradient method has been adopted for spatial discretization. Body force weighted scheme for solving pressure Poisson equation,

and QUICK scheme for solving the convective terms of momentum and energy equations have been used. It should be noted that only the flow equations were solved first, and once the flow became steady and fully developed, the energy equation was solved alone by turning off the flow equations to save the computational time. The surface tension coefficient at the oil-water interface was 0.04925 N/m (Bandara et al. 2015b). The details of the solver parameters used for solving the two-phase flow are tabulated in Table 6.2.

Table 6.2 Solver parameters used in the present study.

Parameters	Details
Discretization method	Finite volume method
Multiphase method	Volume of fluids
Grid size	35000 ─ 55000 elements
Inlet velocity	0.22 ─ 1.1m/s
Courant number (C)	0.25
Grid refinement	Near-wall mesh treatment
Solver details	2D, unsteady, Planar, pressure based absolute velocity formulation.
Pressure-velocity coupling scheme	Fractional step
Transient formulation	First order implicit with non-iterative time advancement (NITA)
Spatial discretisation	Green-Gauss node based method
Pressure discretisation	Body force weighted
Momentum discretisation	QUICK
Energy discretisation	QUICK
Interface reconstruction	Geo-Reconstruct algorithm
Outlet	Pressure outlet
Slip condition	No-slip
Time step size	Variable time stepping for flow equations, $10^{-9} < \Delta t < 10^{-6}$ s, and $\Delta t = 10^{-5}$ s for energy equation
Body force formulation	Implicit body-force

6.3 Results and discussion

6.3.1 *Grid independence*

The entire domain was meshed with square elements except for the region at the vicinity of the wall where near-wall mesh refinement was performed by following the suggestions of Gupta et al. (2009) to capture the thin liquid film between the wall and droplet. Bretherton (1961) proposed a correlation (Eq. 6.11) to estimate the thickness of the continuous phase film existing between the dispersed phase droplet and the channel wall as a function of the Capillary number based on the mixture velocity. Although the model was proposed for circular channels, the film thickness obtained by using the hydraulic diameter of the present computational domain in Bretherton's equation could be considered as the first approximate while meshing to capture the liquid film. Following these guidelines, the numerical studies were performed using three different meshes having 35000, 45000, and 55000 elements. Figure 6.3 shows the computational mesh used in the simulations having near-wall treated elements closer to the walls with the square elements in the core region which consist of 45000 elements with an aspect ratio closer to one. Figures 6.4(a) and 6.4(b) shows the variation of the droplet shape and the dimensionless temperature profile in the liquid slug inside the microchannel with unmodulated wall motion for three different mesh sizes, viz. 35000, 45000, and 55000 elements. In Fig. 6.4(a), the enlarged views of the droplet shapes at four different regions, highlighted by dashed oval boxes, are shown below the main figure. Similarly, the insets in Fig. 6.4(b) give a closer view of dimensionless temperature profiles in the regions highlighted by dashed rectangular boxes. It can be seen from the figure that the droplet shapes and temperature profiles for the mesh sizes of 45000 and 55000 are almost similar. Hence, a mesh having 45000 elements has been used for all further simulations.

Bretherton's model:

$$\frac{\delta_F}{R} = 1.34Ca^{2/3} \tag{6.11}$$

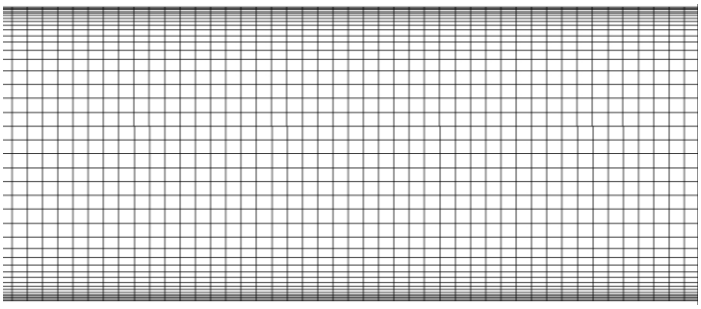

Fig. 6.3. Computational mesh.

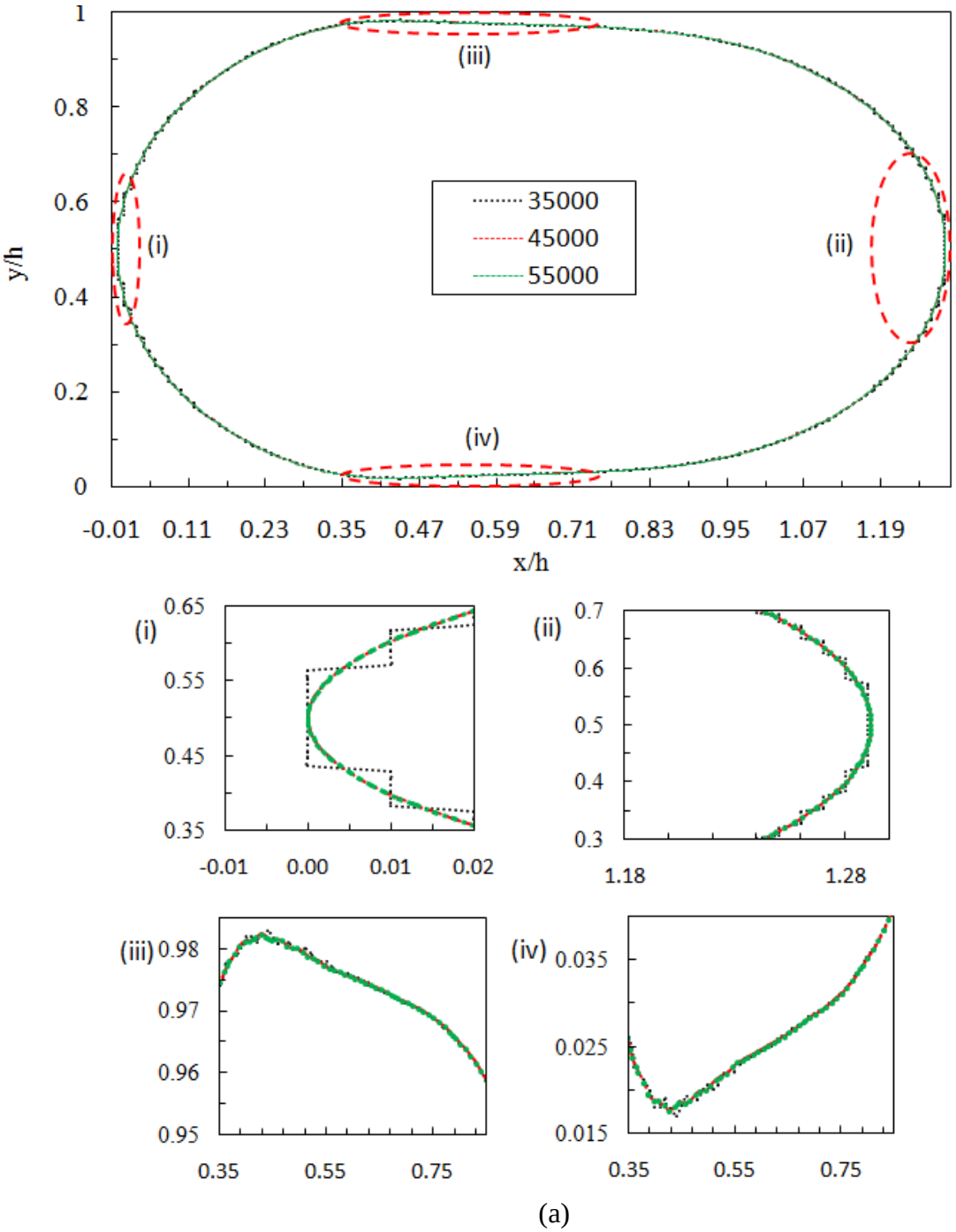
y/h
x/h
35000
45000
55000
(i)
(ii)
(iii)
(iv)
1
0.8
0.6
0.4
0.2
0
-0.01 0.11 0.23 0.35 0.47 0.59 0.71 0.83 0.95 1.07 1.19
0.65
0.55
0.45
0.35
-0.01 0.00 0.01 0.02
0.7
0.6
0.5
0.4
0.3
1.18 1.28
0.98
0.97
0.96
0.95
0.35 0.55 0.75
0.035
0.025
0.015
0.35 0.55 0.75

(a)

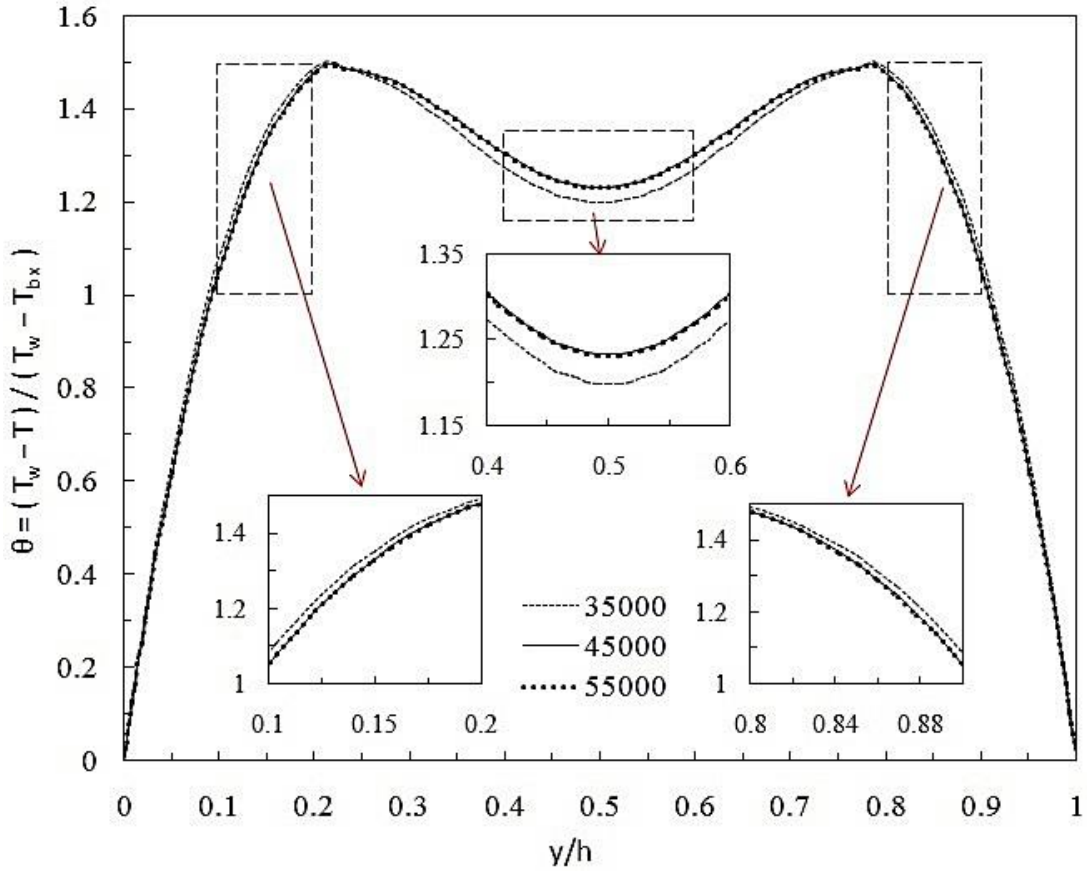

(b)

Fig. 6.4. Grid independence test (a) Droplet profiles, (b) Temperature gradient in slug region (u_{TP} = 0.22m/s, L_S = 280µm, L_D = 115µm).

6.3.2 *Velocity profile: Validation*

Analytically, the fully developed axial velocity profile of a liquid flowing between parallel plates in the slug region can be obtained from Plane-Poiseullie equation given by Eq. (6.12). The present computational fluid dynamics (CFD) source code has been validated against the benchmark analytical equation for the centerline velocity profile of the carrier phase liquid in the slug region. Figure 6.5 shows the comparison of the variation of the fully developed velocity profile achieved from the CFD study and that calculated using Eq. (6.12). It can be seen that a close match is observed between the velocity profiles obtained from the present simulation and the analytical correlation.

$$u_x = 6u_{TP}\frac{y}{h}\left(1-\frac{y}{h}\right) \tag{6.12}$$

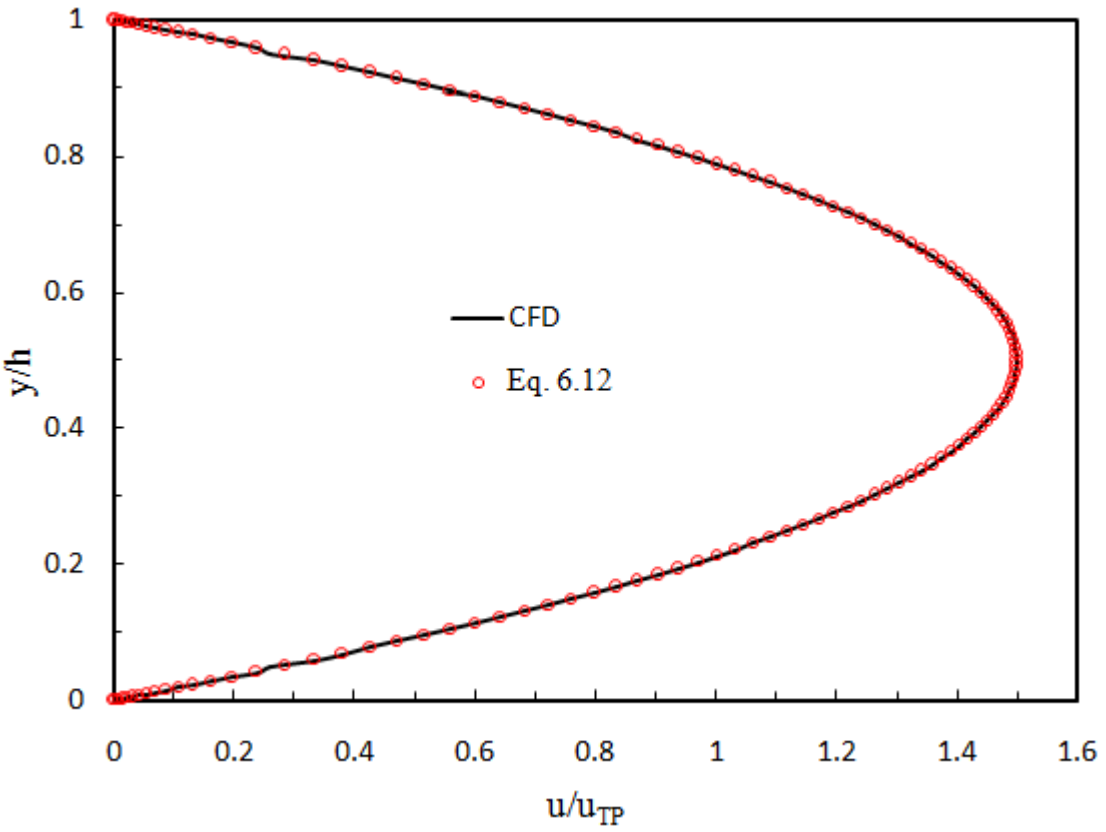

Fig. 6.5. Comparison of the centreline velocity in the liquid zone obtained from the present CFD study and analytical correlation Eq. (6.12) (u_{TP} = 0.22m/s, L_S = 280µm, L_D = 115µm).

6.3.3 *Hydrodynamics*

6.3.3.1 Comparison of droplet shape obtained from SDM and MDM

The slug flow problem can be numerically solved by two approaches namely stationary domain method (SDM) and moving domain method (MDM) (Asadolahi et al. 2011). In the former method, the flow problem needs to be solved by considering the entire computational domain. In such a method, the flow is first allowed to develop fully. To achieve this, the channel walls are prescribed with a temperature equal to the incoming fluid temperature till the hydrodynamic entrance length. The rest of the length of the channel walls is prescribed with higher temperature or heat flux boundary condition to solve the actual heat transfer problem. It should be noted that user-defined C routines have been used in the present study for the formation of continuous oil droplets while using SDM approach by following the guidelines of Asadolahi et al. (2011). In the latter method, due to the periodic nature of the Taylor flow, the flow and heat transfer problem could be solved in a unit cell. A unit cell comprises of a liquid droplet at the center of the microchannel with two halves of the carrier phase liquid surrounding the droplet. In this method, only the flow equations are solved first

to allow the flow to become fully developed after which the energy equation is solved alone to achieve a thermally developed flow. Figure 6.6(a) compares the droplet shape obtained from both the methods. The droplet shapes were found to be similar in both cases without much difference. Figure 6.6(b) graphically depicts the droplet profiles obtained from both the methods. For comparison purpose, the tails of the droplet were made coincident. It can be seen that the droplet profile obtained from MDM closely matches with the droplet profile obtained from the SDM. Since MDM saves a considerable amount of computational time in contrast to the SDM, it has been used in all further simulations.

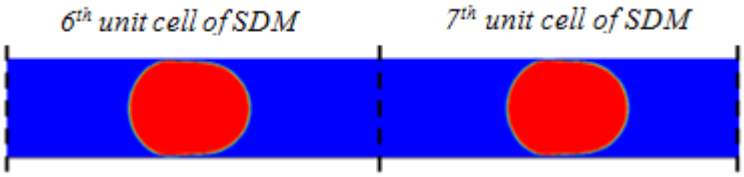

(a)

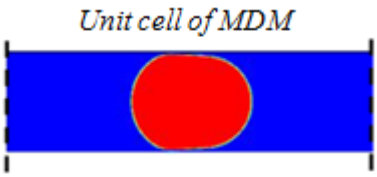

(b)

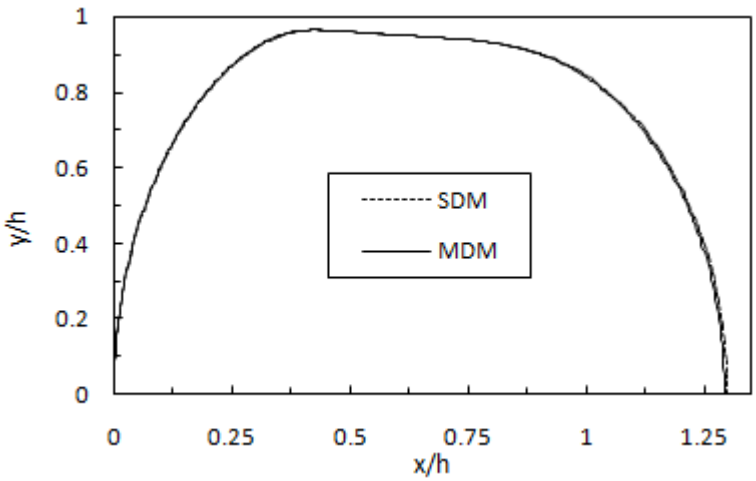

(c)

Fig. 6.6. (a) Contours of the volume fraction of oil droplet obtained using SDM, (b) Contours of the volume fraction of oil droplet obtained using MDM, and (c) Oil droplet profiles obtained using SDM and MDM in the absence of wall modulation (u_{TP} = 0.22m/s, L_S =

280µm, L_D = 115µm). In Figs. 6 (a) and (b), the oil droplets and liquid water slugs are shown in red and blue colors, respectively.

6.3.3.2 Effects of frequency and amplitude of the modulated wall motion on the droplet shape, film thickness, and pressure drop

As mentioned earlier, the walls of the microchannel were subjected to modulated velocity in the transverse direction of the flow (Fig. 6.1). The experimental studies of Shariff (2011) demonstrate the enhancement in flow boiling heat transfer in microchannel when the walls are subjected to high-frequency acoustic vibrations. Whitehill et al. (2010) investigated the influence of low-frequency vibration of droplets (60 to 200 Hz) in the direction normal to the glass slide on which they sit. In the present study, the frequency of the modulated motion of the wall was varied using lower frequencies in the sonic range i.e. $0 < \omega < 750\pi$ rad/s to examine its influence on the flow physics of the Taylor flow. Since the maximum heat transfer rate was obtained at a frequency of 250π rad/s for the selected range of frequencies and capillary numbers ($0.044 < Ca < 0.022$), we restricted our studies to this range of frequency. Figure 6.7 shows the fully developed profiles of the droplet obtained for different values of modulation frequencies. Although the droplet profiles look similar to each other, there exist small instabilities at the interface due to wall modulation. Similar findings can be observed in Fig. 6.8 which shows the droplet profiles obtained by varying the amplitude of the modulated velocity up to four folds w.r.t the base velocity. It can be clearly observed from the figure that small instabilities occur at the two-phase interface when the amplification factor changes from 0 to 4. These instabilities occur due to the existence of small vortices between the wall and interface which will be discussed in detail in subsequent sections. These instabilities alter the heat transfer rates as well. The insets in Fig. 6.7 and Fig. 6.8 give a closer view of droplet profiles in the regions highlighted by dashed rectangular boxes. It should be noted that, in the present study, the range of amplification factor of the modulated wall motion has been selected in a manner such that at any given instant of time the displacement of the wall (i.e. $a\Delta x$) caused due to the modulated motion would not cross the thin film region in the transverse direction. It should also be noted that the film region was captured using near-wall mesh treatment having approximately 10 elements in the film region. However, the maximum displacement of the walls was restricted to a maximum of four elements to avoid the possibilities of rupture of liquid droplets at higher displacements.

Figure 6.9 shows the variation of liquid film thickness with the amplitude of the modulated wall motion. The film thickness has been found to be decreasing for lower values of the amplification factor up to unity. However, the film thickness remained nearly same on further increase in amplification factor up to 4. Figure 6.9 also depicts the comparison of the measured film thickness for different values of the amplitude of modulation with the film thickness calculated using the semi-empirical models proposed by Bretherton (1961), and Aussillous and Quere (A&Q) (2000). The difference between the numerical results and that obtained from the correlations could be attributed to the fact that Bretherton's and Aussillous and Quere's models hold good for slug flows having uniform film thickness inside a circular channel. However, the present study deals with the slug flow inside rectangular microchannel having non-uniform film thickness.

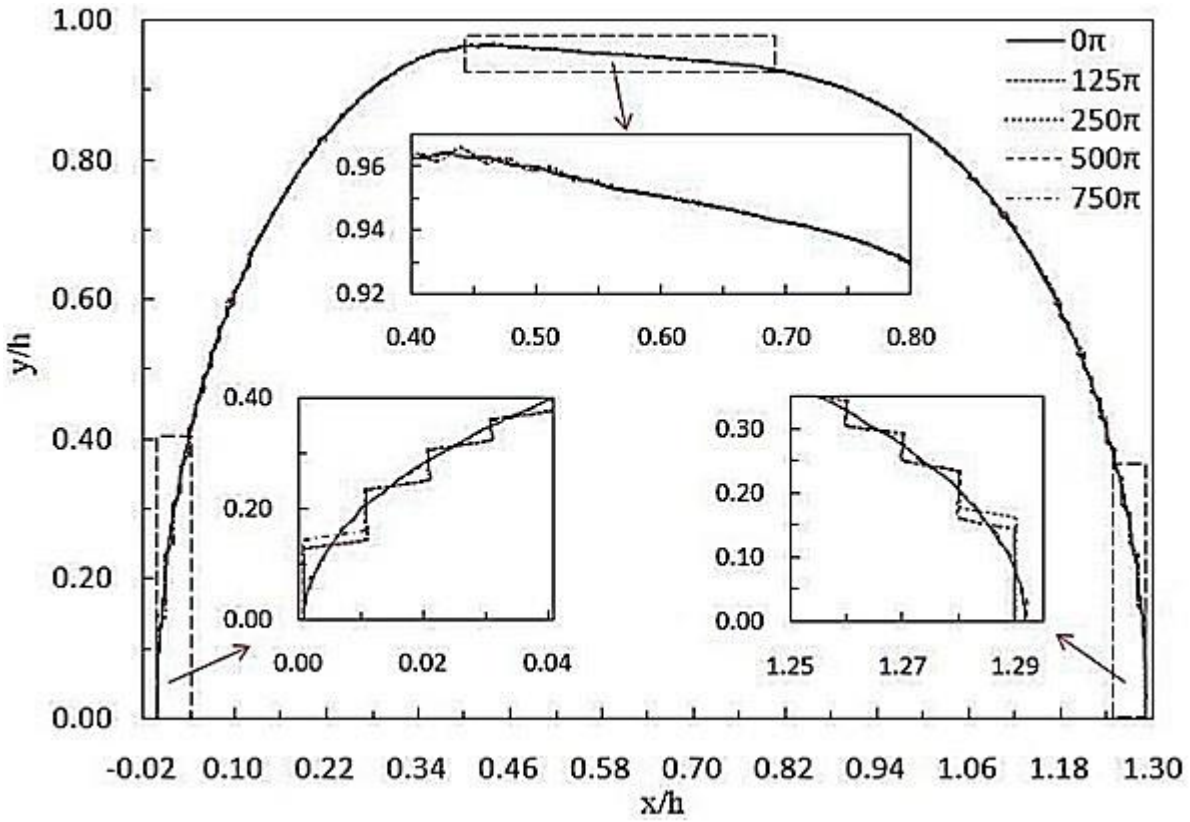

Fig. 6.7. Droplet shape with varying frequency (u_{TP} = 0.22m/s, L_S = 280µm, L_D = 115µm).

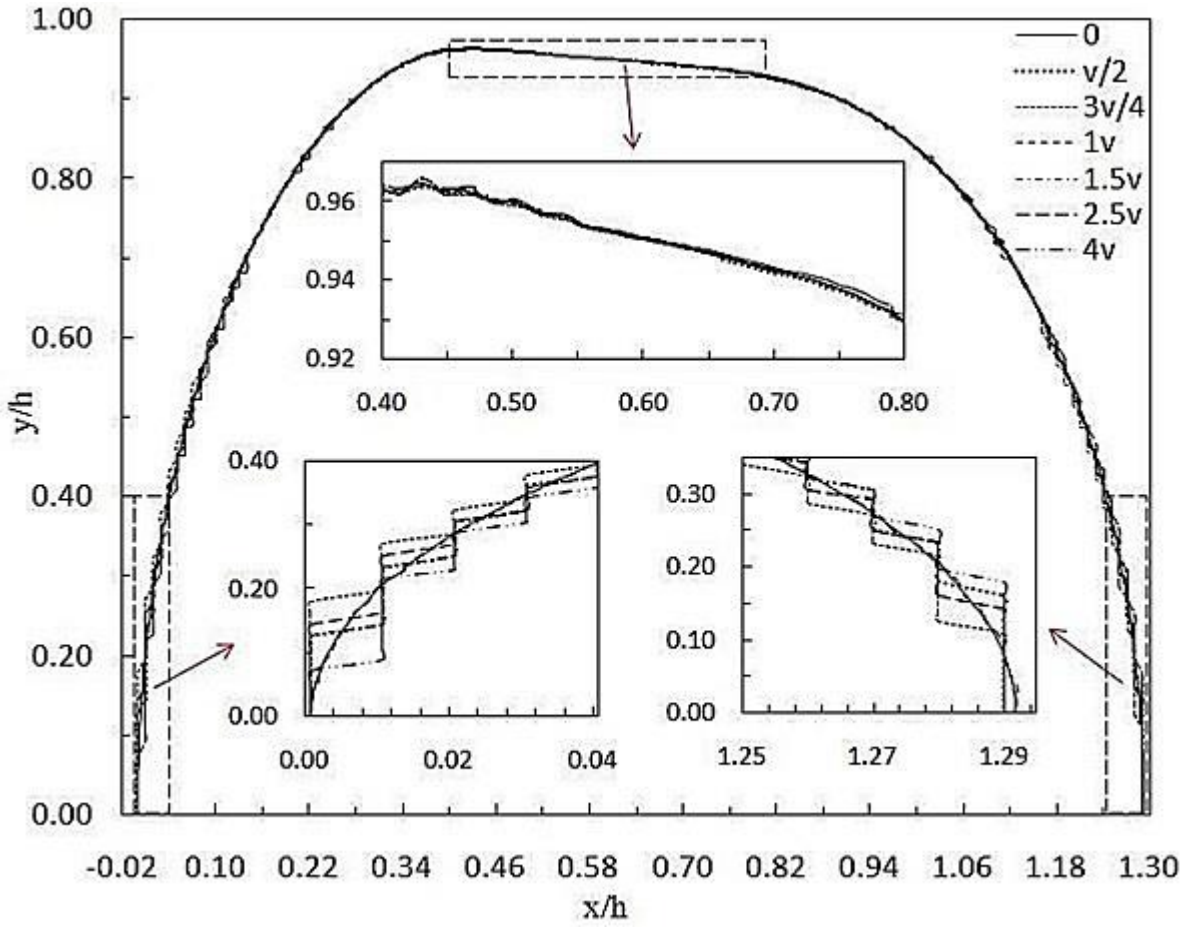

Fig. 6.8. Droplet shape with a varying amplitude (u_{TP} = 0.22m/s, L_S = 280μm, L_D = 115μm).

Aussillous and Que're's model:

$$\frac{\delta_F}{R} = \frac{1.34Ca^{2/3}}{1 + 3.34Ca^{2/3}} \tag{6.13}$$

The instabilities at the interface near the wall occur due to sharp pressure jumps across the interface when the frequency of the modulated motion is changed. Figure 6.10 depicts the contours of static pressure inside the microchannel with varying the frequency of the modulated motion. The presence of high-pressure zones at the interface near the channel walls could be clearly seen in the figure. The pressure at the interface nearer to walls was found to be highest at a frequency of 250π rad/s, as shown in Fig. 6.10(b). The enlarged view of the high pressure zones at the interface has been shown next to the figure. In multiphase flows, the viscous pressure drop and the interfacial pressure drop (also called Laplace pressure) are the two contributing terms in the overall pressure drop.

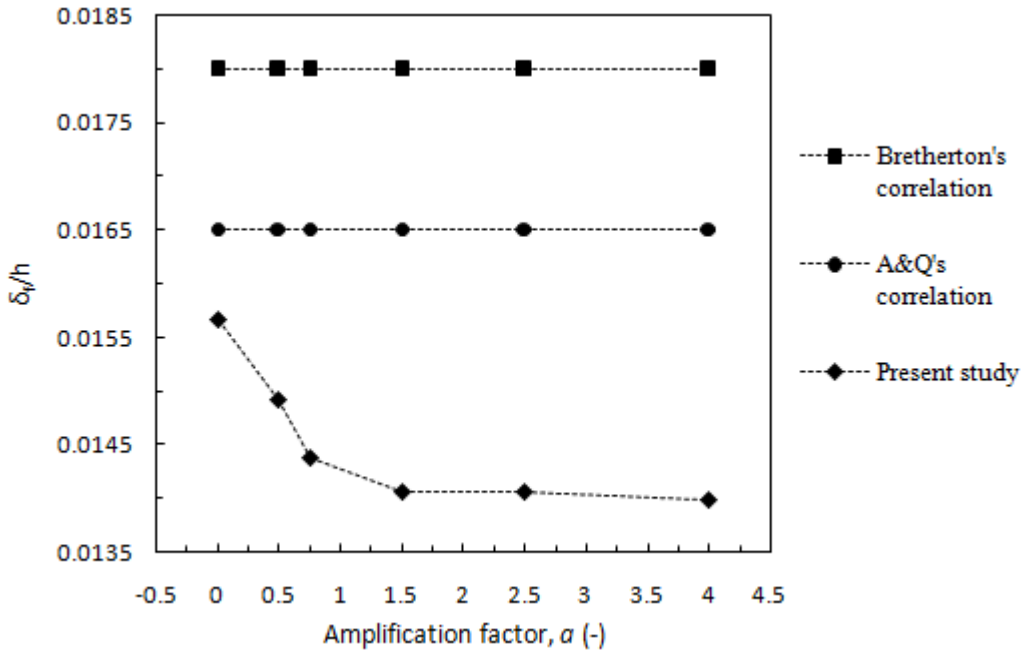

Fig. 6.9. Comparison of film thickness obtained from the present study and some standard models (u_{TP} = 0.22m/s, L_S = 280µm, L_D = 115µm).

The fluid friction at the channel walls leads to the viscous term and the interfacial pressure drop arises due to surface tension between the phases. In addition, the overall pressure drop in slug flow occurs due to three major factors: (a) slug (ΔP_{slug}); (b) film (ΔP_{film}); and (c) the interfacial ($\Delta P_{interface}$) pressure drops (Abiev 2015; Gupta et al. 2013). Figure 6.11 depicts the wall and centerline pressure along the length of the channel at a modulation frequency of 250π rad/s. The region under the top horizontal line shows the portion of the channel covered by the droplet, whereas, the rest of the region represents the portion covered by the continuous phase liquid. The pressure difference between the neighboring carrier phase liquid and the dispersed phase droplet is known as Laplace pressure. The centerline pressure in the droplet region increases in order to balance the interfacial tension force. The curvature of the droplet is stronger (bigger) at the nose and weaker (smaller) at the tail, hence, the nose has a smaller radius of curvature and the tail has a bigger radius of curvature (Fig. 6.7). The key reason for this difference in the radii of curvature of the menisci could be attributed to the higher pressure drop at the frontal interface with respect to the rear interface.

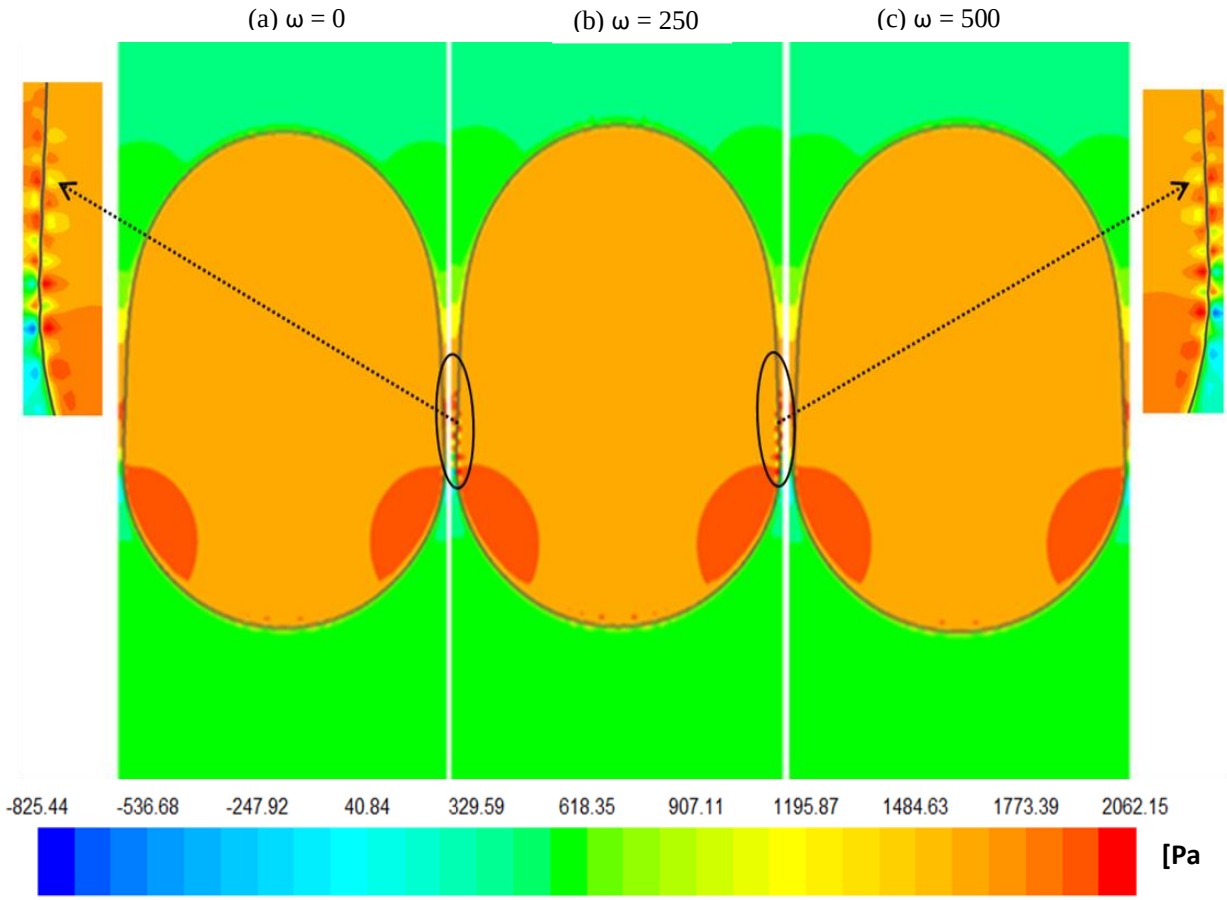

Fig. 6.10. Contours of pressure along with the droplet shape for different frequencies at a fixed amplitude of v_o (u_{TP} = 0.22m/s, L_S = 280µm, L_D = 115µm).

Slug pressure drop can be evaluated from Plane-Poiseuille's equation (Eq. 6.14) due to fully developed flow in the primary phase slug. The same equation was also used by Gupta et al. (2013) in their liquid-liquid Taylor flow study where hexadecane and water were used as continuous and dispersed phases respectively.

$$\Delta P_{slug} = \frac{8\mu_c L_s u_{TP}}{R^2} \tag{6.14}$$

Fouilland et al. (2010) assumed random pressure gradients at the annulus and core. They gave a solution for velocity profile using an analytical, annular, laminar-laminar flow solution for gas-liquid Taylor flows, whereas, Gupta et al. (2013) derived an expression for evaluating the film pressure drop considering equal pressure gradients, unlike arbitrary gradients. (Eq. 6.15).

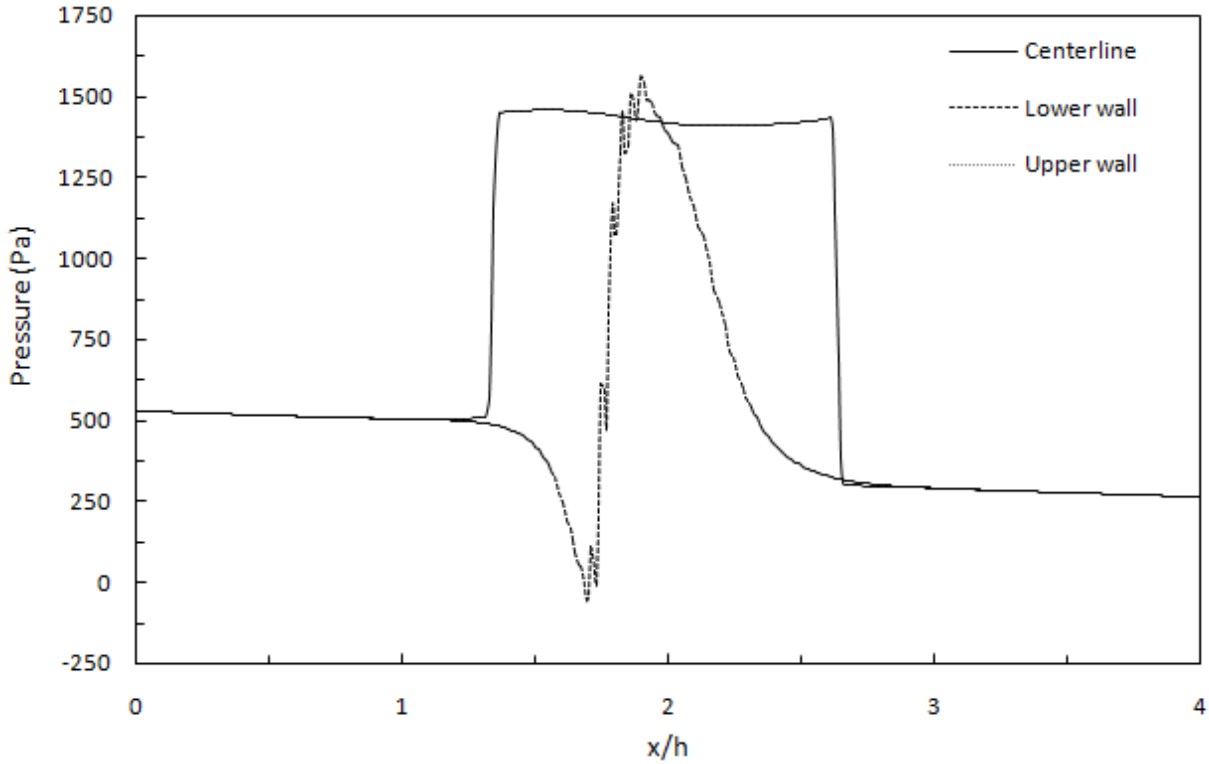

Fig. 6.11. Wall and axial pressure for ω = 250π rad/s and $v = 1v_o$ (u_{TP} = 0.22m/s, L_S = 280μm, L_D = 115μm).

$$\Delta P_{film} = \frac{8\mu_c L_{film} u_{TP}}{R^2(1+[(R_i{}^4)/(R^4)][(1/\lambda)-1]} \tag{6.15}$$

For the evaluation of interfacial pressure drop, Bretherton (1961) proposed an expression which is given in Eq. (6.16). The total pressure drop over a unit cell length, given by Eq. (6.17), can be obtained by summating Eq. (6.14), Eq. (6.15), and Eq. (6.16).

$$\Delta P_{interface} = 4.52\frac{\sigma}{R}(3Ca)^{2/3} \tag{6.16}$$

$$\left(\frac{\Delta P}{L}\right)_{UC} = \frac{8\mu_c u_{TP}}{R^2}\frac{L_s}{L_{UC}} + \frac{8\mu_c u_{TP}}{R^2[(1+(R_i{}^4)/(R^4))((1/\lambda)-1)]}\frac{L_{film}}{L_{UC}} + \frac{4.52}{L_{UC}}\frac{\sigma}{R}(3Ca)^{2/3} \tag{6.17}$$

Figure 6.12 compares the normalized pressure drop in the microchannel obtained from the present simulations and Eq. 6.17. A significant deviation in the overall pressure drop was observed between the numerical results and those obtained from the model, lying

within 35% mean absolute deviation. It should be noted that the model was proposed for circular channels, whereas, in the present study, a two-dimensional analysis has been performed using a non-circular channel with an assumption that the length of the channel in the third dimension is very high as compared to its height. Due to this reason, the effect of the third dimension on the flow properties of the two-phase flow has been neglected. However, for practical applications, the length of the channel in the third dimension is of a finite size which influences the property values inside the flow domain. Hence, a thorough three-dimensional numerical study is required to examine the validity of the model in predicting the pressure drop.

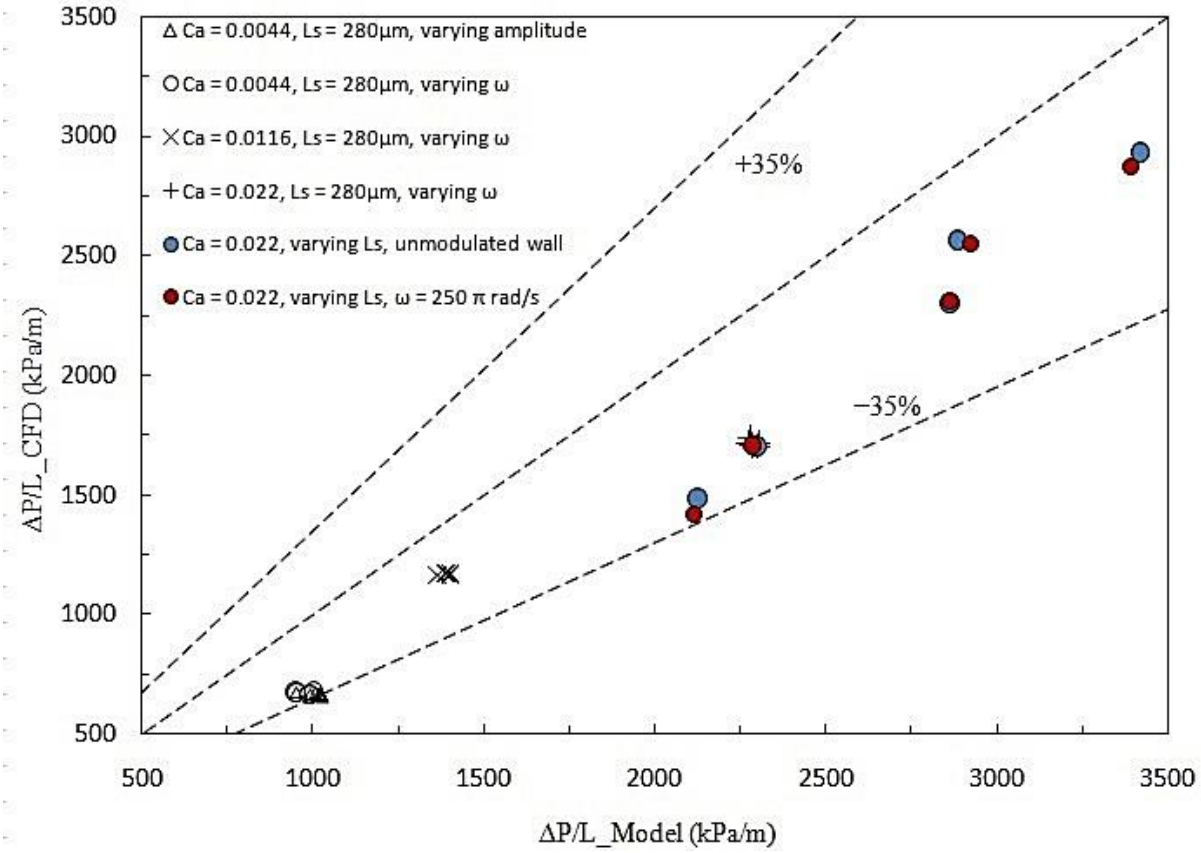

Fig. 6.12. Comparison of pressure drop per unit length obtained from simulations and Eq. 27 ($100 < L_S < 310$ μm, $85 < L_D < 295$ μm, $0.0044 < Ca < 0.022$, $0 < \omega < 750\pi$ rad/s, $0 < a < 4$).

6.3.4 *Heat transfer*

Heat transfer studies have also been carried out in the present work to explore the effect of wall modulation on the heat transfer performance of the slug flow inside the microchannel. The heat transfer rate in a fully developed single-phase flow or slug flow is represented by a non-dimensional number called Nusselt number (Incropera and Dewitt 2002), which is given by:

$$Nu = \frac{q_w}{(T_{w_{avg}} - T_{B_{avg}})} \frac{D_h}{k_C} \tag{6.18}$$

It should be noted that only the thermal conductivity of the carrier phase is considered in Eq. (6.18) because only the carrier phase remained in contact with the walls of the channel in the studies due to the existence of the thin film of the carrier phase between the walls and the interface. If the flow is a sliding slug flow then one needs to consider the thermal conductivity of the dispersed phase too for evaluating the two-phase Nusselt number. Since the Taylor flow is periodic in space as well as in time, the average wall and bulk mean temperature were obtained as follows:

$$T_{w_{avg}} = \frac{\int_t^{t+T} \int_x^{x+L_{UC}} T_w dx dt}{\int_t^{t+T} \int_x^{x+L_{UC}} dx dt} \tag{6.19}$$

$$T_{B_{avg}} = \frac{\int_t^{t+T} \int_x^{x+L_{UC}} \int_A \rho |u_x| c_P T dA dx dt}{\int_t^{t+T} \int_x^{x+L_{UC}} \int_A \rho |u_x| c_P dA dx dt} \tag{6.20}$$

6.3.4.1 Validation

Prior to slug flow studies, a single phase flow and heat transfer study of water under a constant wall heat flux of 420kW/m^2 were carried out using SDM. The heat transfer results were compared with the analytical value of thermally developed flow inside the microchannel having same dimensions as that mentioned in Fig. 6.1. Analytically, the Nusselt number of a thermally developed flow inside a channel under constant wall heat flux is equal to 8.23 (Shah and London 1972). Table 6.3 compares the single-phase Nusselt number which obtained in the CFD study with the analytical value of the single-phase Nusselt number. The single-phase Nusselt number achieved in the present study, which is equal to 8.20, was found be in reasonable with the analytical value (i.e. 8.23).

6.3.4.2 Comparison of two-phase heat transfer obtained from SDM and MDM

In the two-phase studies, initially, the study on LL Taylor flow inside the microchannel without wall velocity modulation was carried out using SDM and MDM approaches to check the consistency of the MDM approach. It can be seen in Table 6.3 that the fully developed value of the two-phase Nusselt number obtained from both the methods is very close to each

other without much deviation. In addition, the two-phase heat transfer rate shows a clear augmentation in the heat transfer performance by approximately 77% as compared to the liquid-only flow. Various researchers have also reported such improvement in the heat transfer performance using LL slug flows in their studies (Bandara et al. 2015b, Dai et al. 2015, Asthana et al. 2011, Eain et al. 2015). It should be noted that in SDM only the zone under the higher temperature walls should be considered for the evaluation of heat transfer rates by excluding the zone under the lower temperature walls since it does not play any role in the heat transfer process. Also, one should allow at least 3 to 4 leading droplets to surpass the high temperature zone from the outlet of the domain before evaluating the heat transfer rate of the thermally developed unit cell in SDM.

Table 6.3 Nusselt numbers for single phase flow obtained from analytical correlation and CFD study, and the Nusselt numbers for two-phase flow with and without modulated wall motion obtained from the CFD study.

Approach/method	**Nusselt number**
Single phase flow (Analytical)	8.23
Single phase flow (CFD)	8.20
Two-phase flow without modulated wall motion (SDM) (u_{TP} = 0.22m/s, L_S = 280µm)	14.26
Two-phase flow without modulated wall motion (MDM) (u_{TP} = 0.22m/s, L_S = 280µm)	14.48
Two-phase flow with modulated wall motion (u_{TP} = 0.22m/s, L_S = 280µm, $v = 1v_o$, $\omega = 250\pi$ rad/s) (MDM)	14.96
Two-phase flow with modulated wall motion (u_{TP} = 0.22m/s, L_S = 280µm, $v = 4v_o$, $\omega = 500\pi$ rad/s) (MDM)	15.23

6.3.4.3 Influence of the frequency of modulated wall velocity on the two-phase heat transfer

The heat transfer performance of the microchannel having oil-water Taylor flow under modulated wall motion has been evaluated at different frequencies of the modulated velocity. The influence of the frequency on the slug flow heat transfer at a fixed amplitude and a mixture velocity of 0.22m/s is depicted in Fig. 6.13. The two-phase Nusselt number increases from 14.48 to 14.96 with an increase in the modulation frequency from 0 to 250 π rad/s. However, a further increase in the frequency has resulted in a decrease of the Nusselt number. Hence, the Nusselt number is found to have a maximum value at a frequency of 250 π rad/s when all other conditions were fixed. The slug length and the film thickness of the

carrier phase remained almost same for different values of the frequency as can be seen in Fig. 6.7. However, there is a huge variation in the Nusselt number. In order to understand this, one should look at the streamlines and the temperature distribution inside the domain at different values of frequency. Figure 6.14 shows the streamlines of the flow in the droplet frame of reference along with the interface at different values of modulation frequency. It can be seen from the figure that there exist some small vortices at the interface near the walls in almost all the cases. The intensity of these vortices was found to be highest for a frequency of 250 π rad/s in contrast to the other cases. In addition, the number of vortices was high in number for the case of $\omega = 250\ \pi$ rad/s over other cases. The enlarged view of these vortex zones at the interface has also been shown beside the figure. Because of these vortices, the carrier phase fluid between the wall and the interface recirculates in the vortex region which aids in the heat transfer enhancement. Figure 6.15 shows the non-dimensional temperature distribution inside the computational unit cell for different values of frequency. As shown earlier in Fig. 6.14, the presence of vortices recirculate the carrier phase fluid inside the domain for a longer time at $\omega = 250\ \pi$ rad/s. This allows a deeper penetration of the wall heat flux from the walls of the channel to the interior region of the domain in contrast to the other cases where the intensities of recirculation were found to be lower. It can be seen from the temperature contours that the thermal heat flux from the channel walls almost reached the centerline of the channel for $\omega = 250\pi$ rad/s unlike in other cases.

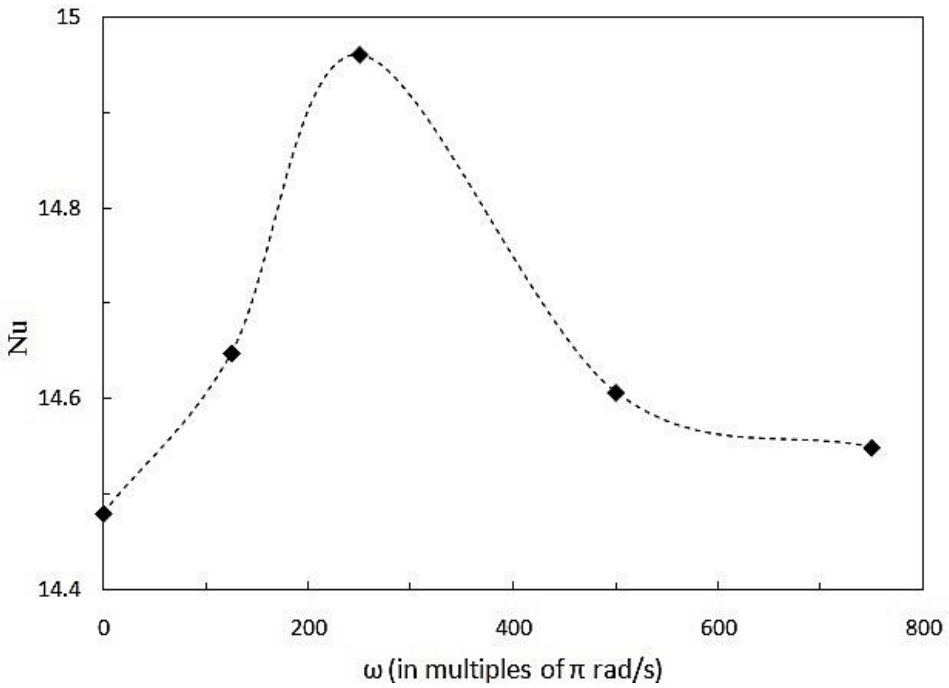

Fig. 6.13. Nusselt number for different frequencies of the modulated wall motion at a fixed amplitude $v = 1v_o$.

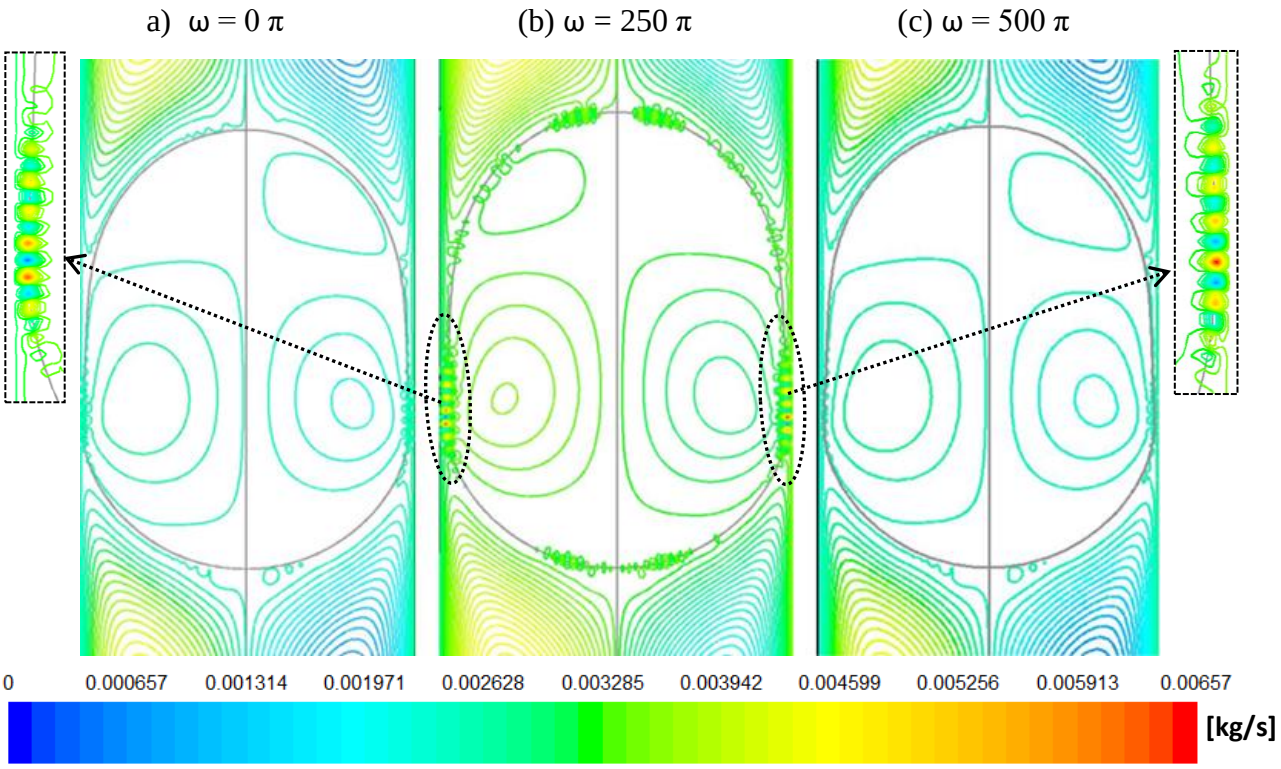

Fig. 6.14. Streamlines with droplet shape for different frequencies of the modulated wall motion at a fixed amplitude $v = 1v_o$.

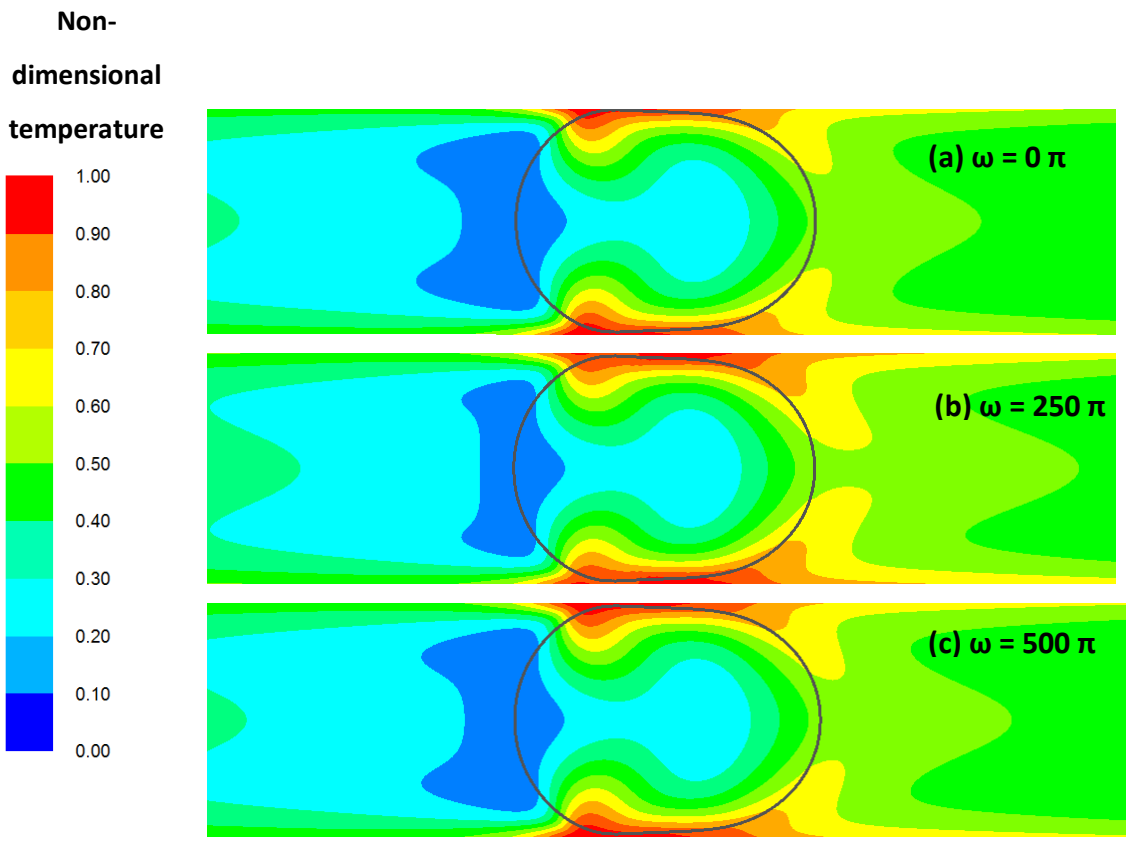

Fig. 6.15. Non-dimensional temperature contours with droplet shape for different frequencies of the modulated wall motion at a fixed amplitude $v = 1v_o$.

6.3.4.4 Influence of the amplitude of modulated wall velocity on the two-phase heat transfer

The influence of the amplitude of modulated wall motion on the heat transfer of LL Taylor flow has also been studied at a fixed frequency of 500π rad/s and a mixture velocity of 0.22m/s. The variation of the Nusselt number with the amplitude of modulated wall motion is depicted in Fig. 6.16. The Nusselt number was found to increase from 14.48 for an amplification factor of 0 to 15.23 for an amplification factor of 4. The Nusselt number showed an independent relationship with the amplitude of the modulation. Figure 6.17 shows the streamlines of the flow for different values of the amplification factor of the modulated wall motion. It can be seen that there exist small vortices at the interface near the walls in almost all cases. The intensity of these vortices was found to be increasing with the increase in the amplification factor. Figure 6.18 shows the non-dimensional temperature distribution for different values of the amplitude. It can be clearly seen that the heat transfer from the walls of the domain propagates increasingly with an increase in the amplitude.

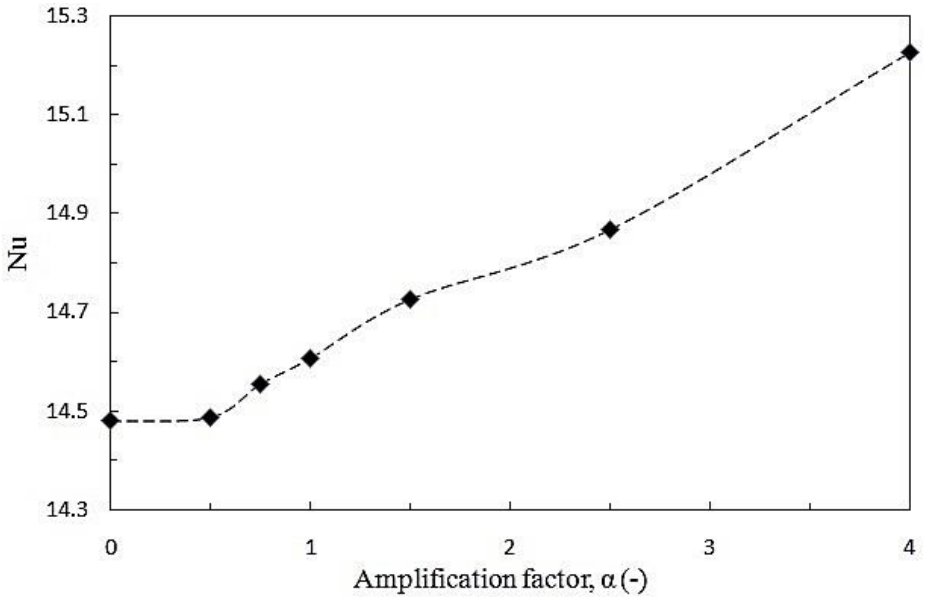

Fig. 6.16. Nusselt number for different amplitude of the modulated wall motion at a fixed frequency of ω = 500π rad/s.

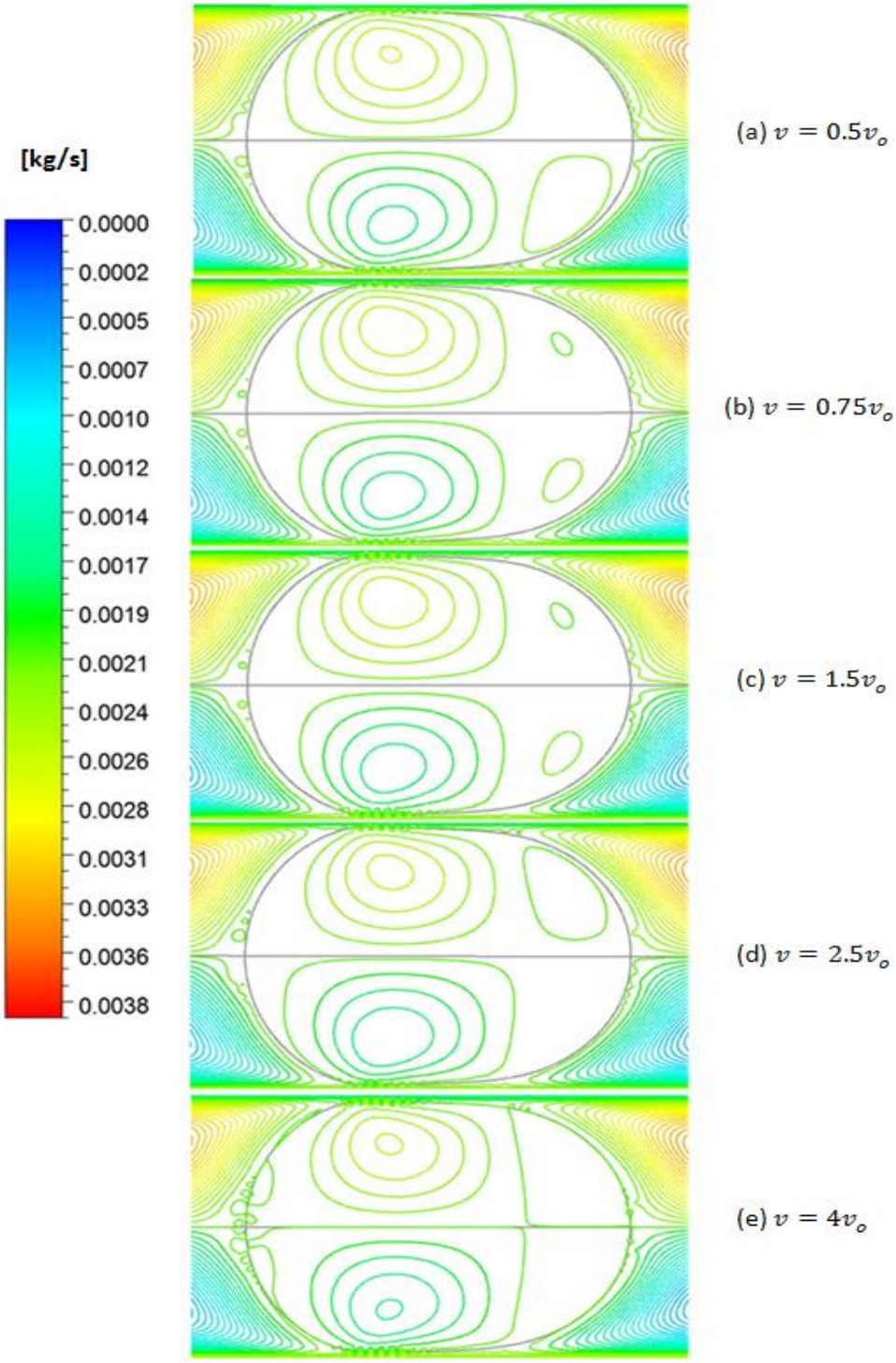

Fig. 6.17 **S**treamlines with droplet shape for different amplitude of the modulated wall motion at a fixed frequency of $\omega = 500\pi$ rad/s.

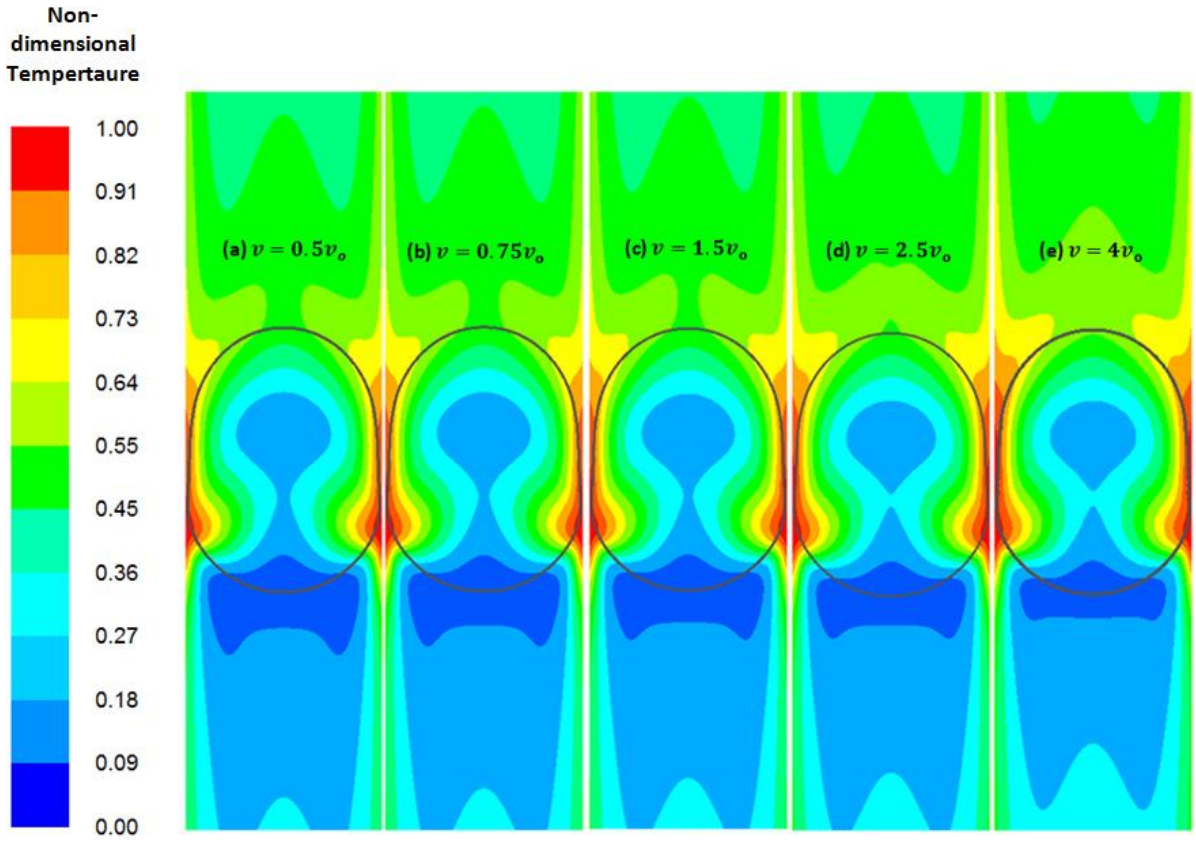

Fig. 6.18. Non-dimensional temperature contours with droplet shape for different amplitude of the modulated wall motion at a fixed frequency of ω = 500π rad/s.

6.3.4.5 Effect of Capillary number on heat transfer under modulated wall motion

The capillary number studies have been performed for the unmodulated as well as modulated wall ($125 < \omega < 750\pi$ rad/s) motion cases. In both the cases, the capillary number of the carrier phase fluid was varied in the range $0.0044 < Ca < 0.022$ (i.e. $0.22 < u_{TP} < 1.1$m/s) keeping other parameters fixed. The droplet and slug lengths were kept constant having values 115µm and 280µm, respectively and a constant heat flux of 420kW/m^2 was prescribed over the walls of the microchannel. Figure 6.19 shows the variation of Nusselt number as a function of capillary number. For the present oil-water system in the unit cell, Nusselt number was found to increase with the increase in capillary number in both the cases. It should be noted that the film thickness was found to increase with the capillary number and the non-uniformity in the film thickness also got increased. At higher capillary numbers, the tail of the droplet became flat with its nose being sharper. This observation is in accordance with the studies of Olbricht and Kung (1963) and Goldsmith and Mason (1992) who reported the presence of such non-uniform film region. Despite the increase in film thickness, the heat transfer rates increased with the capillary which signifies the predominance of convective

heat transfer over conductive heat transfer during the two-phase flow. The heat transfer rates in the modulated wall motion case have been found to be superior in contrast to the unmodulated wall motion case for the chosen range of capillary numbers, as shown in Fig. 6.19. Although the increase in Nusselt numbers at different frequencies of the modulated wall motion was small for the lowest capillary number (maximum increase of approximately 3% at modulation frequency of 250π rad/s), the heat transfer rate improved significantly by an approximate enhancement of up to 23% for the highest capillary number at modulation frequency of 250π rad/s. This implies that higher heat transfer rates could be achieved by providing modulated motion to the microchannel walls. The inference made in section **6.4.3** holds good for the present finding also.

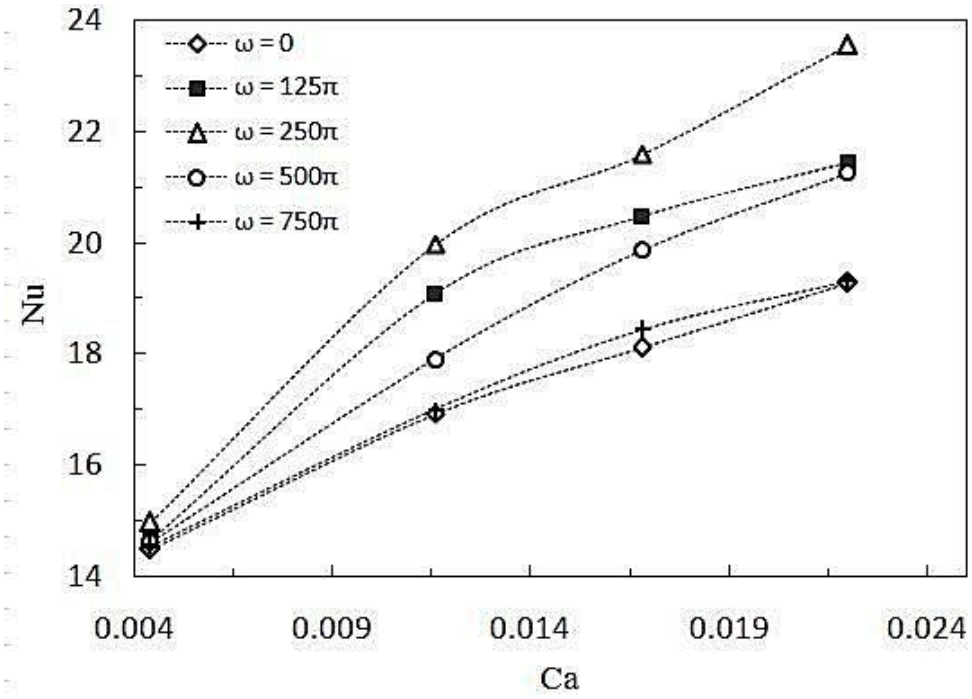

Fig. 6.19. Variation of Nusselt number with Capillary number (L_D = 115µm, L_S = 280µm).

6.3.4.6 *Effect of slug length on heat transfer under modulated wall motion*

Figure 6.20 depicts the impact of liquid slug length on the heat transfer rates for the oil-water system at a given mixture velocity of 1.1 m/s. The slug and droplet lengths were varied in the range $100 < L_S < 310$µm and $85 < L_D < 295$µm, respectively keeping the length of the unit cell constant. The studies were carried out for unmodulated as well as modulated wall motion ($v = 1v_o$ and ω = 250π rad/s) of the microchannel. The heat transfer rate was found to increase with an increase in the liquid slug length from 100 to 280µm for both cases of wall

motion which signifies the importance of smaller and longer droplets in the heat transfer process. On further increase in the liquid slug length, the Nusselt number decreased which implies that the heat transfer rate improves significantly in the presence of shorter droplets. The heat transfer rates improved by 11 to 23% under the modulated wall motion with respect to the unmodulated case. Some researchers have reported that the heat transfer rate enhances with the increase in droplet size in a LL Taylor flow (Che et al. 2015, Dai et al. 2015). However, the reverse has been witnessed in the present study. Recently, Sadhana et al. (2019) reported similar observation in their GL Taylor flow study inside a circular capillary. They reported an improvement in the heat transfer rate with shorter Taylor bubbles having a non-dimensional equivalent sphere radius in the range ~1-1.55. The present work could be extended to explore the effect of non-dimensional equivalent sphere radius of a liquid droplet on the LL Taylor flow heat transfer since it is expected that shorter Taylor droplets may alter the heat transfer process.

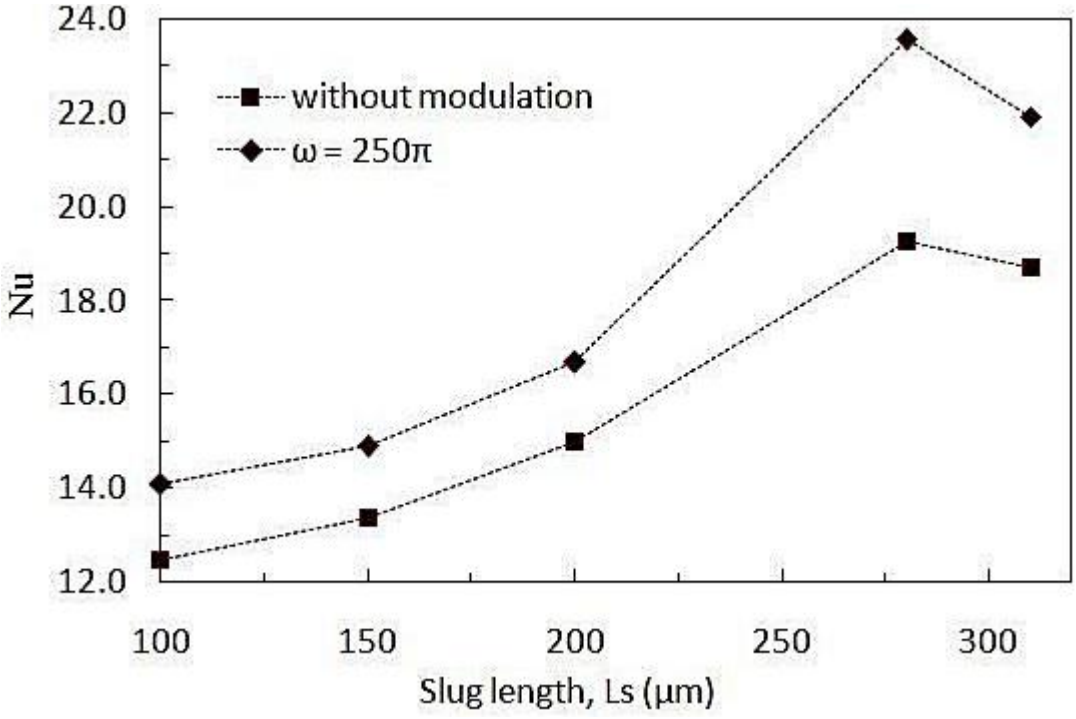

Fig. 6.20. Variation of Nusselt number with liquid slug length at a given mixture velocity of 1.1 m/s.

6.3.4.7 Heat transfer model

In their work, Dai et al. (2015) developed a generalized model (Eq. 6.28) to predict the Nusselt number in GL and LL Taylor flows. The equation was developed by fitting the GL results of Leung et al. (2012) together with the LL results obtained from their CFD simulations. Figure 6.21 shows the schematic diagram of the unit cell comprising one droplet

(bubble) zone (denoted by D), and two halves of the liquid slugs (slug zone denoted by S) on either side of the droplet. The total heat transfer process could be divided into three parts, namely: (i) heat transfer from wall to film, (ii) heat transfer from film to slug, and (iii) heat transfer from film to droplet. These three processes are indicated by 1, 2, and 3, respectively in the figure.

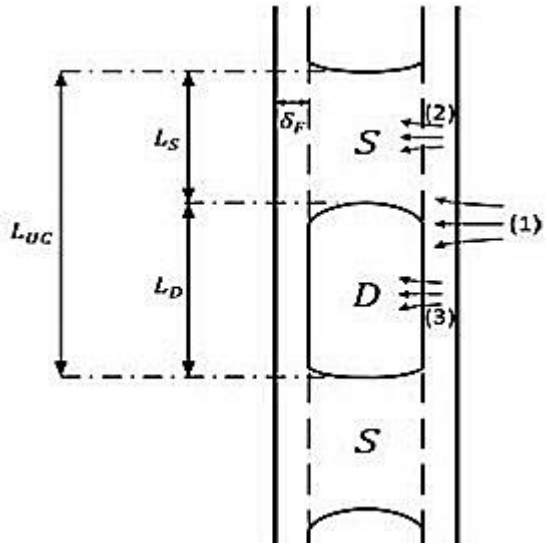

Fig. 6.21. Schematic diagram of the unit cell showing the heat transfer mechanisms from (i) wall to film, (ii) film to slug, and (iii) film to droplet (Dai et al. 2015).

For constant heat flux over the channel wall, the phase temperatures increase at the same rate when the flow is thermally fully-developed. The portion of the total wall heat flux taken up by the dispersed phase droplet can be written as:

$$\frac{Q_D}{Q_w} = \frac{\dot{m}_D c_{pD}}{\dot{m}_D c_{pD} + \dot{m}_C c_{pC}} = \frac{\rho_D \dot{V}_D c_{pD}}{\rho_D \dot{V}_D c_{pD} + \rho_C \dot{V}_C c_{pC}} = \frac{m}{m+1} \tag{6.21}$$

where

$$m = \frac{\rho_D \dot{V}_D c_{pD}}{\rho_C \dot{V}_C c_{pC}} = \left(\frac{\beta}{1-\beta}\right)\frac{\rho_D c_{pD}}{\rho_C c_{pC}} \tag{6.22}$$

Similarly,

$$\frac{Q_C}{Q_w} = \frac{1}{m+1} \tag{6.23}$$

For two-phase flows, the overall heat transfer coefficient is defined as:

$$Q_w = h_{TP}\, A_w\, (\bar{T}_w - \bar{T}_b) \tag{6.24}$$

where $\bar{T}_b$ is given as:

$$\bar{T}_b = \frac{\dot{V}_D \rho_D c_{pD} T_D + \dot{V}_C \rho_C c_{pC} T_S}{\dot{V}_D \rho_D c_{pD} + \dot{V}_C \rho_C c_{pC}} = \frac{m T_D + T_S}{1 + m} \tag{6.25}$$

where, T_S and T_D are the temperatures of slug and droplet, respectively given by Eqs. (6.26, 6.27):

$$T_S = T_{wS} - q_w \left[\frac{1}{h_{wS}} + \frac{L_{UC}}{L_S} \frac{1}{m+1} \frac{1}{h_{FS}}\right] \tag{6.26}$$

$$T_D = T_{wD} - q_w \left[\frac{1}{h_{wD}} + \frac{L_{UC}}{L_D} \frac{m}{m+1} \frac{1}{h_{FD}}\right] \tag{6.27}$$

where T_{wD} and T_{wS} are wall temperatures in droplet and slug regions, respectively, and are considered equal to the wall temperature (T_w). h_{wS}, h_{wD}, h_{FS}, and h_{FD} are the heat transfer coefficients between the: (i) wall and liquid film in slug region, (ii) wall and liquid film in droplet region, (iii) film and liquid slug, and (iv) film and droplet, respectively. h_{wS} and h_{wD}, are assumed to be equal to wall heat transfer coefficient (h_w).

Substituting Eqs. (6.25) and (6.26), (6.27) into Eq. (6.24), the overall heat transfer resistance for two-phase flow can be given as:

$$\frac{1}{h_{TP}} = \frac{1}{h_w} + \frac{L_{UC}}{L_D} \left(\frac{m}{m+1}\right)^2 \frac{1}{h_{FD}} + \frac{L_{UC}}{L_S} \frac{1}{(m+1)^2} \frac{1}{h_{FS}} \tag{6.28}$$

The heat transfer coefficient from wall to film, having film thickness (δ_F), can be obtained by applying Fourier's law of heat conduction Eq. (6.29):

$$h_w = \frac{k_C}{\delta_F} \tag{6.29}$$

The heat transfer coefficient from film to slug (h_{FS}) can be written as:

$$h_{FS} = 4.364 \frac{d}{k_c} + \frac{0.171 \frac{d}{k_c}}{{L^*}_S + 0.0663 {L^*}_S^{1/3}} \tag{6.30}$$

Similarly, the heat transfer coefficient from film to droplet (h_{FD}) can be written as:

$$h_{FD} = \frac{\frac{L_{UC}}{L_D}\left(\frac{m}{1+m}\right)^2}{\frac{1}{h_{TP}} - \frac{1}{h_w} - \frac{L_{UC}}{L_S}\frac{1}{(m+1)^2}\frac{1}{h_{FS}}} \tag{6.31}$$

where h_w and h_{FS} are evaluated according to Eqs. (6.29) and (6.30), respectively.

In dimensionless forms, the above mentioned overall heat transfer coefficient, as well as individual heat transfer coefficients, can be written as given below:

$$\frac{1}{Nu_{TP}} = \frac{1}{Nu_w} + \frac{L_{UC}}{L_D}\left(\frac{m}{m+1}\right)^2 \frac{1}{Nu_{FD}}\frac{k_C}{k_D} + \frac{L_{UC}}{L_S}\frac{1}{(m+1)^2}\frac{1}{Nu_{FS}} \tag{6.32}$$

where,

$$Nu_w = \frac{d}{\delta_F} = 5 + 1.5Ca^{-2/3} \tag{6.33}$$

$$Nu_{FD} = 4.364 + \frac{0.0894}{{L^*}_D + 0.0490{L^*}_D{}^{1/3}} \tag{6.34}$$

with ${L^*}_D = \frac{L_D/d}{Re_D Pr_D}$

$$Nu_{FS} = 4.364 + \frac{0.171}{{L^*}_S + 0.0663{L^*}_S{}^{1/3}} \tag{6.35}$$

with

${L^*}_D = \frac{L_S/d}{Re_{TP} Pr_C}$

The average Nusselt number (Nu_{avg}) for a unit cell has been calculated using Eq. (6.18). Figure 6.22 compares the heat transfer results obtained in the present numerical studies with the results evaluated using the model of Dai et al. (2015). Overall a good agreement is found between the numerical results and that obtained from the model, lying within ±15% deviation.

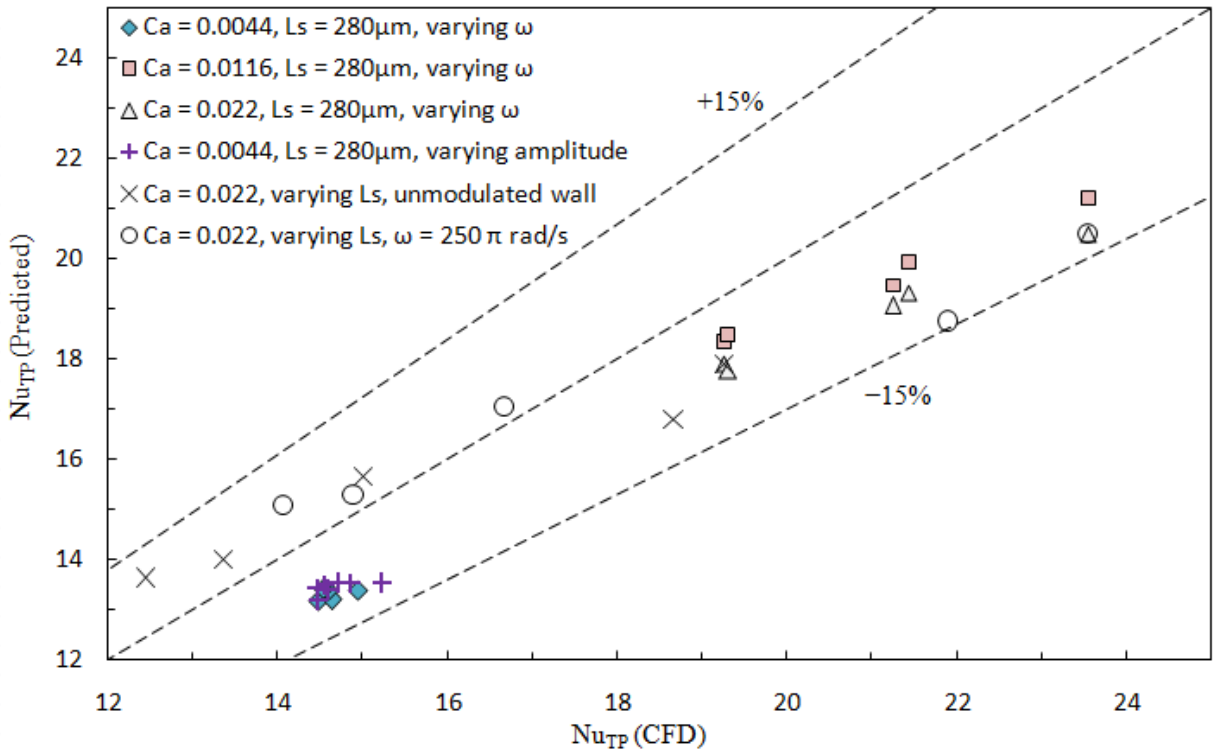

Fig. 6.22. Comparison of Nusselt numbers obtained from the present CFD studies and the model of Dai et al. (2015) ($100 < L_S < 310$ µm, $85 < L_D < 295$ µm, $0.0044 < Ca < 0.022$, $0 < \omega < 750\pi$ rad/s, $0 < a < 4$).

6.4 Summary

The numerical studies of the flow physics and heat transfer behaviour of oil-water Taylor flow inside a rectangular microchannel subjected to modulated wall motion have been discussed in this chapter. VOF method has been used to track the LL interface. The centerline velocity profile in the liquid slug region was found to be in a close match with the profile obtained using Plane-Poiseullie equation. The droplet shapes obtained using SDM and MDM approaches were found to be similar. Small instabilities were witnessed at the interface when the channel wall was subjected to modulated motion in the transverse direction of the flow. This happened due to sharp pressure jumps at the interface. The pressure at the interface nearer to walls has been found to be highest for a modulation frequency of 250π rad/s when the amplitude of the modulation was kept constant. The pressure drop in a unit a cell has also been compared with a pressure drop model. A mean absolute deviation lying within 35% was observed between the numerical results and those calculated using the model. Hence, a better formulation of pressure drop model for evaluating the pressure drop inside a rectangular channel is required. The film thickness of the carrier phase obtained from the numerical studies has been compared with standard models available in the literature for evaluating the

film thickness. Some deviations were found between the CFD results and the models since the effect of modulated motion were not considered in the models. Besides, the models are based on uniform film thickness, whereas, in the present studies, a region of non-uniform film thickness was witnessed.

Heat transfer studies were also carried out under a constant wall heat flux of 420kW/m^2. The average Nusselt number obtained from the simulation of a single-phase flow under constant heat flux condition was found to be in a close match with the analytical value of a fully developed single-phase flow. Later, two-phase LL Taylor flow heat transfer without any modulated wall motion was simulated using SDM and MDM approaches. The fully developed heat transfer results obtained from both the approaches have been found to be in a reasonable agreement. The two-phase heat transfer-rate was also found to be superior to single-phase heat transfer. The studies were then extended to explore the effects of capillary number ($0.0044 < Ca < 0.022$), frequency ($0 < \omega < 750\pi$ rad/s) and amplitude (in terms of the amplification factor, i.e. $0 < a < 4$) of the modulated wall velocity on the heat transfer rate of LL Taylor flow. The heat transfer rates of the slug flow under modulated wall motion of the microchannel improved by 77-186% over liquid-only flow as well as by ~0.47-23% in contrast to slug flow without modulated wall motion for the chosen range of capillary numbers and modulation frequencies. The intensity of vortices was found to be higher for $\omega = 250\pi$ rad/s, as well as the heat transfer from the channel wall to the interior of the domain, was faster at $\omega = 250\pi$ rad/s in contrast to other values of ω. The heat transfer rate was found to vary independently on increasing the amplification factor of the modulated wall motion. This augmentation in the heat transfer could be attributed to the increasing intensity of the vortices at the two-phase interface as well as the better propagation of heat from the channel wall to the core of the domain. The heat transfer rates under modulated wall motion also improved by 11 to 23% with respect to the unmodulated case on varying the slug length. The numerical heat transfer results were compared with the phenomenological model available in the literature for evaluating two-phase Nusselt number in slug flow regime. The numerical results were found to be in close agreement with the results obtained from the model lying within ±15% deviation.

CHAPTER 7

Numerical Study on Evaporation Heat Transfer Characteristics In Inclined Microchannels With Varying Inlet Vapor Quality

7.1 Introduction

Flow boiling inside microchannels has also been an emerging area of research due to its capability of removing high heat fluxes over small areas. The requirement of high cooling performance in cooling systems for electronic devices has always been a point of consideration because of high heat generation within the devices. Conventional cooling systems (fans and fins) mostly fail in meeting such high requirements, whereas, miniaturized systems are found to be very effective in dissipating high heat fluxes in a small area. Due to compactness and high heat transfer coefficient, usage of microchannel based systems is found to be more effective in the thermal management of electronic devices. The involvement of latent heat in evaporative cooling gives high heat transfer rates in contrast to single phase flow.

Experimental studies within multiport microchannel heat sinks using dielectric fluid HFE-7100 shows that heat transfer coefficient for the larger channel is generally inferior than that of the smaller channel (Shing*et al.* 2011). Wang et al. (2012) studied the heat transfer characteristics of the dielectric fluid inside a microchannel. The effect of channel inclination -90^0 (vertically downward) to 90^0 (vertically upward)) on the heat transfer rates was reported in their work where an inclination of $+45^0$ yielded maximum heat transfer coefficient. The results also reveal that the performance of heat transfer always decreases in downward inclinations. Lee & Mudawar (2007) performed rigorous experiments to identify the cooling advantages of water-based nanofluids containing small concentrations of Al_2O_3 inside microchannels. Although augmentation of single-phase heat transfer was observed due to the higher thermal conductivity of the nanoparticles, the commencement of boiling made the deposition of nanoparticles near the channel exit in the form of clusters which led to the

catastrophic failure. Experiments have been performed by Hsu *et al.* (2015) to study the effect of inclination on the heat transfer characteristics of the dielectric fluid during boiling in a microchannel with multiports having a characteristic dimension of 440 microns. The channel inclinations were varied in the range -90^o to 90^o. They observed that the coefficient of heat transfer for downward arrangements was inferior to those for upward arrangements at a given inlet mass flux of 100 kg/m^{2}s and a prescribed heat flux of 25 kWm^{-2} and 40 kWm^{-2}. They reported that the effect of nucleate boiling on the heat transfer mechanisms increases with an increase in heat flux.

Most of the literature mentioned above deals with the experimental studies. However, there are limited numerical studies on two phase fluid flow and heat transfer in inclined microchannels. This chapter presents the numerical modeling of single phase fluid flow in horizontal rectangular channel and validates the numerical results with the experimental results of Lee and Mudawar (2007). Subsequently, modeling of aevaporation heat transfer in inclined rectangular microchannel has been explained. Finally the effect of inclinations on the local and average Nusselt number has been discussed. A comparison of the variation of average Nusselt number with varying inlet vapor qualities for different channel orientations has been shown. All the CFD simulation work has been carried out in ANSYS Fluent 15.0.

7.2 Modeling of single phase fluid flow in horizontal rectangular microchannel

Firstly, a steady state single phase flow of water in a rectangular microchannel is modeled numerically using CFD code ANSYS Fluent. A single microchannel out of 21 channels, as considered in the experimental work of Lee and Mudawar (2007), has been chosen to carry out the numerical study. Figure 7.1 represents the unit cell of the microchannel heat sink with half of surrounding copper walls. Dimensions of the unit cell microchannel are shown in Table 7.1. The obtained results of local heat transfer coefficients have been validated against the experimental results of Lee and Mudawar, (2007).

Table 7.1 Dimensions of the unit cell

$W_w(\mu m)$	$W_{ch}(\mu m)$	$H_{w1}(\mu m)$	$H_{ch}(\mu m)$	$H_{w2}(\mu m)$
125	215	12700	821	5637

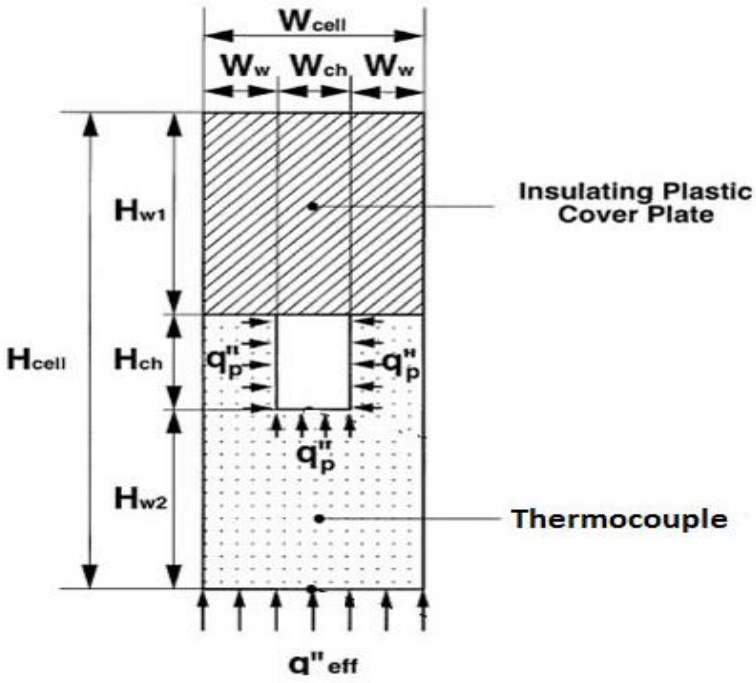

Fig. 7.1 Computational domain for single phase study (Lee and Mudawar, 2007).

7.2.1 Boundary conditions for single phase study

No slip boundary condition is applied at the channel walls. All channel walls except the top wall which is adiabatic, are subjected to a heat flux of 57.24 kW/m^2. Water is used as the working fluid which enters the domain at a Reynolds number of 639 with an inlet temperature of 30^{o}C and outlet is considered to be pressure outlet. As the Reynolds number is within the laminar range, viscous laminar model is chosen. The operating pressure during the entire simulation is kept at 1.12 bar. All the above conditions are taken from the experimental work (Lee and Mudawar, 2007).

7.2.2 Numerical methods for the single phase study

In the present simulations, SIMPLE scheme is used for pressure-velocity coupling. First order UPWIND scheme for the discretisation of convective transport terms along with first order UPWIND scheme for energy terms and PRESTO scheme for pressure terms are also employed. The gradients of velocity, pressure, volume fraction and enthalpy are calculated using Green-Gauss node-based method.

7.3 Results and discussion for the single phase study

Three dimensional steady state simulation for single phase flow in a channel of hydraulic diameter *D*= 341 µm and a length of 4.48 cm has been carried using constant properties of water which are available in the Fluent material database. The simulations for single phase as well as multiphase studies ran on a 64 bit processor having an with 8GB RAM, 3.6GHz processing speed with 8 processors.

7.3.1 Grid independency test for single phase study

A structured mesh has been used for meshing the computational domain with an element size of 30 µm (~11.4D). A grid independence study has been carried out before carrying the actual study. Figure 7.2 shows the variation of heat transfer coefficient along the channel length for different mesh sizes. Based on the results a grid size of 30 microns have been chosen for the present numerical study as the grid size of 20µm and 30µm fetched heat transfer coefficients without much variation.

7.3.2 Validation

The heat transfer coefficient obtained from the single phase study has been validated against the experimental work available in literature. Figure 7.3 compares the variation of predicted local heat transfer coefficient, defined by Eq. (7.1), with that of experimental results of Lee and Mudawar, (2007). The values of obtained heat transfer coefficient are in good agreement with their experimental results with very small deviation (mean absolute error less than 5%).

$$h = \frac{q^{"}}{T_{w_x} - T_{m_x}} \tag{7.1}$$

Here, T_{mx} is bulk mean temperature at a plane perpendicular to the central plane along the channel length, and is computed as a mass weighted average value and the wall temperature T_{wx} is obtained for each point along the channel wall.

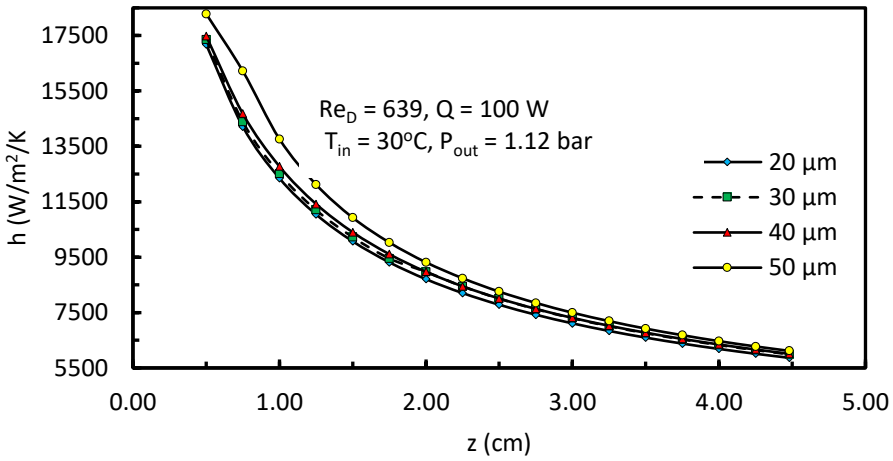

Fig. 7.2 Grid independency test.

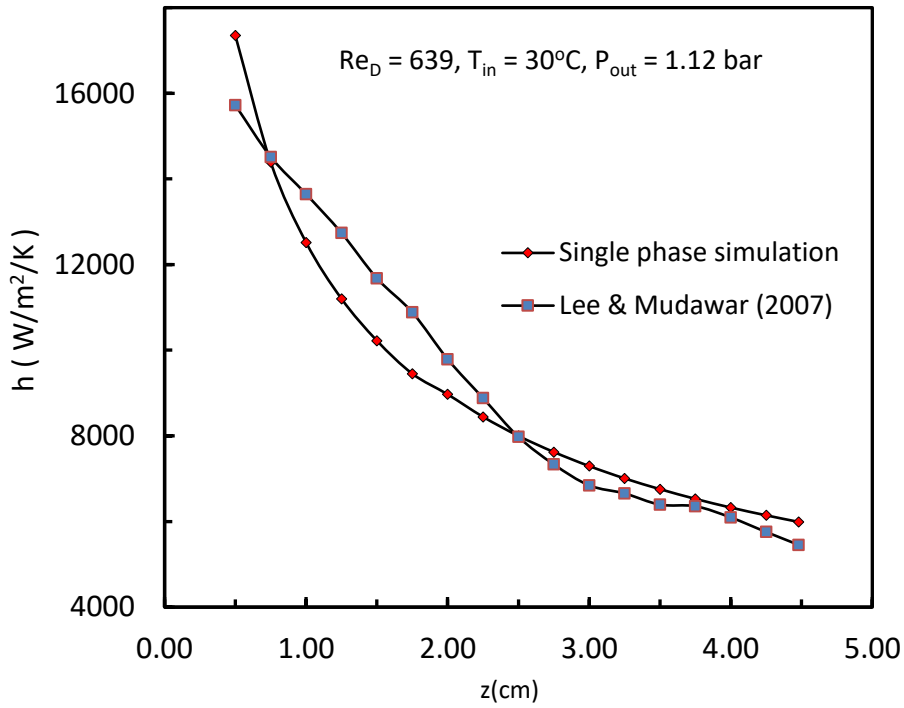

Fig. 7.3 Validation of the single phase study.

7.4 Simulation of evaporation heat transfer in inclined rectangular microchannels with varying inlet vapor qualities

After performing the single phase study and validating the predicted results with the literature results, studies on two-dimensional, unsteady, two-phase fluid flow and evaporation heat transfer of water in inclined rectangular microchannels (Θ varies from 90^0 to 90^0) has been carried out. Volume of fluid multiphase method has been incorporated along with user defined functions for evaporation mass transfer across the interface. In each simulation vapor qualities at inlet has been changed in order to observe the heat transfer variations during the

fluid flow. Surface tension effects (σ = 0.05891N/m) have also beenconsidered in the two phase studies.

7.4.1 Geometry and orientations of the computational domain

The computational domain (Fig. 7.4) consists of a two dimensional rectangular microchannel with a characteristic dimension of 825 µm and length of 25.4 mm. The channel walls have been considered to be made of silicon material. Structured elements of size 5 microns have been chosen for the multiphase flow problem. Figure 7.5 shows the orientations of the rectangular microchannel considered in the present numerical work. The properties of the working fluids are given in Table 7.2.

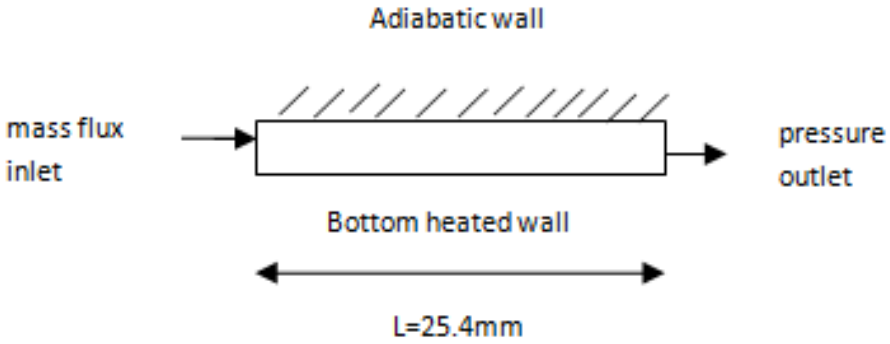

Fig. 7.4 Computational domain for two phase flow study.

Table 7.2 Properties of working fluids

Properties	Water-liquid	Water-vapor
Density (kg/m^3)	1000	0.5542
Specific-heat(J/kg-K)	4182	2014
Thermal conductivity (W/m-K)	0.6	0.0261
Viscosity (kg/m-s)	0.0009	1.34×10^{-5}
Molecular Weight (kg/kgmol)	18.0152	18.0152
Standard State Enthalpy (J/kgmol)	0	$2.992325\times10^{+7}$

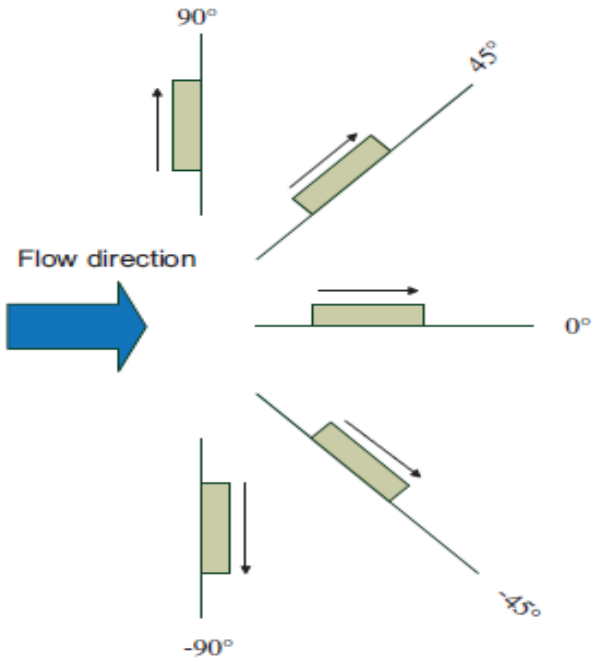

Fig. 7.5 Orientations of the microchannel.

7.4.2 CFD model

Volume of fluid (VOF) (Hirt and Nicholas, 1981), marker points method (Tryggvason and Muradoglu, 2008) and level-set (Sussman *et al.*, 1994), or the phase-field method (Anderson *et al.*, 1998) are some interface capturing techniques which are mostly used in multiphase flow inside microchannels. VOF multiphase approach along with viscous laminar model is used to study the convective boiling heat transfer characteristics of water in inclined microchannels.

The flow and heat transfer equations along with the volume of fluid model governing the evaporation heat transfer process inside the channel are given by Eqs. (2.1-2.3, 2.9) which can be found in Chapter 2.

7.4.3 Boundary conditions for the two phase study

In each simulation the quality of water vapor at inlet of microchannel has been varied in the range 0-0.6, with a fixed mass flux (G = 250 kg/m^{2}s) of the mixture at the inlet. Heat flux of 250 kW/m^2 has been prescribed to the bottom wall of channel, whereas, its upper wall was kept insulated and the operating pressure was set to 1.12 bar. The no-slip condition was considered at the walls of the microchannel.

7.4.4 Numerical methods for the two phase study

Volume of fluids multiphase method has been used to capture the two phase interface. SIMPLE scheme was used for pressure-velocity coupling. The first order UPWIND scheme were used for the discretisation of convective transport terms and energy terms. PRESTO scheme was employed to solve the pressure terms. The gradients of velocity, pressure, volume fraction and enthalpy have been calculated using Green-Gauss node-based method. The pressure gradient and body forces have also been taken into account by using implicit body force treatment. Piecewise linear interface calculation (PLIC) method based Geo-reconstruct scheme, originally proposed by Youngs (1982), has been used for the reconstruction of the two-phase interface.

7.5 Results and discussion for the two phase study

The present section discusses the results obtained from the fluid flow and heat transfer studies carried out in the present work. Effect of channel inclination on the average Nusselt number for a given vapor quality and effect of vapor quality on heat transfer characteristics for a given inclination of channels are discussed in detail.

7.5.1 Effect of channel inclination on heat transfer characteristics

The two-phase heat transfer coefficient is calculated using Eq. (7.2) and in dimensionless form it is represented with the Nusselt number which can be obtained using Eq. (7.3) as shown below:

$$h_{TP} = \frac{q^{"}}{T_w - T_s} \tag{7.2}$$

$$Nu_{TP} = \frac{h_{TP} D}{k_L} \tag{7.3}$$

For a mass flux of G = 250 kg/m^{2}s in inclined microchannels, the results revealed that the heat transfer coefficient is increased by approximately 60% for an inclination angle of 45^0 as compared to that of the horizontal configuration, as shown in Fig. 7.6(a-d). Due to the gravitational effect on the two phase flow, the vapor phase being less dense has the tendency to move away from the heated wall, whereas, the primary phase being heavier tends to move towards the heated wall of the channel. As the conductivity of liquid is higher than vapor phase and also aperture of the liquid being small during this process, its velocity increases resulting in the augmentation of heat transfer. This way a high amount of heat from the walls

gets carried away by the liquid lying in contact with the walls and the same is transferred to the secondary phase more efficiently in contrast to the single-phase flows. Therefore, the heat transfer coefficient has been found to be always lower in case of downward inclination (-45^0) by around 43% as compared to upward inclination of 45^0.

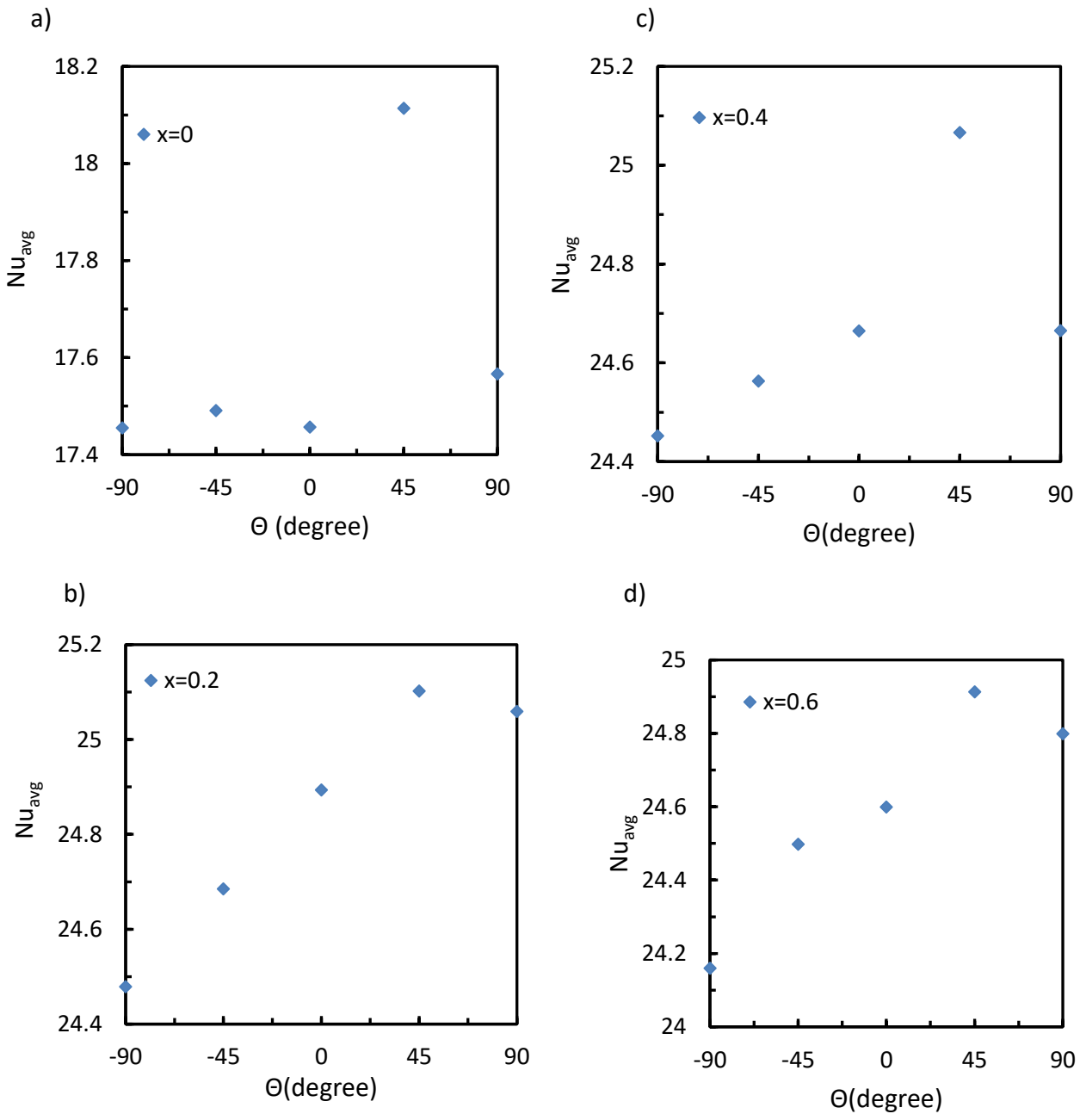

Fig. 7.6(a-d). Variation of average Nusselt no. with θ for a given inlet vapor quality (*x*).

7.5.2 Effect of vapor quality on heat transfer characteristics

It is observed that for a given heat flux of 250 kW/m^2, the boiling heat transfer coefficient increases significantly at very high quality region except at the low quality region where it remains roughly unchanged due to partial dry out (Fig. 7.7).

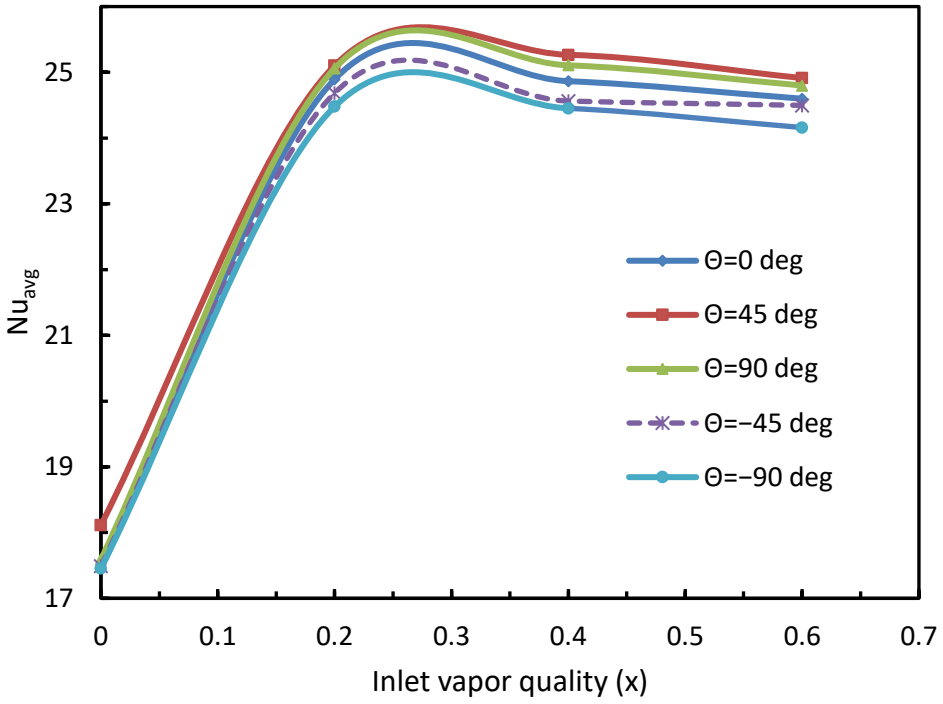

Fig. 7.7. Variation of average Nusselt no. with inlet vapor quality for different channel inclination (θ).

7.6 Summary

Single phase flow of water inside a rectangular microchannel was simulated and the obtained results of heat transfer coefficients were validated against the experimental work available in literature. The obtained numerical results were inline with the experimental work available in the literature which shows the consistency of the models used during the simulation. Using the same models along with VOF multiphase approach a two phase study of flow and heat transfer was carried out in ANSYS Fluent to find the effects of varying the vapor quality at the inlet of inclined microchannels during evaporation heat transfer. The heat transfer coefficients was found to be highest in 45^0 upward orientation and also it was observed that the downward orientations always impair the heat transfer. The possible reason for this nature is that the residence time of the fluid inside the channel is less in downward orientation as compared to upward orientation of the channel. Also, in 90^0 (upward and

downward) orientation, the heat transfer was comparatively less as compared to 45^0 (upward and downward) because of symmetry of the vapor bubble inside the channel due to which the liquid-vapor interface lies away from the channel walls resulting in lesser heat transfer.

CHAPTER 8 CONCLUSION AND FUTURE SCOPE

8.1. Conclusion

In this thesis, the fluid flow and heat transfer characteristics of two-phase slug flow inside microchannels have been studied by considering the effect of several parameters *viz.*: wall wettability, thermal wall boundary conditions (both modulated and unmodulated), and oscillatory wall motion of the microchannel. In addition, the effects of channel inclination and inlet vapor quality on the evaporation heat transfer in microchannel have also been explored. The first study concerns with the effect of wall wettability on the pressure drop and slug lengths during a gas-liquid Taylor flow in microchannel. The second study deals with the heat transfer characteristics of liquid-liquid Taylor flow in a circular microchannel subjected to different thermal wall conditions. The third study is concerned with the flow and heat transfer characteristics of liquid-liquid Taylor flow inside a rectangular microchannel under modulated wall temperature boundary conditions. The fourth study deals with the hydrodynamics and heat transfer characteristics of liquid-liquid Taylor flow inside a rectangular microchannel under modulated wall motion in the transverse direction of the flow. The last study is concerned with the evaporation heat transfer characteristics of water in inclined rectangular microchannels.

The hydrodynamics of a gas-liquid Taylor flow in a *T*-junction microchannel has been examined. The effects of contact angle and carrier phase fluid velocity on the bubble, liquid slug length and pressure drop have been investigated. The bubble shape became asymmetric and the pressure drop increased in hydrophobic channels in contrast to the hydrophilic channels. This happened due to an increase in the frictional pressure drop in hydrophobic channels as the length of contact between the channel wall and bubble was higher in the non-wetting channels with respect to that in the wetting channels for same volume fraction of the gas phase. The reason for such increase in the frictional pressure drop could also be attributed

to the increase in the overall liquid slug length and a decrease in the overall bubble length with increasing contact angle. The obtained numerical results of pressure drop have also been found to be in good agreement with the existing pressure drop models in the literature. Besides, the bubble and liquid slug lengths decreased with wall contact angle due to convex shape of the menisci in hydrophilic channels unlike in hydrophobic channels where the nose and tail of the bubble were of concave shape. The bubble and liquid slug lengths were found to increase and decrease, respectively with an increase in the incoming fluid velocity. The variation of the bubble and liquid slug lengths with incoming fluid velocity have also been compared with the standard models and the obtained trends were found to be in close match with the models.

The hydrodynamics and heat transfer characteristics of a liquid–liquid Taylor flow in a vertical circular microchannel of 100μm diameter have been examined. The thin liquid film of the carrier phase fluid between the wall and the two-phase interface has been captured using the mesh which was adapted dynamically based on the gradients of the volume fraction of the dispersed phase. It was noticed that the nose of the droplets has higher curvature with respect to their tail since the pressure drop at the frontal interface was higher than that at the tail. The heat transfer studies revealed that higher heat transfer rates over single-phase flow could be achieved by introducing liquid droplets along with the carrier phase fluid in the channel under both isothermal and constant heat flux wall heating conditions. It was noticed that the average heat transfer rate was enhanced by 187% for isothermal wall condition and by 210% for the constant heat flux wall condition with respect to the liquid-only flow under identical operating conditions. The presence of internal recirculation within the slug and droplet regions in the Taylor flow causes such enhancement in the heat transfer over single-phase flow in which such recirculation does not exist.

The hydrodynamics and thermal behavior of a liquid-liquid Taylor flow in a rectangular microchannel under modulated wall heating conditions have also been numerically explored. Prior to two-phase studies, the single phase flow of water under isothermal wall conditions was studied and the results were compared with the analytical results for validating the numerical code. Later, two-phase heat transfer studies were carried out in which two immiscible dispersed phase oil droplets were introduced into the channel subjected to identical conditions as that of single-phase flow. It was witnessed that the average heat transfer rate increased by 42% in contrast to single-phase flow. After this study, the hotter walls of the channel were prescribed with temperature-modulated wall heating conditions of

four different kinds. Out of these four conditions, the one which fetched the optimum heat transfer rate was selected as the base case for studying the impact of frequency ($0 < \omega < 750\pi$ rad/s) and amplitude ($0 < \varepsilon < 0.03$) of the modulated wall temperature profiles on the heat transfer rate. The temperature gradient along the transverse direction of the flow, evaluated at the middle of the droplet, was found to be highest for $\varepsilon = 0.02$ and $\omega = 500\pi$ rad/s in the above-mentioned base case. This resulted in the maximum heat transfer rate in contrast to other value of the amplitude and frequency of the modulated temperature profile. An approximate enhancement of 50% in the heat transfer was achieved using the two-phase flow under modulated temperature boundary condition as compared to single-phase flow. Although film thickness increased with the capillary number, heat transfer coefficient was found to increase as the convective heat transfer dominated the conduction heat transfer. Besides, for the chosen range of Capillary numbers ($0.0044 < Ca < 0.022$), the average heat transfer rate improved by 50% to 126% under modulated wall temperature condition with $\varepsilon = 0.02$ and $\omega = 500\pi$ rad/s in contrast to liquid-only flow.

The flow physics and heat transfer characteristics of oil-water Taylor flow inside a rectangular microchannel subjected to constant heat flux condition and modulated wall motion in the transverse direction of the flow have been studied. The presence of sharp pressure jumps due to modulated wall motion caused instabilities at the two-phase interface which altered the heat transfer process. The slug flow heat transfer improved significantly when the walls of the microchannel were subjected to modulated wall motion. Approximately, 77-186% enhancement in heat transfer rate was achieved over liquid-only flow. Whereas, an approximate augmentation of 0.47-23% in the heat transfer rates were obtained in contrast to slug flow under unmodulated wall motion for the studied range of capillary numbers($0.0044 < Ca < 0.022$) and modulation frequencies($0 < \omega < 750\pi$ rad/s). The intensity of vortices was found to be higher for $\omega = 250\pi$ rad/s, as well as the heat transfer from the channel wall to the interior of the domain, was faster at $\omega = 250\pi$ rad/s as compared to other values of ω. The intensity of the vortices increased on increasing the amplification factor of the modulated wall motion in the range $0 < a < 4$ which resulted in higher heat transfer rates.The heat transfer rates also improved by 11 to 23% with modulated wall motion in the presence of shorter droplets as compared to that of unmodulated case when the slug length was varied in the range $100 < L_S < 310\mu m$.

The effect of gravity on the flow boiling of water inside microchannel has been numerically examined. The inclination of the channel (was) varied fromthe downward

arrangement (-90^0) to upward arrangement (90^0) and the bottom wall of the channel was subjected to constant heat flux heating condition with its upper wall being insulated. The vapour being less dense, has the tendency to move towards the upper wall. This offered higher heat transfer rate in contrast to the flow in downward orientations. The heat transfer coefficient has been found to be maximum in 45^0 upward orientation. Water being more dense and higly conductive in nature,it comes in contact with the heated wall. In addition, the residence time of the fluid inside the channel increases in the upward orientation of the channel as the fluid flows against the gravity. The flow became asymmetric on changing the channel inclination, except for vertically upward and downward orientations where the flow remained symmetric and the vapor bubble translated symmetrically along the centerline of the channel. Hence, the heat transfer was comparatively lesser in 90^0 (upward and downward) orientations in contrast to 45^0 (upward and downward) orientations as the liquid-vapor interface lies away from the channel walls.

8.2. Contribution made in the thesis

Following are the key findings of the present research work:

1. Contact angle influences the two-phase pressure drop across a microchannel. It is also observed that hydrophilic channels result in lower pressure drop as compared to hydrophobic channels.
2. The sinusoidal temperature boundary condition enhances the heat transfer rate (~126%) as compared to isothermal heating in slug flow in microchannels.
3. Oscillatory motion of the microchannel walls improves the heat dissipation rate (~23%) as compared to the stationary walls during two-phase slug flow.

8.3. Future scope

The present research work could be extended in the future to investigate the effect of droplet size on the flow and heat transfer characteristics of a liquid-liquid Taylor flow inside microcapillaries. A three-dimensional numerical study could be performed in the future to examine the validity of the pressure drop and heat transfer models in predicting the pressure drop and heat transfer in a LL slug flow regime inside the microchannel under modulated wall motion. The present studies can be also extended to explore flow physics and heat transfer behavior of slug flow inside wavy microchannels. In addition, the heat transfer characteristics of Taylor flow inside wavy microchannels under modulated motion can also be explored.

REFERENCES

Abiev, R.Sh., 2011. Modeling of pressure losses for the slug flow of a gas–liquid mixture in mini– and microchannels. *Theoretical Foundations of Chem. Eng*., 45(2):156–163.

Abiev, R. S., 2012. Modern state and perspectives of microtechnique application in chemical industry. *Russ. J. Gen. Chem.*, 82(12): 2019–2024.

Abiev, R.S. & Lavretsov, I. V., 2012. Intensification of mass transfer from liquid to capillary wall by Taylor vortices in minichannels, bubble velocity and pressure drop. *Chemical Engineering Science*, 74:59–68.

Abiev, R.S., 2013. Bubbles velocity, Taylor circulation rate and mass transfer model for slug flow in milli- and microchannels. *Chemical Engineering Journal*, 227:66–79.

Abiev, R.S., 2015. Effect of contact-angle hysteresis on the pressure drop under slug flow conditions in minichannels and microchannels. *Theoretical Foundations of Chemical Engineering*, 49(4):414–421.

Abiev, R.Sh., 2017. Analysis of local pressure gradient inversion and form of bubbles in Taylor flow in microchannels. *Chem. Eng. Sci.*, 174:403–412.

Akbar, M.K., Plummer, D.A., Ghiaasiaan, S.M., 2003. On gas-liquid two-phase flow regimes in microchannels. *Int. J. Multiph. Flow*, 29(5):855–865.

Anderson, D.M., McFadden, G.B., Wheeler, A.A., 1998. Diffuse-interface methods in fluid mechanics, *Annual Review of Fluid Mechanics*, 30(1):139–165.

ANSYS FLUENT 12.0 Theory Guide, *Access date: 13th March 2019*.

Asadolahi, A. N., Gupta, R., Fletcher, D. F. & Haynes, B. S., 2011. CFD approaches for the simulation of hydrodynamics and heat transfer in Taylor flow. *Chem. Eng. Sci.*, 66:5575–5584.

Asadolahi, A. N., Gupta, R., Leung, S.S.Y., Fletcher, D. F. & Haynes, B. S., 2012. Validation

of a CFD model of Taylor flow hydrodynamics and heat transfer. *Chem. Eng. Sci.*, 69(1):541–552.

Asthana, A., Zinovik, I., Weinmueller, C., Poulikakos, D., 2011. Significant Nusselt number increase in microchannels with a segmented flow of two immiscible liquids: An experimental study. *International Journal of Heat and Mass Transfer*, 54(7–8):1456–1464.

Aussillous, P. & Quere, D., 2000. Quick deposition of a fluid on the wall of a tube. *Physics of Fluids*, 12(10):2367–2371.

Bandara, T., Nguyen, N.-T. & Rosengarten, G., 2015a. Slug flow heat transfer without phase change in microchannels: A review. *Chemical Engineering Science*, 126:283–295.

Bandara, T., Cheung, S.C.P, Rosengarten, G., 2015b. Slug flow heat transfer in microchannels: A numerical study. *Computational Thermal Sciences*, 7(1): 81–92.

Bauer, T. et al., 2006. Intensification of heterogeneous catalytic gas-fluid interactions in reactors with a multichannel monolithic catalyst. *Russian Journal of Applied Chemistry*, 79(7):1047–1056.

Betz, A.R. & Attinger, D., 2010. Can segmented flow enhance heat transfer in microchannel heat sinks? *International Journal of Heat and Mass Transfer*, 53(19–20):3683–3691.

Bogojevic, D. et al., 2009. Two-phase flow instabilities in a silicon microchannels heat sink. *International Journal of Heat and Fluid Flow*, 30(5):854–867.

Brackbill, J.U., Kothe, D.B. & Zemach, C., 1992. A continuum method for modeling surface tension. *Journal of Computational Physics*, 100(2):335–354.

Bretherton, F.P., 1961. The motion of long bubbles in tubes. *Journal of Fluid Mechanics*, 10(2):166–188.

Celata, G.P. et al., 2006. Microtube liquid single-phase heat transfer in laminar flow. *International Journal of Heat and Mass Transfer*, 49(19–20):3538–3546.

Cengel, Y.A. & Cimbala, J.M., 2017. *Fluid Mechanics: fundamentals and applications* Fourth edi., New York,: McGraw-Hill Education.

Cetin, B., 2005. Analysis of Single Phase Convective Heat Transfer in microtubes and microchannels. *Thesis submitted to Middle East Technical University*.

Che, Z. et al., 2015. Three dimensional features of convective heat transfer in droplet-based microchannel heat sinks. *International Journal of Heat and Mass Transfer*, 86:455–464.

Che, Z., Wong, T.N. & Nguyen, N.T., 2011. An analytical model for plug flow in microcapillaries with circular cross section. *International Journal of Heat and Fluid*

Flow, 32(5):1005–1013.

Che, Z., Wong, T.N. & Nguyen, N.T., 2012. Heat transfer enhancement by recirculating flow within liquid plugs in microchannels. *International Journal of Heat and Mass Transfer*, 55(7–8):1947–1956.

Che, Z., Wong, T.N. & Nguyen, N.T., 2013. Heat transfer in plug flow in cylindrical microcapillaries with constant surface heat flux. *International Journal of Thermal Sciences*, 64:204–212.

Choi, Y.S. et al., 2018. Pressure drop characteristics for two-phase flow of FC-72 in microchannel. *Proceedings of the Institution of Mechanical Engineers, Part C: Journal of Mechanical Engineering Science*, 232(6):987–997.

Cole, K.D., 2010. Steady-periodic heating in parallel-plate microchannel flow with participating walls. *Int. J. Heat and Mass Transfer*, 53(5–6):870–878.

Coleman, J.W. & Garimella, S., 2003. Two-phase flow regimes in round, square and rectangular tubes during condensation of refrigerant R134a, *Int. J. Refrig*. 26:117–128.

Courant, R., Friedrichs, K., Lewy, H., 1967. On the partial difference equations of mathematical physics. *IBM Journal of Research and Development*, 11(2):215-234.

Cubaud, T., Ulmanella, U., Ho, C-M., 2006. Two-phase flow in microchannels with surface modifications. *Fluid Dynamics Res*., 38:772–786.

Dai, Z., Guo, Z., Fletcher, D.F., &Haynes, B.S., 2015. Taylor flow heat transfer in microchannels – Unification of liquid – liquid and gas – liquid results. *Chemical Engineering Science*, 138:140–152.

Duran Martinez, F.L., Billet, A.M., Julcour-Lebigue, C., Larachi, F., 2015. Hydrodynamics And Mass Transfer In Taylor Flow. COMSOL Conference, Grenoble, France, 14–16 Oct 2015.

Eain, M.M.G., Egan, V. & Punch, J., 2013. Film thickness measurements in liquid–liquid slug flow regimes. *International Journal of Heat and Fluid Flow*, 44:515–523.

Eain, M.M.G., Egan, V. & Punch, J., 2015. Local Nusselt number enhancements in liquid-liquid Taylor flows. *International Journal of Heat and Mass Transfer*, 80:85–97.

Fabbri, M., Jiang, S. & Dhir, V.K., 2005. A comparative study of cooling of high power density electronics using sprays and microjets. *Journal of Heat Transfer*, 127(1):38–48.

Faircloth, J.M., & Schaetzle, W.J., 1969. Effect of vibration on heat transfer for flow normal to a cylinder. *Journal of Heat Transfer*, 91(1): 140–144.

Farhangi, M.M., Passandideh-Fard, M. & Moin, H., 2010. Numerical study of bubble rise

and interaction in a viscous liquid. *International Journal of Computational Fluid Dynamics*, 24(1-2):13–28.

Ferrari, A., Magnini, M. & Thome, J.R., 2018. Numerical analysis of slug flow boiling in square microchannels. *International Journal of Heat and Mass Transfer*, 123:928–944.

Fischer, M., Juric, D. & Poulikakos, D., 2010. Large Convective Heat Transfer Enhancement in Microchannels With a Train of Coflowing Immiscible or Colloidal Droplets. *Journal of Heat Transfer*, 132(11):1–10.

Fouilland, T.S., Fletcher, D.F. & Haynes, B.S., 2010. Film and slug behaviour in intermittent slug-annular microchannel flows. *Chemical Engineering Science*, 65(19):5344–5355.

Fukagata, K. et al., 2007. Numerical simulation of gas-liquid two-phase flow and convective heat transfer in a micro tube. *International Journal of Heat and Fluid Flow*, 28(1 Special Issue.):72–82.

Ganapathy, H. et al., 2013. Volume of fluid-based numerical modeling of condensation heat transfer and fluid flow characteristics in microchannels. *International Journal of Heat and Mass Transfer*, 65:62–72.

Gao, W., Xu, X. & Liang, X., 2018. Flow boiling of R134a in an open-cell metal foam mini-channel evaporator. *International Journal of Heat and Mass Transfer*, 126:103–115.

Garstecki, P., Fuerstman, M.J., Stone, H.A., Whitesides, G.M., 2006. Formation of droplets and bubbles in a microfluidic T-junction–scaling and mechanism of break-up. *Lab on a Chip*, 6:437–446.

Gawali, D.B.S., Swami, V.B. & Thakre, S.D., 2014. Theoretical and Experimental Investigation of Heat Transfer Characteristics through a Rectangular Microchannel Heat Sink. *International Journal of Innovative Research in Science, Engineering and Technology*, 3(8):15631–15640.

Goldsmith, H.L. & Mason, S.G., 1963. The flow of suspensions through tubes. II. Single large bubbles. *Journal of Colloid Science*, 18(3):237–261.

Gupta, R., Leung, S. S. Y., Manica, R., Fletcher, D. F. & Haynes, B. S., 2013. Hydrodynamics of liquid-liquid Taylor flow in microchannels. *Chem. Eng. Sci.*, 92:180–189.

Gupta, R., Fletcher, D.F. & Haynes, B.S., 2010a. CFD modelling of flow and heat transfer in the Taylor flow regime. *Chemical Engineering Science*, 65(6):2094–2107.

Gupta, R., Fletcher, D.F. & Haynes, B.S., 2010b. Taylor Flow in Microchannels: A Review of Experimental and Computational Work. *Journal of Computational Multiphase Flows,*

2(1):1-31.

Gupta, R., Fletcher, D.F. & Haynes, B.S., 2009. On the CFD modelling of Taylor flow in microchannels. *Chemical Engineering Science*, 64(12):2941–2950.

Haase, S., 2017. Characterisation of gas-liquid two-phase flow in minichannels with co-flowing fluid injection inside the channel, part II: gas bubble and liquid slug lengths, film thickness, and void fraction within Taylor flow. *International Journal of Multiphase Flow*, 88:251–269.

Han, Y. & Shikazono, N., 2009. Measurement of the liquid film thickness in micro tube slug flow. *International Journal of Heat and Fluid Flow*, 30(5):842–853.

He, Q., Hasegawa, Y. & Kasagi, N., 2010. Heat transfer modelling of gas-liquid slug flow without phase change in a micro tube. *International Journal of Heat and Fluid Flow*, 31(1):126–136.

Hetsroni, G., Mosyak, A., Pogrebnyak, E., Yarin, L.P., 2005. Heat transfer in micro-channels: Comparison of experiments with theory and numerical results. *International Journal of Heat and Mass Transfer*, 48:5580–5601.

Hirt, C.W. & Nichols, B.D., 1981. Volume of fluid (VOF) method for the dynamics of free boundaries. *Journal of Computational Physics*, 39(1):201–225.

Horvath, C., Solomon, B.A. & Engasser, J.M., 1973. Measurement of Radial Transport in Slug Flow Using Enzyme Tubes. *Industrial and Engineering Chemistry Fundamentals*, 12(4):431–439.

Hosseinian, H., and Meghdadi I.A.H., 2018. Experimental study of heat transfer enhancement due to the surface vibrations in a flexible double pipe heat exchanger. *Heat and Mass Transf.*, 54(4):1113–1120.

Hsu, L.C. et al., 2015. An experimental study of inclination on the boiling heat transfer characteristics of a micro-channel heat sink using HFE-7100. *International Communications in Heat and Mass Transfer*, 62:13–17.

Hu, J.S. & Chao, C.Y.H., 2007. An experimental study of the fluid flow and heat transfer characteristics in micro-condensers with slug-bubbly flow. *International Journal of Refrigeration*, 30(8):1309–1318.

Iqbal, A. & Pandey, M., 2018. Effect of local thermophysical properties and flashing on flow boiling pressure drop in microchannels. *International Journal of Multiphase Flow*, 106:311–324.

Irandoust, S. & Andersson, B., 1989. Liquid Film in Taylor Flow through a Capillary.

Industrial and Engineering Chemistry Research, 28(11):1684–1688.

Incropera, F.P., and D. P. Dewitt, D.P., 2002. Fundamentals of Heat and Mass Transfer. 5th ed. New York: John Wiley & Sons.

Issa, R.I., 1986. Solution of the implicitly discretised fluid flow equations by operator-splitting. *J. Comput. Phys*. 62(1):40–65.

Jeffers, N.M.R., Punch, J., Walsh, E.J., 2009. Heat transfer from novel target surface structures to a normally impinging, submerged and confined water jet. *Journal of Thermal Science and Engineering Applications*, 1(3):1–9.

Jovanović, J., Zhou, W., Rebrov, EV., Nijhuis, TA., Hessel, V., Schouten, JC, 2011. Liquid-liquid slug flow: hydrodynamics and pressure drop. *Chem. Eng. Sci*. 66:42–54.

Kandlikar, S.G., 2002. Fundamental issues related to flow boiling in minichannels and microchannels. *Experimental Thermal and Fluid Science*, 26(2–4):389–407.

Kandlikar, S.G., 2004. Heat transfer mechanisms during flow boiling in microchannels. *Journal of Heat Transfer*, 126:8–16.

Kashid, M.N. et al., 2005. Internal circulation within the liquid slugs of a liquid-liquid slug-flow capillary microreactor. *Industrial and Engineering Chemistry Research*, 44(14):5003–5010.

Kawahara, A., Sadatomi, M., Nei, K., Matsuo, H., 2011. Characteristics of two-phase flows in a rectangular microchannel with a T-junction type gas-liquid mixer. *Heat Transfer Engineering*. 30(7–8):585–594.

Khan, W. et al., 2018. Slug formation mechanism for air–water system in T-junction microchannel: a numerical investigation. *Chemical Papers*, 72(11):2921–2932.

Kim, S.M., Kim, J. & Mudawar, I., 2012. Flow condensation in parallel micro-channels - Part 1: Experimental results and assessment of pressure drop correlations. *International Journal of Heat and Mass Transfer*, 55(4):971–983.

Kreutzer, M.T., Kapteijn, F., Moulijn, J.A., Kleijn, C.R., Heiszwolf, J.J., 2005. Inertial and interfacial effects on pressure drop of Taylor flow in capillaries. *AIChE J.*, 51(9):2428–2440.

Kuan, W.K. & Kandlikar, S.G., 2006. Experimental study on the effect of stabilization on flow boiling heat transfer in microchannels. *Journal of Heat transfer*, 28:746–752.

Kunert, C. & Harting, J., 2008. Simulation of fluid flow in hydrophobic rough microchannels. *International Journal of Computational Fluid Dynamics*, 22(7):475–480.

Laborie, S., Cabassud, C., Durand-Bourlier, L., Laine, J.M., 1999. Characterisation of gas-liquid two-phase flow inside capillaries. *Chem. Eng. Sci.*, 54:5723–5735.

Lac, E., & Sherwood, J.D., 2009. Motion of a drop along the centreline of a capillary in a pressure-driven flow. *Journal of Fluid Mechanics*, *640*:27–54.

Lakehal, D., Larrignon, G. & Narayanan, C., 2008. Computational heat transfer and two-phase flow topology in miniature tubes. *Microfluidics and Nanofluidics*, 4(4):261–271.

Lee, J. & Mudawar, I., 2007. Assessment of the effectiveness of nanofluids for single-phase and two-phase heat transfer in micro-channels. *International Journal of Heat and Mass Transfer*, 50(3–4):452–463.

Lelea, D., Nishio, S. & Takano, K., 2004. The experimental research on microtube heat transfer and fluid flow of distilled water. *International Journal of Heat and Mass Transfer*, 47(12–13):2817–2830.

Leung, S.S.Y., Gupta, R., Fletcher, D.F., Haynes, B.S., 2012. Effect of Flow Characteristics on Taylor Flow Heat Transfer. *Industrial & Engineering Chemistry Research*, 51(4):2010–2020.

Leung, S.S.Y., Liu, Y., Fletcher, D.F., Haynes, B.S., 2010. Heat transfer in well-characterised Taylor flow. *Chemical Engineering Science*, 65(24):6379–6388.

Li, W., Yang, F., Alam, T., Qu, X., Peng, B., Khan, J., Li, C., 2018. Enhanced flow boiling in microchannels using auxiliary channels and multiple micronozzles (I): Characterizations of flow boiling heat transfer. *International Journal of Heat and Mass Transfer*, 116:208–217.

Lim, T.W. et al., 2014. Two-phase pressure drop due to friction in micro-channel. *Proceedings of the Institution of Mechanical Engineers, Part C: Journal of Mechanical Engineering Science*, 228(5):921–931.

Liu D, Wang S (2011) Gas–liquid mass transfer in Taylor flow through circular capillaries. Ind Eng Chem Res. 50(4):2323–2330.

Liu, D., Ling, X. & Peng, H., 2016. Comparative analysis of gas-liquid flow in T-junction microchannels with different inlet orientations. *Advances in Mechanical Engineering*, 8(3):1–14.

Lockhart, R. W., & Martinelli, R. C., 1949. Proposed Correlation of Data for Isothermal Two-Phase, Two-Component Flow in Pipes. *Chemical Engineering Progress*. 45(1):39-48.

Lou, Q., Yang, M. & Xu, H., 2018. Numerical investigations of gas–liquid two-phase flows

in microchannels. *Proceedings of the Institution of Mechanical Engineers, Part C: Journal of Mechanical Engineering Science*, 232(3):466–476.

Mantle, J., Kazmierczak, M., Hiawy, B., 1994. The effect of temperature modulation on natural convection in a horizontal layer heated from below: high-rayleigh-number experiments. *Journal of Heat Tranfer*, 116(3):614–620.

Markal, B., Aydin, O. & Avci, M., 2016. Effect of aspect ratio on saturated flow boiling in microchannels. *International Journal of Heat and Mass Transfer*, 93:130–143.

Mehdizadeh, A., Sherif, S. A. & Lear, W. E., 2011. Numerical simulation of thermofluid characteristics of two-phase slug flow in microchannels. *Int. J. Heat Mass Transf*. 54:3457–3465.

Morini, G.L., 2006. Scaling effects for liquid flows in microchannels. *Heat Transfer Engineering*, 27(4):64–73.

Morini, G.L., 2004. Single-phase convective heat transfer in microchannels: A review of experimental results. *International Journal of Thermal Sciences*, 43(7):631–651.

Morini, G.L., 2018. The Challenge to Measure Single-phase Convective Heat Transfer Coefficients in Microchannels. *Heat Transfer Engineering*, 7632:1–16.

Mukherjee, A. & Kandlikar, S.G., 2009. The effect of inlet constriction on bubble growth during flow boiling in microchannels. *International Journal of Heat and Mass Transfer*, 52(21–22):5204–5212.

Muzychka, Y. S., Walsh, E., & Walsh, P., 2010. Simple Models for Laminar Thermally Developing Slug Flow in Noncircular Ducts and Channels. *J. Heat Transfer*, 132:1–10.

Navier C (1823) Me´moiresur les lois du mouvement de fluids. Memoires de l'Academie Royale des Sciences de l' Institut de France 6:389–440.

Nichita, B.A., Zun, I., Thome, J.R., 2010. A level set method coupled with a volume of fluid method for modeling of gas-liquid interface in bubbly flow. *J. Fluids Eng.* 132:1-15.

Nikkhah, Z., Karimipour, A., Safaei, M.R., Forghani-Tehrani, P., Goodarzi, M., Dahari, M. & Wongwises, S., 2015. Forced convective heat transfer of water/functionalized multi-walled carbon nanotube nanofluids in a microchannel with oscillating heat flux and slip boundary condition. *Int. Comm. in Heat and Mass Transfer* 68:69–77.

Oishi, M., Kinoshita, H., Fujji, T., Oshima, M., 2009. Confocal micro-PIV measurement of droplet formation in a T-shaped micro-junction. *Journal of Physics: Conference Series*, 147:1–9.

Olbricht, W.L., Kung, D.M., 1992. The deformation and breakup of liquid drops in low Reynolds number flow through a capillary. *Physics of Fluids*, 4:1347–1354.

Ookawara, S., Ishikawa, T. & Ogawa, K., 2007. Applicability of a miniaturized micro-separator/classifier to oil-water separation. *Chemical Engineering and Technology*, 30(3):316–321.

Peng, X.F. & Peterson, G.P., 1995. The effect of thermofluid and geometrical parameters on convection of liquids through rectangular microchannels. *International Journal of Heat and Mass Transfer*, 38(4):755–758.

Pohorecki, R., Kula, K., 2008. A simple mechanism of bubble and slug formation in Taylor flow in microchannels. *Chem. Eng. Res. and Des.* 86:997– 1001.

Prajapati, Y.K., Pathak, M., & Khan, M.K., 2016. Transient heat transfer characteristics of segmented finned microchannels. *Experimental Thermal and Fluid Science*, 79:134–142.

Qian, D. & Lawal, A., 2006. Numerical study on gas and liquid slugs for Taylor flow in a T-junction microchannel. *Chemical Engineering Science*, 61(23):7609–7625.

Rosa, P., Karayiannis, T.G. & Collins, M.W., 2009. Single-phase heat transfer in microchannels: The importance of scaling effects. *Applied Thermal Engineering*, 29(17–18):3447–3468.

Roy S, Bauer T, Al-Dahhan M., Lehner P, Turek T (2004) Monoliths as multiphase reactors: a review. AIChE J. 50(11):2918–2938.

Sadhana, K., Kumar, N. & Gupta, R., 2018. Effect of gas–liquid ratio on the wall shear stress in slug flow in capillary membranes. *Asia-Pacific Journal of Chemical Engineering*, 13(6):1–13.

Sadhana, K., Kumar, N. & Gupta, R., 2019. Flow and heat transfer in slug flow in microchannels: Effect of bubble volume. *Int. J. Heat Mass Transf*. 129: 812–826.

Sahar, A.M., Ozdemir, M.R., Fayyadh, E.M., Wissink, J., Mahmoud, M.M., Karayiannis, T.G., 2015. Single phase flow pressure drop and heat transfer in rectangular metallic microchannels. *Applied Thermal Engineering*, 93:1324–1336.

Salman, W., Gavriilidis, A. & Angeli, P., 2006. On the formation of Taylor bubbles in small tubes. *Chemical Engineering Science*, 61(20):6653–6666.

Santos, R.M., Kawaji, M., 2010. Effect of contact angle on gas slug formation, shape and flow in a microchannel T-junction by numerical simulation. *19th Int. Congr. Chem. Process Eng.*, p. 673.

Santos, R.M., Kawaji, M., 2012. Developments on wetting effects in microfluidic slug flow. *Chem. Eng. Comm*. 199(12):1626-1641.

Schilder, B. et al., 2010. Flow visualization and local measurement of forced convection heat transfer in a microtube. *Journal of Heat Transfer*, 132(3):1-9.

Shah, R.K., and London, A.L., 1972. Laminar flow forced convection heat transfer and flow friction in straight and curved ducts-A summary of analytical solutions. Technical report no. 75, Stanford university, California.

Shah, R.K., 1975. Laminar flow friction and forced convection heat transfer in ducts of arbitrary geometry. *Int J Heat and Mass Transfer* 18:849–862.

Shariff, Y.M., 2011. Acoustics vibrations to enhance flow boiling in microchannels. *Int. J. of Thermal & Environmental Engineering*, 2(1):19-25.

Shing, K.Y., Jeng, Y.R., Huang, C.-M., and Wang, C.-C., 2011. Heat transfer and flow pattern characteristics for HFE-7100 within microchannel heat sinks, *Heat Transfer Engineering*, 32(7–8):697–704.

Slezkin NA (1955) Dinamikavyazkoineszhimaemoizhidkosti (Dynamics of Viscous Incompressible Liquid). Moscow: Gostekhteorizdat.

Song, H., Chen, D.L. & Ismagilov, R.F., 2006. Reactions in droplets in microfluidic channels. *Angewandte Chemie - International Edition*, 45(44):7336–7356.

Sowayan, A.S., 2013. Effect of bottom wall vibration on heat transfer enhancement for a square cavity domain. *Adv. Sci. Lett.*, 19(3): 889–892.

Sussman, M., Smereka, P. and Osher, S. (1994), A Level Set Approach for computing solutions to incompressible two phase flow, *Journal of Computational Physics*, 114: 146–159.

Svetlov, S.D. & Abiev, R.S., 2018. Formation mechanisms and lengths of the bubbles and liquid slugs in a coaxial-spherical micro mixer in Taylor flow regime. *Chemical Engineering Journal*, 354:269–284.

Taha, T. & Cui, Z. F., 2006. CFD modelling of slug flow in vertical tubes. *Chem. Eng. Sci*. 61:676–687.

Talimi, V., Muzychka, Y.S. & Kocabiyik, S., 2012. A review on numerical studies of slug flow hydrodynamics and heat transfer in microtubes and microchannels. *Int. J. Multiph. Flow*, 39: 88–104.

Talimi, V., Muzychka, Y.S. & Kocabiyik, S., 2013. Slug flow heat transfer in square microchannels. *International Journal of Heat and Mass Transfer*, 62(1):752–760.

Triplett, K. A., Ghiaasiaan, S.M., Abdel-Khalik, S.I. & Sadowski, D.L., 1999. Gas–liquid two-phase flow in microchannels Part I: two-phase flow patterns. *International Journal of Multiphase Flow*, 25(3):377–394.

Triplett, K. A., Ghiaasiaan, S.M., Abdel-Khalik, S.I., LeMouel, A., et al., 1999. Gas–liquid two-phase flow in microchannels Part II: void fraction and pressure drop. *International Journal of Multiphase Flow*, 25(3):395–410.

Tryggvason, G. and Muradoglu, M. (2008), A front-tracking method for computation of interfacial flows with soluble surfactants, *Journal of Computational Physics*, 227: 2238–2262.

Tuckerman, D.B. & Pease, R.F.W., 1981. High-performance heat sinking for VLSI. *IEEE Electron Device Letters*, 2(5):126–129.

Urbant, P., Leshansky, A. & Halupovich, Y., 2008. On the forced convective heat transport in a droplet-laden flow in microchannels. *Microfluidics and Nanofluidics*, 4(6):533–542.

Vandu, C.O., Liu, H. & Krishna, R., 2005. Mass transfer from Taylor bubbles rising in single capillaries. *Chemical Engineering Science*, 60(22):6430–6437.

Vivekanand, S. V. B. & Raju, V. R. K., 2015. Simulation of Evaporation Heat Transfer in a Rectangular Microchannel. *Procedia Engineering*, 127:309-316.

Vivekanand, S. V. B. & Raju, V. R. K., 2018. Numerical study of the hydrodynamics and heat transfer characteristics of liquid-liquid Taylor flow in microchannel. *Heat Transf. Asian Res.*, 47(6):794–805.

Vivekanand, S.V.B., Raju, V.R.K., 2019. Effect of wall contact angle and carrier phase velocity on the flow physics of gas–liquid Taylor flows inside microchannels. *Chemical Papers*, 75(5):1173–1188.

Vocale, P. et al., September 2014. Experimental and numerical analysis of single phase flow in a micro T- junction. *, 4th Micro and Nano Flows Conference UCL, London, UK,* pg, 1-8.

Walsh, P. A., Walsh, E. J. & Muzychka, Y. S., 2010. Heat transfer model for gas-liquid slug flows under constant flux. *Int. J. Heat Mass Transf*. 53:3193–3201.

Wang, C.C. et al., 2012. Effect of inclination on the convective boiling performance of a microchannel heat sink using HFE-7100. *Experimental Thermal and Fluid Science*, 36:143–148.

White, E. T. & Beardmore, R.H., 1962. The velocity of rise of single cylindrical air bubbles through liquids contained in vertical tubes. *Chem. Eng. Sci*. 17:351–361.

Whitehill, J., Martyn, S., Neild, A., and Wah, T.N, August 2010. Droplet behaviour under high intensity acoustic vibration. *Proceedings of 20th International Congress on Acoustics, ICA*, Sydney, Australia: 23-27.

Wu, H.Y. & Cheng, P., 2005. Condensation flow patterns in silicon microchannels. *International Journal of Heat and Mass Transfer*, 48(11):2186–2197.

Youngs, D.L., 1982. Time-dependent multi-material flow with large fluid distortion. In: Morton, K.W., Baines, M.J. (Eds.), Numerical Methods for Fluid Dynamics New York. Academic, New York: 273–285.

Yun, R., Hyeok Heo, J. & Kim, Y., 2006. Evaporative heat transfer and pressure drop of R410A in microchannels. *International Journal of Refrigeration*, 29(1):92–100.

Zhang, J., Fletcher, D. F. & Li, W., 2016. Heat transfer and pressure drop characteristics of gas–liquid Taylor flow in mini ducts of square and rectangular cross-sections. *Int. J. Heat Mass Transf.*, 103:45–56.

Zheng, Y., Chen, J., Shang, Y., Chang, H., Chen, H., and Shu, S., 2017. Numerical analysis of the influence of wall vibration on heat transfer with liquid hydrogen boiling flow in a horizontal tube. *Int. J. Hydrogen Energy*, 42(52): 30804–30812.

PUBLICATIONS

Publications in International/National Journals

1. S.V.B. Vivekanand and V.R.K. Raju, "Effect of wall temperature modulation on the heat transfer characteristics of droplet-train flow inside a rectangular microchannel" *Chinese Journal of Chemical Engineering*, Elsevier 2019 (Accepted for publication).

2. S.V.B. Vivekanand and V.R.K. Raju, "Effect of wall contact angle and carrier phase velocity on the flow physics of gas–liquid Taylor flows inside microchannels" *Chemical Papers*, Springer, 73:1173–1188, 2019. DOI:10.1007/s11696-018-0668-3.

3. S.V.B. Vivekanand and V.R.K. Raju, "Numerical study of the hydrodynamics and heat transfer characteristics of liquid–liquid Taylor flow in microchannel", *Heat Transfer-Asian Research*, Wiley, 47:794–805, 2018. DOI: 10.1002/htj.21341.

4. S.V.B. Vivekanand, S. Chandrasekhar, and V.R.K. Raju, "Influence of capillary number on the droplet shape, film thickness, and pressure drop in a liquid-liquid Taylor flow inside a microcapillary", *International Journal of Mathematical, Engineering and Management Sciences*,4(6):1407–1419, 2019. DOI: 10.33889/IJMEMS.2019.4.6-111.

5. S.V.B. Vivekanand and V.R.K. Raju, "Numerical study on evaporation heat transfer characteristics of water in inclined microchannels with varying inlet vapor quality", *World Journal of Engineering*, Emerald, 16(1):125–131, 2019. DOI: 10.1108/WJE-12-2017-0417.

6. S.V.B. Vivekanand and V.R.K. Raju, "Simulation of evaporation heat transfer in a rectangular microchannel", *Procedia Engineering*, Elsevier, 127: 309-316, 2015. DOI: 10.1016/j.proeng.2015.11.374.

7. S.V.B. Vivekanand and V.R.K. Raju, "Effect of modulated wall motion on flow and heat transfer in the Taylor flow regime in a rectangular microchannel", 2019 (*Communicated*)

National/International Conferences Attended

1. S.V.B. Vivekanand and V.R.K. Raju, *"Simulation of evaporation heat transfer in a rectangular microchannel",* Proceedings of the International Conference Computational Heat and Mass Transfer NIT Warangal, India – Nov 30-Dec 2, 2015.

2. S.V.B. Vivekanand and V.R.K. Raju, *"Influence of Capillary number on the droplet shape, film thickness, and pressure drop in a liquid-liquid Taylor flow inside a microcapillary"* Proceedings of the National Conference on Computational Modeling of Fluid Dynamics Problems (CMFDP-2019) NIT Warangal, India – Jan 18-20, 2019.

3. S.V.B. Vivekanand, S Chandrasekhar, V.R.K. Raju, *"Effect of homogeneous void fraction, slug and droplet lengths, and mixture velocity on the heat transfer characteristics of a liquid-liquid Taylor flow inside a circular microcapillary"* 2nd International Conference on New Frontiers in Chemical, Energy and Environmental Engineering (INCEEE 2019) 15-16 Feb, 2019, NIT Warangal, India.